Volume 3 Issue 1 (2017) · ISSN 2424-7723

INTERNATIONAL JOURNAL OF BIOPRINTING

WHIOCE PUBLISHING PTE. LTD.
PROVIDING
FIRST-CLASS SCIENTIFIC INFORMATION
FOR TOP SCHOLARS

Editorial Board

Editor-in-Chief
Chee Kai Chua
Nanyang Technological University, Singapore
mckchua@ntu.edu.sg

Associate Editor
Wai Yee Yeong
Nanyang Technological University, Singapore
wyyeong@ntu.edu.sg

Assistant Editor
Jia An
Nanyang Technological University, Singapore
anjia@ntu.edu.sg

Editorial Board Members
Paulo Jorge Da Silva Bartolo
University of Manchester, UK
paulojorge.dasilvabartolo@manchester.ac.uk

Richard Bibb
Loughborough University, UK
r.j.bibb@lboro.ac.uk

Martin Birchall
University College London, UK
m.birchall@ucl.ac.uk

Frederik Claeyssens
University of Sheffield, UK
f.claeyssens@sheffield.ac.uk

Charlotte Hauser
Nanyang Technological University, Singapore
chauser@ibn.a-star.edu.sg

Jiankang He
Xi'An Jiaotong University, China
jiankanghe@mail.xjtu.edu.cn

Geun Hyung Kim
Sungkyunkwan University, South Korea
gkimbme@skku.edu

Vladimir Mironov
Center for Information Technology Renato Archer, Brazil
vladimir.mironov54@gmail.com

Makoto Nakamura
University of Toyama, Japan
maknaka@eng.u-toyama.ac.jp

Roger Narayan
University of North Carolina and North Carolina State University, USA
roger_narayan@unc.edu

Ibrahim Tarik Ozbolat
University of Iowa, USA
ibrahim-ozbolat@uiowa.edu

Cijun Shuai
Central South University, China
shuai@csu.edu.cn

Lay Poh Tan
Nanyang Technological University, Singapore
lptan@ntu.edu.sg

Xiaohong Wang
Tsinghua University, China
wangxiaohong@mail.tsinghua.edu.cn

Shoufeng Yang
University of Southampton, UK
s.yang@soton.ac.uk

Dong Jin Yoo
Daejin University, South Korea
djyoo@daejin.ac.kr

Permission is granted to quote from the contents of this journal with customary acknowledgement of the source.
For subscriptions, or single-copy orders, please contact us at editorial@whioce.com for enquiries.
Printed in Singapore.

Volume 3 Issue 1• 2017
ISSN 2424-7723 (print) ISSN 2424-8002 (online)

INTERNATIONAL JOURNAL OF BIOPRINTING

Editor-in-Chief
Chee Kai Chua
Nanyang Technological University, Singapore

WHIOCE PUBLISHING PTE. LTD.

Volume 3 | Issue 1 | 2017 | Page 1 – 86 |

International Journal of Bioprinting

https://ijb.whioce.com/index.php/int-j-bioprinting

CONTENTS

EDITORIAL

Cell powered biobots and more perspectives for IJB

Editor–in-Chief: Chee Kai CHUA

Executive Director and Professor, Singapore Centre for 3D Printing, School of Mechanical & Aerospace Engineering, College of Engineering, Nanyang Technological University, Singapore

http://dx.doi.org/10.18063/IJB.2017.01.003.

At the end of 2016, *International Journal of Bioprinting* (IJB) is able to estimate its first mock impact factor. Based on one issue published in 2015, the 2016 mock impact factor for IJB is calculated to be 6, excluding self-citations! This result is surprising, impressive and encouraging. However, this is just a beginning and more and more quality articles and reviews are needed in order to maintain it.

Tissue transplants and *in vitro* tissue models are common applications of bioprinting. Recently, a new application of bioprinting is emerging, namely cell powered biobots. Cell powered biobots are biohybridmotile microsystems that are made from freeform deposition of living cells and other materials. Cells are used to power the motility of the microsystem such as walking, swimming or flying, depending on design intent. Cells can also be genetically engineered for remote control. These battery-free dynamic microsystems may have unimaginable applications in biomedical science and engineering in future. We do welcome submissions from this interesting research area as well.

We would also like to take this opportunity to invite any person or organization to express their honest views on bioprinting, to share what they think are the crucial questions in bioprinting. These perspective or commentary papers can be shorter than a standard article but must convey a clearly outlined point of view. Bioprinting is a super exciting topic all over the world now. Many approaches and diverse focuses co-exist with one another. Some views are even opposing. Advancement in bioprinting is certainly important, but perspectives from other professions are equally important.

In this issue, there are 3 reviews, 4 original research articles and 1 perspective. Liew and Zhang review *in vitro* pre-vascularization strategies for tissue engineered constructs[1]. Whitford and Hoying review recent development in bioinks that support vascularization[2]. Lee *et al*. review recent bioprinter modifications for developing new cell printing systems[3]. Koch *et al*. present a parametric study of laser for laser-assisted bioprinting[4]. Murphy *et al*. report a solvent evaporation method to print polymer/bioactive glass composite scaffolds with stem cells incorporated[5]. Sing *et al*. investigate titanium/tantalum/ collagen-based biphasic implants for repairing osteochondral defects[6]. Liu *et al*. study the morphology of polycaprolactone scaffold made by electrohydrodynamic jetting[7]. Suntornnond provides a perspective on the role of support materials in bioprinting[8].

References

1. Liew A W L and Zhang Y, 2017, *In vitro* pre-vascularization strategies for tissue engineered constructs — bioprinting and others. *International Journal of Bioprinting*, vol.3(1): 3–17. http://dx.doi.org/10.18063/IJB.2017.01.008
2. Whitford W and Hoying J B, 2017, Digital biomanufacturing supporting vascularization in 3D bioprinting. *International Journal of Bioprinting*, vol.3(1): 18–26. http://dx.doi.org/10.18063/IJB.2017.01.002
3. Lee H, Koo Y, Yeo M, *et al*., 2017, Recent cell printing systems for tissue engineering. *International Journal of Bioprinting*, vol.3(1): 27–41. http://dx.doi.org/10.18063/IJB.2017.01.004
4. Koch L, Brandt O, Deiwick A, *et al*., 2017, Laser assisted bioprinting at different wavelengths and pulse durations with a metal dynamic release layer: a parametric study. *International Journal of Bioprinting*, vol.3(1):

Cell powered biobots and more perspectives for IJB. © 2017 Chee Kai CHUA. This is an Open Access article distributed under the terms of the Creative Commons Attribution-NonCommercial 4.0 International License (http://creativecommons.org/licenses/by-nc/4.0/), permitting all non-commercial use, distribution, and reproduction in any medium, provided the original work is properly cited.

42–53. http://dx.doi.org/10.18063/IJB.2017.01.001

5. Murphy C, Kolan K, Li W, *et al.*, 2017, 3D bioprinting of stem cells and polymer/bioactive glass composite scaffolds for bone tissue engineering. *International Journal of Bioprinting*, vol.3(1): 54–64. http://dx.doi.org/10.18063/IJB.2017.01.005
6. Sing S L, Wang S, Agarwala S, *et al*., 2017, Fabrication of titanium based biphasic scaffold using selective laser melting and collagen immersion. *International Journal of Bioprinting*, vol.3(1): 65–71. http://dx.doi.org/10.18063/IJB.2017.01.007
7. Liu H, Vijayavenkataraman S, Wang D, *et al*., 2017, Influence of electrohydrodynamic jetting parameters on the morphology of PCL scaffolds. *International Journal of Bioprinting*, vol.3(1): 72–82. http://dx.doi.org/10.18063/IJB.2017.01.009
8. Suntornnond R, An J and Chua C K, 2017, Roles of support materials in 3D bioprinting — present and future. *International Journal of Bioprintin*g, vol.3(1): 83–86. http://dx.doi.org/10.18063/IJB.2017.01.006

RESEARCH ARTICLE

In vitro pre-vascularization strategies for tissue engineered constructs–Bioprinting and others

Andy Wen Loong Liew and Yilei Zhang*

Singapore Centre for 3D Printing, School of Mechanical and Aerospace Engineering, Nanyang Technological University, Singapore 639798, Singapore

Abstract: Tissue-engineered products commercially available today have been limited to thin avascular tissue such as skin and cartilage. The fabrication of thicker, more complex tissue still eludes scientists today. One reason for this is the lack of effective techniques to incorporate functional vascular networks within thick tissue constructs. Vascular networks provide cells throughout the tissue with adequate oxygen and nutrients; cells located within thick un-vascularized tissue implants eventually die due to oxygen and nutrient deficiency. Vascularization has been identified as one of the key components in the field of tissue engineering. In order to fabricate biomimetic tissue which accurately recapitulates our native tissue environment, *in vitro* pre-vascularization strategies need to be developed. In this review, we describe various *in vitro* vascularization techniques developed recently which employ different technologies such as bioprinting, microfluidics, micropatterning, wire molding, and cell sheet engineering. We describe the fabrication process and unique characteristics of each technique, as well as provide our perspective on the future of the field.

Keywords: vascularization, vasculogenesis, endothelial, microfluidics, micropatterning, cell-sheet engineering, wire-molding

*Correspondence to: Yilei Zhang, Singapore Centre for 3D Printing, School of Mechanical and Aerospace Engineering, Nanyang Technological University, Singapore 639798, Singapore: E-mail: ylzhang@ntu.edu.sg

Received: November 11, 2016; **Accepted:** December 14, 2016; **Published Online:** January 23, 2017

Citation: Liew A W L and Zhang Y, 2017, *In vitro* pre-vascularization strategies for tissue engineered constructs — Bioprinting and others. *International Journal of Bioprinting*, vol.3(1): 3–17. http://dx.doi.org/10.18063/IJB.2017.01.008.

1. Introduction

There is a wide spectrum of human pathologies which plague mankind and affect our quality of life. These diseases often lead to organ failure and even death of the patient. The conventional treatment for organ failure would be an organ transplant, where the patient's damaged organ is replaced by a functional and compatible donor organ. Although organ transplantation has proven its efficacy over the years, thousands of people continue to lose their lives every year due to organ failure. The reason for this is the demand and supply disparity of donor organs. The demand for donor organs far exceeds the supply, and there are simply not enough donor organs to go around. Research by the U.S. Department of Health and Human Services found that in the United States alone, 22 people waiting for organ transplants die each day due to shortage of donor organs[1]. Moreover, the percentage gap between the number of patients on the waiting list and the number of organ donors has been steadily increasing every year. Tissue engineering has shown promising signs to be a solution to this problem.

The term *tissue engineering* was first coined in 1993 by Langer and Vacanti in their highly influential paper[2]. Tissue engineering is a cross-disciplinary field of research, comprising the principles of biology and engineering to create functional tissue in a lab in order to replace or restore damaged tissue in a patient. A patient suffering from tissue injury, such as skin burn,

In vitro pre-vascularization strategies for tissue engineered constructs–Bioprinting and others. © 2017 Andy Wen Loong Liew. This is an Open Access article distributed under the terms of the Creative Commons Attribution-NonCommercial 4.0 International License (http://creativecommons.org/licenses/by-nc/4.0/), permitting all non-commercial use, distribution, and reproduction in any medium, provided the original work is properly cited.

can be treated using this approach. A biopsy is first performed to extract healthy autologous (skin) cells from the patient. These cells are cultured and expanded *in vitro* to obtain a sufficient number of cells needed for the treatment. The cells are then seeded onto a biodegradable scaffold which will then be cultured to maturity. When the tissue-engineered graft is fully matured, it can then be transplanted onto the patient's injury site to enhance the wound healing process.

Research in this field is expanding quickly and has given rise to many tissue engineering companies which carry out research and manufacture human Tissue-Engineered Products (hTEPs) for clinical use today. Tissue engineering is still in its early initial phases, thus only few hTEPs have been successfully translated into commercial availability. These commercially available hTEPs mainly comprise skin products, followed by cartilage, and lastly bone products. By 2003, more than 20 skin replacement products were available in USA and Europe[3]. Tissue-engineered cartilage products have found widespread application today to treat traumatic knee joint damage by undergoing Autologous Chondrocyte Transplantation (ACT) surgery[3]. The application of tissue-engineered bone products is limited to the treatment of small bone lesions as larger defect sites still remain untreatable by this approach and autologous bone grafts still remain the preferred approach. With the successful translation of these hTEPs into clinical application, tissue engineering has proven its legitimacy as a promising candidate for the treatment of injured tissue, sparking more and more research in the field. Today, research groups all over the world are working to create hTEPs from various tissues such as cardiac[4,5], liver[6], cornea[7], trachea[8], artery[9] and many others.

Various research groups have published works reporting the successful engineering of functional tissue *in vitro*, such as bladder[10] tissue, although they have not yet been used in clinical trials due to its early stage of development. Many of these published works report the successful engineering of only very thin, microscale tissue constructs. One of the main reasons for this is the fact that cells encapsulated deep within a large tissue construct have limited access to oxygen and nutrients, causing them to die during long-term culture. We know that cells located more than 200 μm away from a nutrient source (blood vessels) do not receive sufficient nutrients for survival[11]. With the ultimate goal of tissue engineering in mind, which is to successfully engineer complete organs, new techniques need to be developed to allow the fabrication of larger tissue constructs which demonstrate long-term viability post implantation. A promising approach to this problem is the pre-vascularization of tissue implants, where techniques are used to incorporate functional vascular networks within a tissue construct *in vitro* before implantation. Compared to an un-vascularized tissue construct, a pre-vascularized tissue construct has shown enhanced anastomosis with host vasculature post implantation, thus providing adequate nutrients to encapsulated cells and improving viability. The vascularization of tissue engineered constructs is deemed to be vital to the progress of tissue engineering today and in the future[12]. In this review, we highlight the significance of pre-vascularization and its impact on tissue engineering. We also identify recently developed *in vitro* vascularization techniques which have shown promising results, categorized based on the technologies they employ, and describe each of their fabrication processes.

2. Significance of Pre-Vascularization

2.1 Tissue Engineering for Regenerative Medicine

With avascular tissue products such as skin and cartilage already made commercially available, tissue engineers are now looking to engineer larger, more complex tissue which could potentially be used as a viable treatment option for patients suffering from critical diseases. However, there are a host of crucial challenges to be addressed to meet this goal. Our native tissues possess highly specific architectures, and different tissues have their own unique structural organization. It is imperative that tissue engineers accurately emulate the intrinsic heterogeneous architecture of these complex tissues when fabricating their tissue engineered construct as there is a well-accepted correlation between tissue architecture and pathogenesis[13]. Tissue-engineered constructs that do not accurately mimic the heterogeneous nature of native tissues could lead to disease and be carcinogenic when implanted into a patient. The successful engineering of complex tissue also requires control of differentiated function of the cells within the tissue engineered construct, failing which could cause the tissue-engineered construct to be dysfunctional and malignant. There are many other challenges in the pursuit of engineering large, complex tissue constructs such as matrix stiffness, molecular gradients and hierarchical structure[14], but one of the main challenges is the one we

will be focusing on in this report—the problem of vascularization.

As previously mentioned, the incorporation of a mature, inter-connected vascular network within a tissue construct is vital in tissue engineering as it helps to prevent the development of a necrotic core due to nutrient deficiency of cells deep within the construct, and provides a readily perfusable network for nutrient perfusion throughout the construct during the fabrication stage, or after implantation in a patient[15]. The implantation of a pre-vascularized tissue construct minimizes the need for vasculogenic and angiogenic processes to occur after implantation, and has been shown to induce rapid vascularization and inosculation with host vasculature upon implantation into mice when compared to un-vascularized constructs[16]. These studies demonstrate the importance of pre-vascularizing a tissue construct *in vitro* before implantation. Today, success in the vascularization of tissue constructs has been limited to the vascularization of thin (2D) tissue slices, and the vascularization of large 3D tissue constructs has seen slower progress. The lack of viable fabrication techniques has been a prime hindrance to our progress in this area. Successful vascularization of large 3D tissue constructs would undoubtedly provide invaluable contribution in the field of tissue engineering and bring us a step closer to fabricating whole organs.

2.2 *In Vitro* Tissue Models

Besides its obvious applications in regenerative medicine, the ability to vascularize large 3D tissue constructs would also contribute to the development of *in vitro* tissue models which better replicate our native tissues. The use of animal models and *ex vivo* (cadaveric) human tissue models for various studies, such as pathophysiology and pharmacology, has resulted in groundbreaking findings over the years. However, there are inherent limitations with the use of these models. Cadaveric human tissue models offer exceptional replication of native tissue; however, they suffer from limited availability. The use of animal models brings rise to issues with species-specific tissue response[17], as well as ethical issues with regards to the well-being of lab animals. These shortcomings have driven researchers to develop more advanced *in vitro* tissue models which accurately mimic native tissue and are easily fabricated without the need for donor tissue and animal experiments. The most common *in vitro* model still being used in scientific research today is the cell monolayer, i.e., 2D cell culture[18]. As we know, the cells in our bodies are enclosed within a 3D extra-cellular matrix (ECM) environment where they attach and proliferate. The results of experiments utilizing these 2D *in vitro* models may not be an accurate representation as it is known that cells function differently when cultured in 2D vs 3D cellular environments, affecting cellular cues, differentiation, adhesion, and morphogenesis, among others[19–21]. 3D *in vitro* models are able to more closely replicate the cellular environment found in our native tissue, thus providing researchers with more reliable results compared to using 2D *in vitro* models[22]. However, the fabrication and application of 3D *in vitro* models are not as trivial as cell monolayers. A common problem faced by the application of 3D *in vitro* models is the loss of cell viability in long-term culture[23], thus driving research to improve the lifespan of these models through modifications to the system[24]. Vascularized 3D tissue models have the potential to remain viable for long periods while still able to accurately replicate native vascularized tissue. As we know, cell-cell interactions and signaling plays a vital role in determining cell functionality *in vivo*. As such, monoculture tissue models may not accurately depict and account for the cellular interactions between parenchymal cells (i.e., hepatocytes and cardiomyocytes) and endothelial cells (ECs) which occur repeatedly in our organs, given that blood vessels are found throughout our entire body. The development of vascularized 3D tissue models is crucial in this regard. Moreover, vascularized 3D tissue models could also be used to boost our understanding of vascular physiology such as vasculogenesis, angiogenesis, and the physiology involved in vascular pathogenesis which would help to improve treatment of patients suffering from arterial diseases such as thrombosis and atherosclerosis. Vascularized 3D tissue models could also be useful in pharmacology studies and drug screening.

3. Current *In Vitro* Vascularization Approaches

Different vascularization techniques have been recently reported in literature, including the *in vivo* approach where perforated, un-vascularized tissue constructs are implanted to allow the host's peripheral vascular system to naturally vascularize the tissue construct[25]. This method requires the timely invasion of the host vasculature into the un-vascularized tissue construct through angiogenic sprouting in order to provide the cells within the tissue construct with adequate nutrients to survive. Naturally, it would take a longer time to vascularize larger tissue constructs by this approach. Thus, this approach may not be viable

for large 3D tissue constructs as the time taken for *in vivo* vascularization may be too long causing necrosis before a functional vascular network is formed, leading to premature failure of the construct. This disadvantage has driven many researches to develop *in vitro* vascularization techniques to fabricate pre-vascularized tissue constructs before implantation, which has clear advantages over un-vascularized constructs. The use of *in vitro* pre-vascularized tissue constructs would speed up the process of anastomosis with host vasculature and provide cells with quick access to a nutrient supply[26]. We will now look at the current methods developed by various research groups to fabricate blood vessels *in vitro*, and discuss their advantages as well as disadvantages.

3.1 Bioprinting

The term bioprinting refers to any additive manufacturing technique which uses biological ink to produce living tissue constructs for a variety of applications including regenerative medicine and cellular studies[27]. There are numerous bioprinting techniques which rely on fundamentally different principles of fabrication such as extrusion, ink-jet, and laser-based approaches. Bioprinting technology has been a hot topic of research in recent years, given its potential advantages over other conventional techniques, with research groups striving to improve the performance of existing bioprinters as well as developing new bioprinting technologies. This pursuit has given rise to novel bioprinting technologies in recent years such as the development of the "freeform reversible embedding of suspended hydrogels" process, able to produce 3D constructs with complex architecture not achievable by conventional approaches[28]. Today, advanced bioprinters with state-of-the-art features such as temperature and viscosity are now commercially available in the market, and researchers have been utilizing these bioprinters to produce groundbreaking researches. Researchers have demonstrated the ability of bioprinting technology to fabricate hybrid constructs made of multiple hydrogel materials and cell types, offering control of the construct's mechanical stiffness and composition[29]. Scaffold-free, large diameter tubular tissue constructs have also been produced by bioprinting for vascular tissue engineering applications using an indirect agarose molding technique[30]. The technique offers control of the tube's shape, dimension and hierarchical branching. The same approach was utilized to fabricate fused toroid-shaped, scaffold-free tissue from an alginate-based mold produced by bioprinting, showcasing the ability to produce viable tissue with customizable architecture[31].

Novel laser-based bioprinting approaches have also been developed in recent years including the Laser-Induced-Forward-Transfer (LIFT) technique and stereolithography (SLA). The LIFT technique involves the focusing of a high powered laser beam onto a photo-absorbent material coated with biological ink. When the photo-absorbent material is exposed to sufficient laser intensity it vaporizes and causes a high-pressure zone which propels a small volume of biological ink onto a donor slide where the ink is collected. By controlling the laser intensity and axial motion, high resolution patterns of biological material can be printed[33,34]. Stereolithography was patented in the 1980's but only recently has the technology found applications in the field of tissue engineering as researchers demonstrated its ability to be used for cell encapsulation and the fabrication of 3D tissue scaffolds. Projection stereolithography (PSL) has been utilized to fabricate living tissue constructs with controllable, porous architecture and demonstrated that cell viability was improved due to enhanced nutrient delivery within the porous scaffolds compared to solid scaffolds[35]. Commercially available SLA systems have also been modified to improve and expand the system capabilities for tissue engineering applications such as the ability to fabricate 3D tissue constructs comprising distinct layers of different cell types and material composition, thus improving the long-term viability of encapsulated cells[36].

The bioprinting approach has also shown potential applications in the field of vascularization of tissue constructs. A key advantage of using bioprinting technology is the ability to fabricate truly three-dimensional microchannel networks which are perfusable and can be lined with ECs. These 3D networks can be fabricated into pre-designed patterns which could be useful in studying the effects of vascular network spatial organization. Using a newly developed extrusion-based bioprinting approach, 3D tissue constructs consisting of multiple cell types were successfully produced and Human Umbilical Vein Endothelial Cells (HUVECs) were observed to line the lumen of embedded microchannels simulating perfusable blood vessels[37]. Microchannel networks were incorporated into the bulk ECM through the bioprinting of fugitive ink which was later removed, leaving behind microchannels which were then seeded with HUVECs. A similar study, using the same prin-

ciples but slightly different methodology, was carried out where researchers were able to incorporate an interconnected vascular network within bulk hydrogel containing hepatocytes and showed that perfusion of the vascular network with cell medium was able to sustain metabolic activity of the surrounding hepatocytes[32] (**Figure 1**). Recently, a technique capable of printing cell-laden tubular hydrogel constructs was developed using a multilayered coaxial extrusion system[38]. The technique demonstrated high cell viability, tunable tube dimensions, perfusability and complex architecture.

Despite its obvious advantages, bioprinting does suffer from several drawbacks when applied to vascularization of tissue constructs. Firstly, potential problems arising from the use of fugitive ink include the biocompatibility of the fugitive ink, as well as the removal process. Many reports found in literature today utilize the same fugitive ink approach to tackle the problem of vascularization[39] (**Figure 2**). Fugitive ink may contain cytotoxic compounds which are detrimental to cell viability and affect cell phenotype. The process of removing the fugitive ink, such as chemical dissolution and heat treatment, may also affect cell phenotype and lead to abnormal cell function and necrosis. Secondly, 3D printing technologies, such as Selective Laser Melting (SLM) and Fused Deposition Modelling (FDM), are known for their ability to fabricate objects with complex architecture. However, bioprinting technology may be less capable in this aspect considering the fact that the bioprinted material is soft and gel-like, featuring high water content and incorporating live cells. This limits the level of structural complexity achieved in the printed tissue constructs.

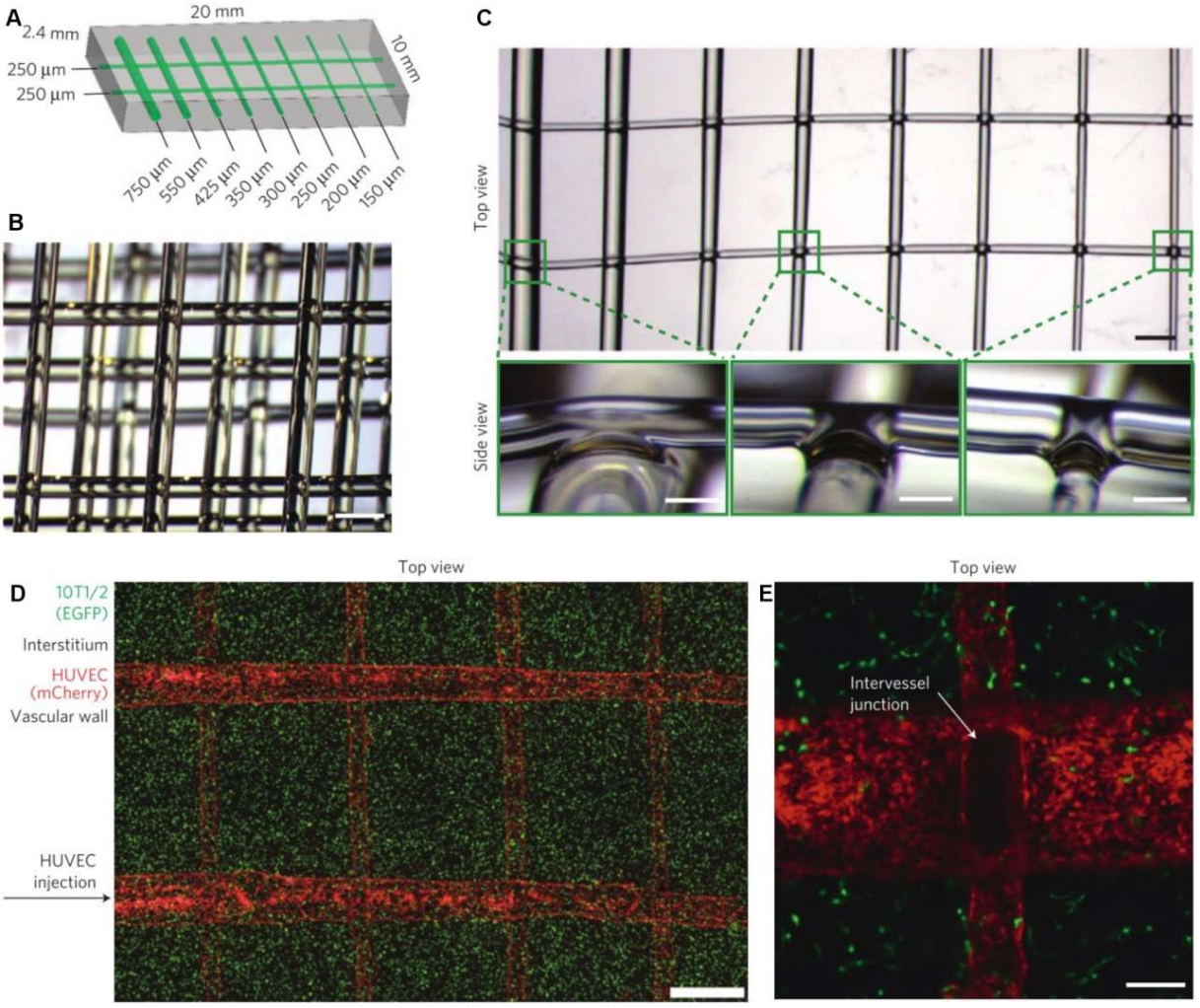

Figure 1. 3D printed carbohydrate-glass lattice used as sacrificial template in engineered tissues containing living cells to generate interconnected networks lined with endothelial cells and perfused with blood. Scale bars: (B, D, C top-view) 1 mm; (C side-view, E) 200 µm. (Adopted from Miller *et al.*[32])

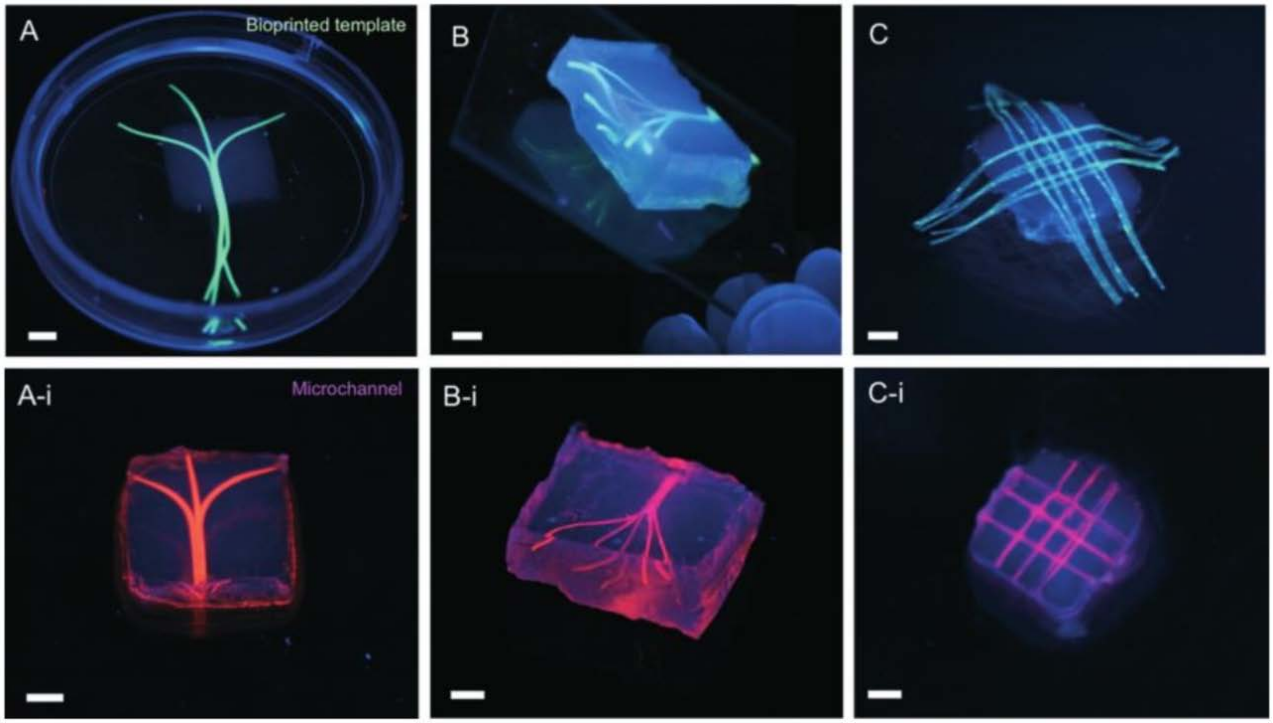

Figure 2. Bioprinted agarose template to fabricate microchannel networks within Gelatin Methacrylated (Gelma) hydrogel. Scale bars: 3 mm. (Adopted from Betassoni *et al*.[39])

3.2 Microfluidics (Lithography)

Microfluidic technology has been gaining popularity in research over the past two decades with more and more papers containing the keyword "microfluidic" being published[40]. This technology has found applications in many different fields of research, one of which being the vascularization of tissue constructs. Today, advanced lithographic technology allows us to fabricate complex microfluidic networks with ultra-high resolution, giving the user superb control over the networks' geometrical features. Its small scale minimizes the amount of consumables needed (such as cell medium) for each experimental run, thus reducing cost and increasing throughput. Microfluidic technology has been used in various ways to achieve vascularization. In one approach, microchannel networks were produced within bulk collagen matrix and seeded with HUVECs to simulate perfusable blood vessels[41] (**Figure 3**). The biofunctionality of the fabricated *in vitro* vessels was demonstrated including HUVEC interaction with pericytes which affected barrier function. In another approach, microfluidic channels were fabricated within bulk agarose hydrogel encapsulating murine fibroblasts. The microfluidic channels were not seeded with ECs but murine fibroblast viability was shown to improve by the perfusion of medium thorough the microchannel networks[42].

Another commonly used and exciting approach today involves the encapsulation of ECs within bulk hydrogel where they spontaneously self-assemble into perfusable vascular networks. Microfluidic technology is used in this method to fabricate the device, as well as to provide the encapsulated cells with medium and supplement perfusion with controlled parameters such as flow rate, flow direction, and pressure. Various microfluidic designs have been developed to suit the objectives of each research project including the replication of dynamic angiogenesis *in vitro*[43], the creation of a perfusable vascular network on a chip[44] (**Figure 4**) under physiologically relevant shear rates[45], the vascularization of cardiac tissue for improved functionality[46], and the controlled formation and characterization of capillary networks using a microfluidic device[47]. In these studies, directed angiogenic sprouting has been achieved and strong barrier function, as well as perfusable network interconnectivity has been demonstrated. The advantages of this approach include that it has high throughput, and the vascular networks are formed through natural vasculogenic and angiogenic processes which rely on self-assembly of the ECs, allowing the ECs to degrade and migrate

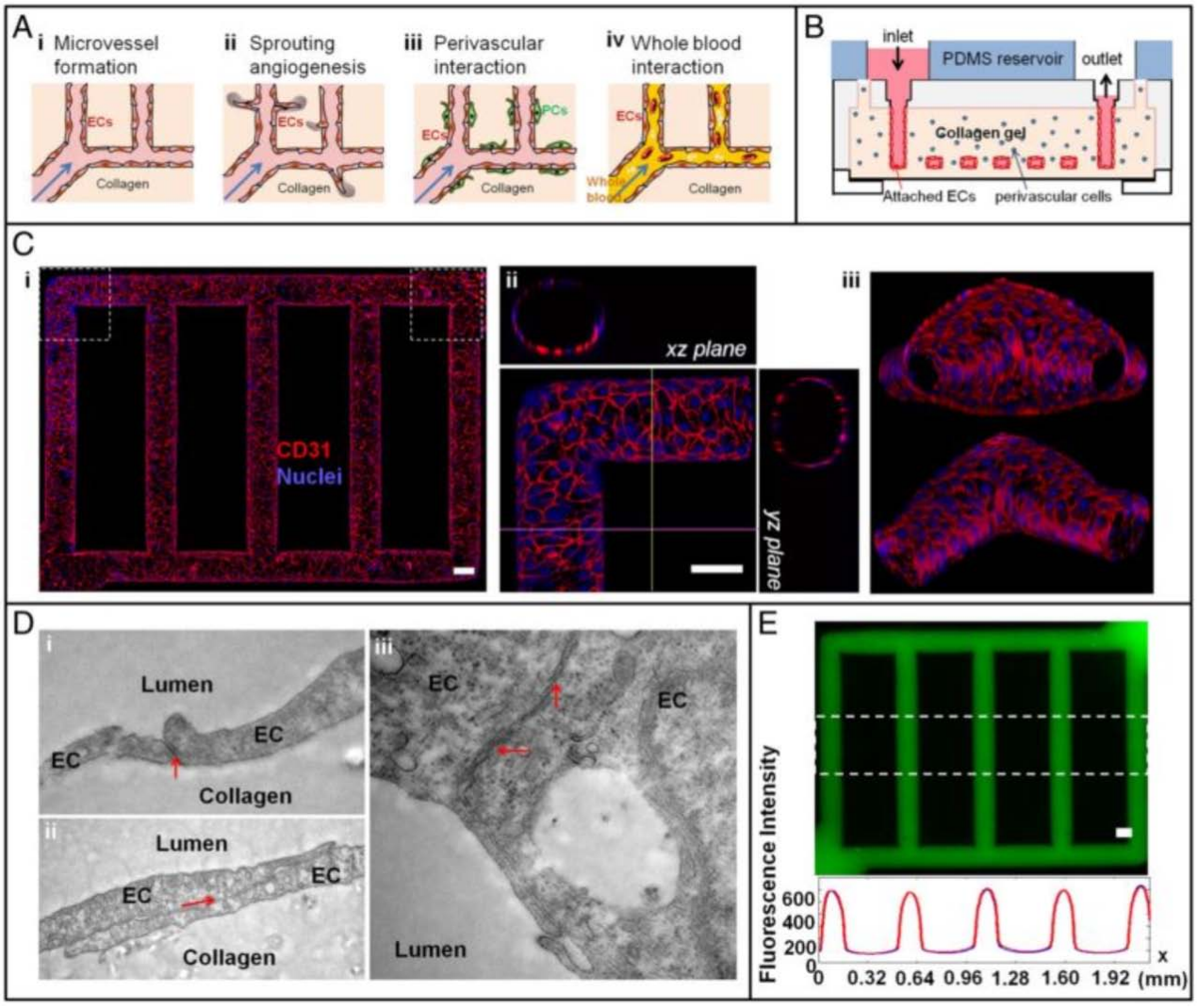

Figure 3. Microfluidic technology used to engineer microvascular networks within 3D tissue scaffolds for applications in vascular tissue modelling. Scale bars: 100 μm. (Adopted from Zheng *et al*.[41])

through their surrounding Extra-Cellular Matrix (ECM) freely which is beneficial compared to mechanically constraining the ECs into their lumenized structures[48]. However, the vascular networks formed using this approach are limited to a thin tissue, unlike the networks formed using the bioprinting approach, which may not accurately recapitulate our native vascular networks which are arranged in 3D. Another limitation would be that the formed vascular networks are confined within the microfluidic system and cannot be easily separated for implantation, thus its application for regenerative medicine is diminished.

3.3 Micropatterning

The micro-patterning approach to vascularization involves the patterning of biological material or adhesive proteins on a substrate to induce vasculogenesis with controlled spatial organization. In one study, researchers used standard photolithographic techniques to produce PDMS stamps, which were subsequently used to pattern Fibronectin (Fn) strips on glass coverslips following the procedure shown in **Figure 5A**[49]. Human Endothelial Progenitor Cells (hEPCs) showed preferential adhesion on the Fn surface compared to the non-adhesive PEG surface while also demonstrating directed elongation along the Fn strips after 24 hours post seeding (**Figure 5B**). Optimal strip width for directed cell elongation was found to be 50 μm. After 5 days in culture, immunostaining was performed to show confinement of hEPCs within the Fn strips with sparse migration to neighbouring strips (**Figure 5C**). Another common approach is the use of

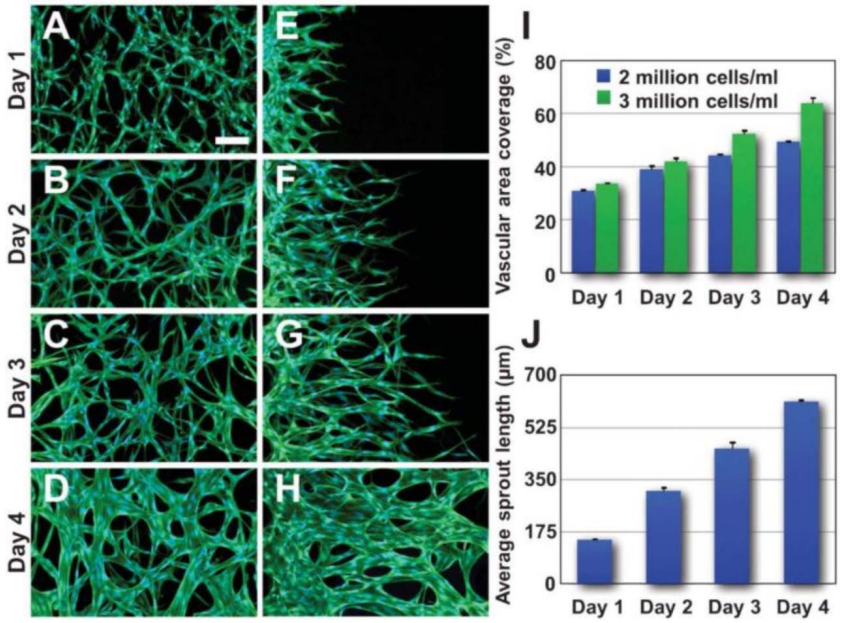

Figure 4. Microfluidic technology used to form perfusable 3D vascular networks along with tumor vasculature by the spatially controlled co-culture of endothelial cells with stromal fibroblasts, pericytes or cancer cells. Scale bars: 100 μm. (Adopted from Kim *et al*.[44])

photolithographic techniques to produce substrates with design-specific microgrooves which can be filled with cellular material and cultured *in vitro*. Raghavan *et al*. utilized this technique in their work which successfully produced lumenized vascular tubes with controlled diameters by varying the dimensions of their microgrooves. By culturing cellular material within branched microgrooves with varying designs, lumenized vascular tubes were also observed to branch into multiple tubes while maintaining their lumenized structure[50]. The branching patterns could be controlled by fabricating microgrooved structures with different designs. Using a similar technique, Chaturvedi *et al*. developed a technique to successfully produce vascular tubes within microgrooved structures which could be harvested and encapsulated within bulk fibrin hydrogel to produce vascularized tissue used for *in vivo* implantation to study the impact of various design parameters on the vascularization of tissue engineered constructs upon implantation in rats[51]. This is an advantage over the closed microfluidic systems where vascularized tissue could not be harvested for subsequent *in vivo* implantation. However, the harvesting process needs to be further developed to increase throughput and achieve 3D vascularized tissue.

Photolithographic techniques have also been used directly to pattern photo-crosslinkable cellular material onto adhesive substrates for vascularization applications. In one study, a UV source, a photomask, and photo-crosslinkable Gelma hydrogel were used to pattern cell-laden Gelma strips, containing ECs and other cells self-aligning cells, onto treated glass slides to demonstrate the ability to control cell alignment and elongation orientation by mechanically confining the cells within a 3D architecture[52]. In another study using a similar approach, strips of Gelma micro-constructs containing ECs and of varying dimensions were patterned onto a treated glass slide where after culture endothelial tubes formed within the patterned strips[53]. They found that optimal tube formation was only achieved at a given micro-construct size. A variety of other micropatterning techniques have also been used for vascularization applications such as soft lithography[54] and laser-assisted micropatterning[55]. In all the abovementioned papers, successful engineering of lumenized endothelial tubes were reported with controlled spatial organization.

3.4 Wire Molding

The incorporation of microchannels within a tissue engineered construct allows immediate perfusion of medium throughout the tissue construct to supply cells with adequate nutrients for survival. The wire molding technique is a simple and effective method of producing microchannels within a tissue construct which

can be perfused with medium to enhance the viability of cells within the surrounding polymerized gel[56]. The fabrication procedure used previously by another research group is shown schematically in **Figure 6**[57]. A pre-polymer solution (with or without cells) is cast and polymerized around a wire held in suspension by mechanical supports. After complete polymerization, the wire is then manually withdrawn from the polymerized material, leaving behind a perfusable microchannel which provides nutrients to encapsulated cells thus simulating our native microvessels. In their report, the generation of microporous cell-laden hydrogel constructs through sucrose crystal leaching was shown to enhance diffusivity through the construct and increase viability of encapsulated cells. A clear advantage of this approach is the ability to incorporate

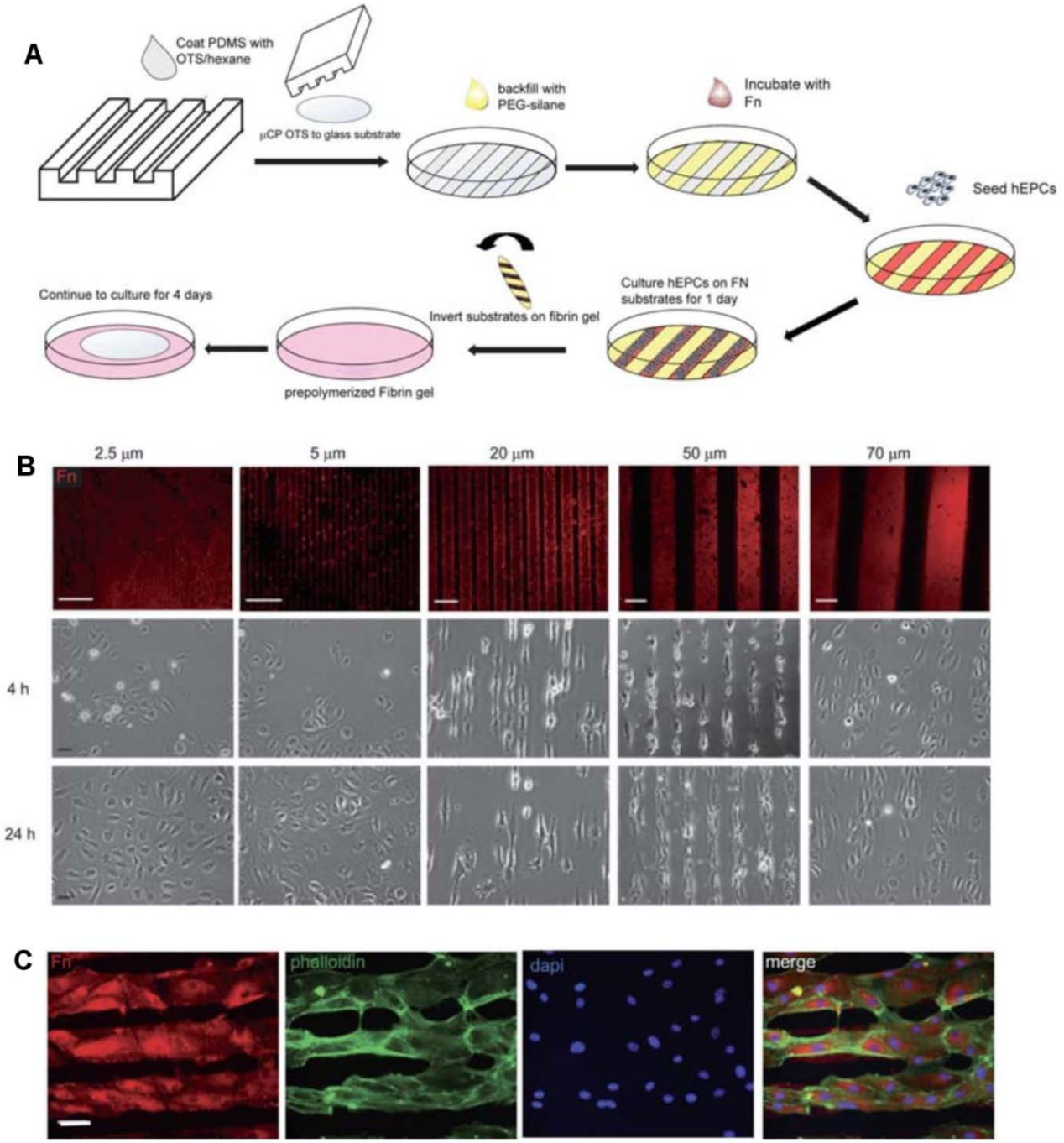

Figure 5. PDMS stamping technique used for Fn micropatterning on coverslips. hEPCs were confined within Fn strips and demonstrated controlled elongation along strip direction. Scale bars are 50μm. (Adopted from Raghavan *et al.*[49])

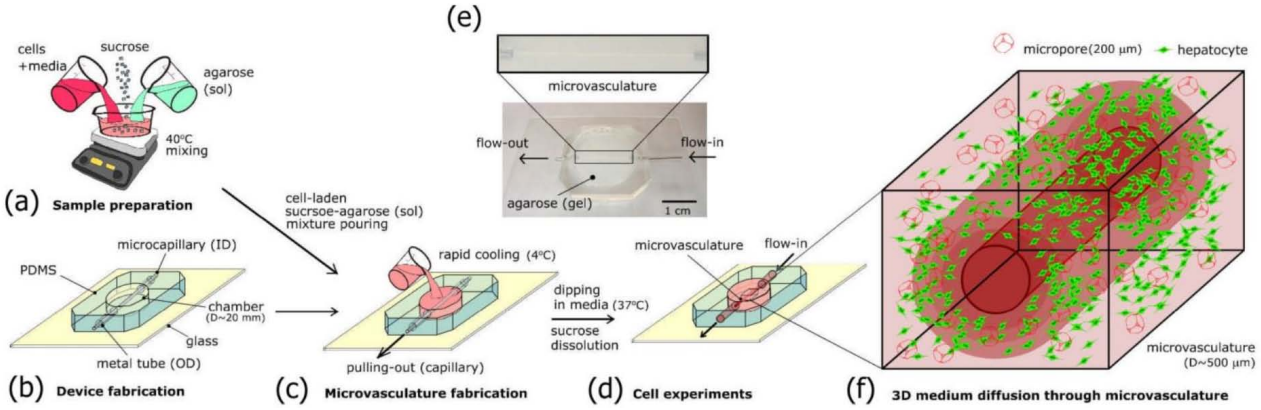

Figure 6. Wire molding technique employed to fabricate perfusable 3D microvascular tubes within microporous cell-laden hydrogels to produce biomimetic tissue constructs. (Adopted from Yao *et al*.[57])

evenly distributed microchannels within large tissue constructs in true 3D form where microchannels are stacked on various Z-planes. This was demonstrated by Yao *et al*. in their work where multichannel (up to 7) collagen conduits were fabricated using this technique to demonstrate the potential of using multichannel nerve guide conduits, instead of commercially available single channel conduits, to minimize dispersion of regenerating axons[58]. The same approach was utilized for vascularization applications where ECs were seeded onto the inner walls of microchannels within their tissue construct, and after implantation *in vivo*, demonstrated quicker vascular infiltration compared to tissue constructs without microchannels[25]. In a different paper, Chrobak *et al*. used the wire molding technique to create a single microchannel within bulk collagen gel, after which ECs were seeded and grown to confluence on the inner walls of the microchannel[59] (**Figure 6**). The relationship between channel diameter and gelling temperature was established, as well as the relationship between EC invasion into the surrounding matrix and collagen concentration. The vascular tubes also demonstrated appropriate response to inflammatory stimuli such as Histamine and Thrombin, which showed that they were functioning as native vessels would *in vivo*. Our native vessels are composed of more complex architectures than just a monolayer of ECs. Capillaries mostly comprise a bilayer structure of ECs surrounding by a Smooth Muscle Cell (SMC) layer responsible for defining vascular tone. By utilizing a modified wire molding technique in combination with other unique procedures, the ability to recapitulate this bilayer structure *in vitro* was demonstrated in recent reports, specifically using SAM-based cell transfer mechanisms[60] and hierarchical cell manipulation techniques[61]. In a separate report, a cell-seeded microchannel fabricated by wire molding was also used to determine the impact of mechanical signals on the stability and barrier function of engineered microvasculature simulating native vessels[62]. These works show the variety of research applications where the wire molding technique could be used to help us increase our understanding of vascular biology through the use of *in vitro* models.

Although the vascular network architecture cannot be precisely controlled using this technique, such as network branching and interconnectivity, wire molding has proven to be a promising technique for the vascularization of large 3D tissue constructs. It is elegantly simple and offers immediate perfusability as well as precise control over microvascular diameter. Endothelial layers seeded onto microchannel walls demonstrated healthy phenotype similar to our native vessels. The ability to vascularize thick 3D constructs could also prove advantageous over other techniques which are confined to thin sheets of tissue.

3.5 Cell Sheet Engineering

A novel approach to tissue engineering is the use of cell sheet technology. Cell sheet technology allows the user to harvest confluent cell monolayers from culture dishes with the use of thermo-responsive polymers which allow easy detachment without chemical treatment. The harvested cell sheets remain viable and intact with their naturally deposited ECM which allow for easy reattachment onto another substrate after harvest. Cell sheet engineering has been used to engineer biomimetic tissue *in vitro* such as corneal epithelium[63], skin[64], and myocardial tissue[65].

Asakawa *et al*. applied cell sheet technology to fa-

bricate vascularized tissue constructs made of stacked cell sheet layers[66]. EC monoculture sheets were stacked with fibroblast monoculture sheets in multiple different configurations to study the effect of EC positioning within the tissue construct on vascularization. After 3 days in culture, *in vitro* vascular networks were formed within the cell sheet stacks, and these pre-vascularized constructs showed enhanced vasculogenesis upon implantation *in vivo*. Subsequent reports managed to control the alignment of endothelial networks through cell-cell interactions with surrounding focally oriented fibroblast sheets[67]. In another study, a thick (30 cell sheets, close to 1 mm thick) myocardial tissue stack with an interconnected, perfusable vascular network was fabricated using cell sheet technology in tandem with *in vivo* vascularization achieved by subcutaneous poly-surgery (up to 10 cycles) implantation into nude rats[68]. This approach may not be feasible for clinical translation as it would require the patient to undergo repetitive surgical procedures. A technique able to vascularize thick cell sheet stacks *in vitro* would negate the need for poly-surgery. Sakaguchi *et al*. proposed a strategy for thick cardiac tissue vascularization *in vitro* using cell sheet technology in combination with a perfusion bioreactor and microfluidics[4,69] (**Figure 7**). Stacks of cell sheets consisting of cardiac and ECs were layered on top of a collagen construct containing microchannels and cultured in a bioreactor. ECs within the cell sheets were seen migrating through the collagen ECM to form vascular networks which were connected to the pre-fabricated perfusable microchannels, thus allowing medium perfusion throughout the layered tissue construct. As more sheets were stacked on the layered construct (12 sheets, more than 100 μm in thickness), ECs continued to form new vessels and connect with pre-existing microvessels to form an interconnected vascular network. Using a similar method, Sekine *et al*. demonstrated in a study that stacked layers of cell sheets composed of neonatal rat cardiomyocytes and ECs improved cardiac function when implanted into infarcted rat hearts with increasing EC density, and showed higher capillary density and inosculation[70].

Overall, cell sheet technology offers a unique method for the vascularization of tissue constructs with distinct advantages. Firstly, the ECM material is deposited naturally by the cells themselves, thus negating the need to fabricate a biodegradable scaffold which may require the use of cytotoxic chemicals. Secondly, the high cell-density and homogeneous distribution achieved in a cell sheet leads to higher regenerative function[4], and the method of cell sheet harvesting

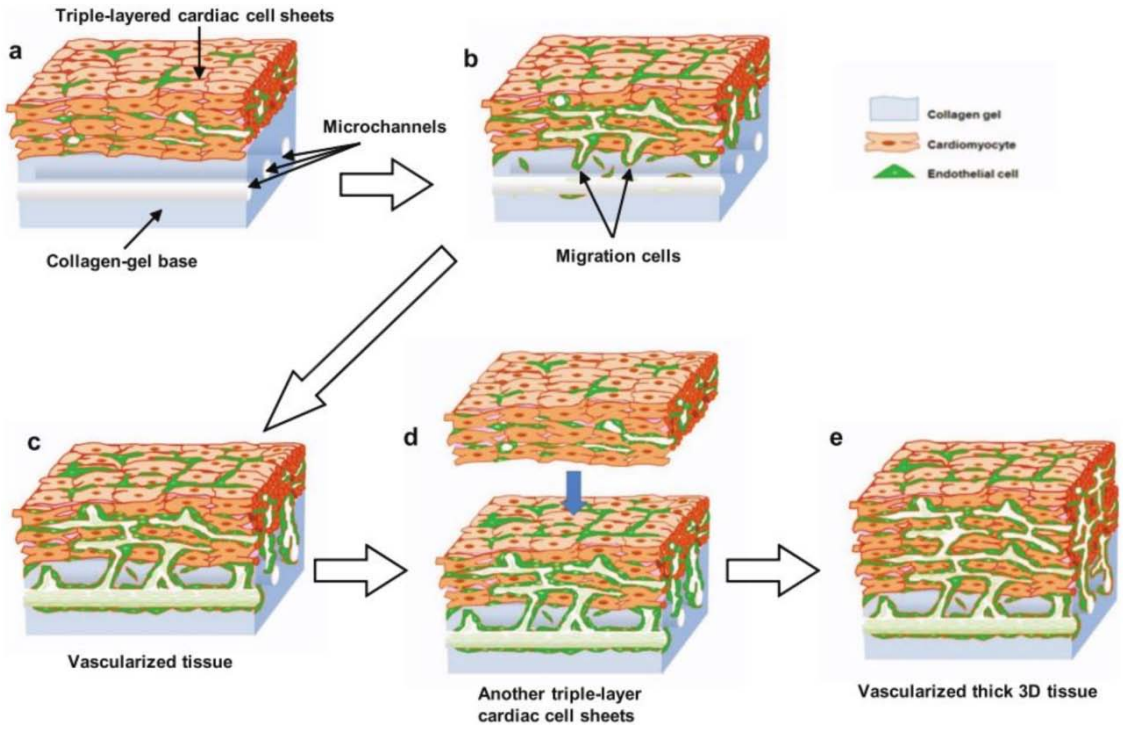

Figure 7. Cell sheet technology combined with a collagen based perfusion bioreactor for the preservation of cell viability by the vascularization of 3D tissues. (Adopted from Sakaguchi *et al*.[69])

Table 1. Characteristics possessed by each of the five techniques described

	Bioprinting	Microfluidics	Micropatterning	Wire molding	Cell-sheet
Vascularization of thick 3D tissue	✓			✓	✓
Control of tube dimensions	✓	✓	✓	✓	
Control of network architecture	✓		✓		
Perfusable networks	✓	✓		✓	✓
Multicellular vascularized tissue	✓	✓	✓	✓	✓
Suitability for *in vitro* models	✓	✓	✓	✓	
Tubulogenesis through self-assembly		✓	✓		✓
Ability for vascularized tissue to be harvested for downstream experiments	✓			✓	✓

and stacking only requires slight thermal treatment which does not significantly harm the cells. Thirdly, the ability to form thick layers of vascularized tissue and control over the orientation of vascular networks has been demonstrated using cell sheet technology.

4. Conclusion

In vitro vascularization techniques play a critical role in the advancement of tissue engineering. In the field of regenerative medicine, scientists have identified vascularization as a key hurdle that needs to be overcome. To date, the variety of tissue-engineered products successfully translated for clinical use has been limited to thin avascular tissue due to the inability of current technology to incorporate functional vascular networks into thick tissue constructs. The ability to fabricate physiologically accurate *in vitro* tissue models has also been hindered by the lack of effective *in vitro* vascularization techniques. Although 2D vascular models have been successfully fabricated and proven their efficacy, thick 3D vascular models remain elusive. Today, biologists and engineers are working hand in hand to develop working techniques for *in vitro* vascularization. We have described several enabling techniques being developed today which show promising signs of being able to achieve this goal. Each of these techniques has its own unique capabilities which make it particularly suitable for certain applications, such as for fabricating 3D perfusable networks within a tissue construct (bioprinting, cell sheet engineering), for controlled branching patterns and vessel diameter (micropatterning, wire molding), and for fabricating 2D *in vitro* vascular models (microfluidics, wire molding). **Table 1** shows a compiled checklist of characteristics possessed by the 5 techniques covered in this review. Admittedly, there are other approaches being applied to achieve *in vitro* vascularization such as electrospinning[71] and cell-accumulation[72] which were not covered in this review but also demonstrate potential for future development.

With the increasing flow of research into bioprinting technology, it is not surprising that the technology has experienced a rapid boost in development. Bioprinting technology now allows us to print multicellular constructs with high precision which mimics the hierarchal architecture of native tissue. It also possesses the ability to fabricate perfusable 3D microchannel networks within bulk tissue which is particularly useful in our efforts to achieve *in vitro* vascularization. Compared to other technologies like photolithography, bioprinting is young in terms of its development, thus it has the potential to be improved significantly and to find new applications in the years ahead. We believe that bioprinting represents the future of tissue engineering and could potentially evolve into becoming the gold-standard of biofabrication technology.

Conflict of Interest and Funding

No conflict of interest was reported by all authors. Y.Z. acknowledges the Tier-1 Academic Research Funds from the Singapore Ministry of Education (RGC 1/14), the A*STAR Industrial Robotics Programme (1225100007) and the SHS-NTU/017/2016.

References

1. U.S. Department of H ealth & Human Services, 2015, *Organ donation statistics*, viewed on October 2, 2016, <http://www.organdonor.gov/statistics-stories/statistics.html>
2. Langer R and Vacanti J P, 1993, Tissue engineering. *Science*, vol.260(5110): 920–926. http://doi.org/10.1126/science.8493529
3. Hüsing B, Bührlen B, Gaisser S, *et al*. 2003, Human tissue-engineered products: today's markets and future prospects. *Science and Technology*: 1–58.
4. Sakaguchi K, Shimizu T and Okano T, 2015, Construction of three-dimensional vascularized cardiac tissue with cell sheet engineering. *Journal of Controlled Release*, vol.205: 83–88. http://dx.doi.org/10.1016/j.jconrel.2014.12.016

5. Yeong W Y, Sudarmadji N, Yu H Y, *et al*. 2010, Porous polycaprolactone scaffold for cardiac tissue engineering fabricated by selective laser sintering. *Acta Biomaterialia*, vol.6(6): 2028–2034. http://dx.doi.org/10.1016/j.actbio.2009.12.033
6. Lee P J, Hung P J and Lee L P, 2007, An artificial liver sinusoid with a microfluidic endothelial-like barrier for primary hepatocyte culture. *Biotechnology and Bioengineering*, vol.97(5): 1340–1346. http://dx.doi.org/10.1002/bit.21360
7. Tonsomboon K and Oyen M L, 2013, Composite electrospun gelatin fiber-alginate gel scaffolds for mechanically robust tissue engineered cornea. *Journal of the Mechanical Behavior of Biomedical Materials*, vol.21: 185–194. http://dx.doi.org/10.1016/j.jmbbm.2013.03.001
8. Jungebluth P, Alici E, Baiguera S, *et al*. 2011, Tracheobronchial transplantation with a stem-cell-seeded bioartificial nanocomposite: a proof-of-concept study. *The Lancet*, vol.378(9808): 1997–2004. http://dx.doi.org/10.1016/S0140-6736(11)61715-7
9. Hasan A, Memic A, Annabi N, *et al*. 2014, Electrospun scaffolds for tissue engineering of v ascular grafts. *Acta Biomaterialia*, vol.10(1): 11–25. http://dx.doi.org/10.1016/j.actbio.2013.08.022
10. Atala A, Bauer S B, Soker S, *et al*. 2006, Tissue-engineered autologous bladders for patients needing cystoplasty. *Lancet*, vol.367(9518): 1241–1246. http://dx.doi.org/10.1016/S0140-6736(06)68438-9
11. Folkman J and Hochberg M, 1973, Self-regulation of growth in three dimensions. *The Journal of Experimental Medicine*, vol.138(4): 745–753. http://dx.doi.org/10.1084/jem.138.4.745
12. Rouwkema J, Rivron N C and van Blitterswijk C A, 2008, Vascularization in tissue engineering. *Trends in Biotechnology*, vol.26(8): 434–441. http://dx.doi.org/10.1016/j.tibtech.2008.04.009
13. Schmeichel K L and Bissell M J, 2010, Modeling tissue-specific signaling and organ function in three dimensions. *Journal of Cell Science*, vol.116(Pt 12): 2377–2388. http://dx.doi.org/10.1242/jcs.00503
14. Griffith L G and Swartz M A, 2006, Capturing complex 3D tissue physiology *in vitro*. *Nature Reviews: Molecular Cell Biology*, vol.7(3): 211–224. http://dx.doi.org/10.1038/nrm1858
15. Auger F A, Gibot L and Lacroix D, 2013, The pivotal role of vascularization in tissue engineering. *Annual Review of Biomedical Engineering*, vol.15: 177–200. http://dx.doi.org/10.1146/annurev-bioeng-071812-152428
16. Baranski J D, Chaturvedi R R, Stevens K R, *et al*. 2013, Geometric control of vascular networks to enhance engineered tissue integration and function. *Proceedings of the National Academy of Sciences of the United States of America*, vol.110(19): 7586–7591. http://dx.doi.org/10.1073/pnas.1217796110
17. Krewski D, Acosta Jr D, Andersen M, *et al*. 2010, Toxicity testing in the 21st century: a vision and a strategy. *Journal of Toxicology and Environmental Health. Part B: Critical Reviews*, vol.13(2–4), 51–138. http://dx.doi.org/10.1080/10937404.2010.483176
18. Elliott N T and Yuan F, 2011, A review of three-dimensional *in vitro* tissue models for drug discovery and transport studies. *Journal of Pharmaceutical Sciences*, vol.100: 59–74. http://dx.doi.org/10.1002/jps.22257
19. Naito H, Yoshimura M, Mizuno T, *et al*. 2013, The advantages of three-dimensional culture in a collagen hydrogel for stem cell differentiation. *Journal of Biomedical Materials Research. Part A*, vol.101(10): 2838–2845. http://dx.doi.org/10.1002/jbm.a.34578
20. Baker B M and Chen C S., 2012, Deconstructing the third dimension—how 3D culture microenvironments alter cellular cues. *Journal of Cell Science*, vol.125(13): 3015–3024. http://dx.doi.org/10.1242/jcs.079509
21. Soucy P A and Romer L H, 2009, Endothelial cell adhesion, signaling, and morphogenesis in fibroblast-derived matrix. *Matrix Biology*, vol.28(5): 273–283. http://dx.doi.org/10.1016/j.matbio.2009.04.005
22. Wang R, Xu J, Juliette L, *et al*. 2005, Three-dimensional co-culture models to study prostate cancer growth, progression, and metastasis to bone. *Seminars in Cancer Biology*, vol.15(5): 353–364. http://dx.doi.org/10.1016/j.semcancer.2005.05.005
23. Burke A S, MacMillan-Crow L A and Hinson J A, 2010, The hepatocyte suspension assay is superior to the cultured hepatocyte assay for determining mechanisms of acetaminophen hepatotoxicity relevant to *in vivo* toxicity. *Chemical Research in Toxicology*, vol.23(12): 1855–1858. http://dx.doi.org/10.1021/tx1003744
24. Mingoia R T, Nabb D L, Yang C-H, *et al*. 2007, Primary culture of rat hepatocytes in 96-well plates: effects of extracellular matrix configuration on cytochrome P450 enzyme activity and inducibility, and its application in *in vitro* cytotoxicity screening. *Toxicology in Vitro*, vol.21(1): 165–173. http://dx.doi.org/10.1016/j.tiv.2006.10.012
25. Zhang W, Wray L S, Rnjak-Kovacina J, *et al*. 2015, Vascularization of hollow channel-modified porous silk scaffolds with endothelial cells for tissue regeneration. *Biomaterials*, vol.56: 68–77. http://dx.doi.org/10.1016/j.biomaterials.2015.03.053
26. Mitchell G M and Morrison W A, 2014, *In vivo* vascularization for large-volume soft tissue-engineering. *Vascularization—Regenerative Medicine and Tissue Engineering*: 343–362. http://dx.doi.org/10.1201/b16777-23
27. Dababneh A B and Ozbolat I T, 2014, Bioprinting technology: a current state-of-the-art review. *Journal of Manufacturing Science and Engineering*, vol.136(6): 61016. http://dx.doi.org/10.1115/1.4028512

28. Hinton T J, Jallerat Q, Palchesko R N, *et al*. 2015, Three-dimensional printing of complex biological structures by freeform reversible embedding of suspended hydrogels. *Science Advances*, vol.1(9): e1500758. http://dx.doi.org/10.1126/sciadv.1500758
29. Schuurman W, Khristov V, Pot M W, *et al*. 2011, Bioprinting of hybrid tissue constructs with tailorable mechanical properties. *Biofabrication*, vol.3(2): 21001. http://dx.doi.org/10.1088/1758-5082/3/2/021001
30. Norotte C, Marga F S, Niklason L E, *et al*. 2009, Scaffold-free vascular tissue engineering using bioprinting. *Biomaterials*, vol.30(30): 5910–5917. http://dx.doi.org/10.1016/j.biomaterials.2009.06.034
31. Tan Y, Richards D J, Trusk T C, *et al*. 2014, 3D printing facilitated scaffold-free tissue unit fabrication. *Biofabrication*, vol.6(2): 24111. http://dx.doi.org/10.1088/1758-5082/6/2/024111
32. Miller J S, Stevens K R, Yang M T, *et al*. 2012, Rapid casting of patterned vascular networks for perfusable engineered three-dimensional tissues. *Nature Materials*, vol.11(9): 768–774. http://dx.doi.org/10.1038/nmat3357
33. Ovsianikov A, Gruene M, Pflaum M, *et al*. 2010, Laser printing of cells into 3D scaffolds. *Biofabrication*, vol.2(1): 14104. http://dx.doi.org/10.1088/1758-5082/2/1/014104
34. Ringeisen B R, Othon C M, Barron J A, *et al*. 2006, Jet-based methods to print living cells. *Biotechnology Journal*, vol.1(9): 930–948. http://dx.doi.org/10.1002/biot.200600058
35. Lin H, Zhang D, Alexander P G, *et al*. 2013, Application of visible light-based projection stereolithography for live cell-scaffold fabrication with designed architecture. *Biomaterials*, vol.34(2): 331–339. http://dx.doi.org/10.1016/j.biomaterials.2012.09.048
36. Chan V, Zorlutuna P, Jeong J H, *et al*. 2010, Three-dimensional photopatterning of hydrogels using stereolithography for long-term cell encapsulation. *Lab on a Chip*, vol.10(16): 2062–2070. http://dx.doi.org/10.1039/c004285d
37. Kolesky D B, Truby R L, Gladman A S, *et al*. 2014, 3D bioprinting of vascularized, heterogeneous cell-laden tissue constructs. *Advanced Materials*, vol.26(19): 3124–3130. http://dx.doi.org/10.1002/adma.201305506
38. Jia W, Gungor-Ozkerim P S, Zhang Y S, *et al*. 2016, Direct 3D bioprinting of perfusable vascular constructs using a blend bioink. *Biomaterials*, vol.106: 58–68. http://dx.doi.org/10.1016/j.biomaterials.2016.07.038
39. Bertassoni L E, Cecconi M, Manoharan V, *et al*. 2014, Hydrogel bioprinted microchannel networks for vascularization of tissue engineering constructs. *Lab on a Chip*, vol.14(13): 2202–2211. http://dx.doi.org/10.1039/c4lc00030g
40. Van Der Meer A D, Poot A A, Duits M H G, *et al*. 2009, Microfluidic technology in vascular research. *Journal of Biomedicine and Biotechnology*, vol.2009: 823148. http://dx.doi.org/10.1155/2009/823148
41. Zheng Y, Chen J, Craven M, *et al*. 2012, *In vitro* microvessels for the study of angiogenesis and thrombosis. *Proceedings of the National Academy of Sciences of the United States of America*, vol.109(24): 9342–9347. http://dx.doi.org/10.1073/pnas.1201240109
42. Tocchio A, Tamplenizza M, Martello F, *et al*. 2015, Versatile fabrication of vascularizable scaffolds for large tissue engineering in bioreactor. *Biomaterials*, vol.45: 124–131. http://dx.doi.org/10.1016/j.biomaterials.2014.12.031
43. Song J W, Bazou D and Munn L L, 2012, Anastomosis of endothelial sprouts forms new vessels in a tissue analogue of angiogenesis. *Integrative Biology,* vol.4(8): 857–862. http://dx.doi.org/10.1039/c2ib20061a
44. Kim S, Lee H, Chung M, *et al*. 2013, Engineering of functional, perfusable 3D microvascular networks on a chip. *Lab on a Chip*, vol.13: 1489–1500. http://dx.doi/org/10.1039/c3lc41320a
45. Moya M L, Hsu Y-H, Lee A P, *et al*. 2013, *In vitro* perfused human capillary networks. *Tissue Engineering Part C: Methods*, vol.19(9): 730–737. http://dx.doi.org/10.1089/ten.TEC.2012.0430
46. Chiu L L Y, Montgomery M, Liang Y, *et al*. 2012, Perfusable branching microvessel bed for vascularization of engineered tissues. *Proceedings of the National Academy of Sciences of the United States of America*, vol.109(50): E3414–3423. http://dx.doi.org/10.1073/pnas.1210580109
47. Yeon J H, Ryu H R, Chung M, *et al*. 2012, *In vitro* formation and characterization of a perfusable three-dimensional tubular capillary network in microfluidic devices. *Lab on a Chip*, vol.12(16): 2815. http://dx.doi.org/10.1039/c2lc40131b
48. Jakab K, Norotte C, Marga F, *et al*. 2010, Tissue engineering by self-assembly and bio-printing of living cells. *Biofabrication*, vol.2(2): 22001. http://dx.doi.org/10.1088/1758-5082/2/2/022001
49. Dickinson L E, Moura M E and Gerecht S, 2010, Guiding endothelial progenitor cell tube formation using patterned fibronectin surfaces. *Soft Matter*, vol.6(20): 5109. http://dx.doi.org/10.1039/C0SM00233J
50. Raghavan S, Nelson C M, Baranski J D, *et al*. 2010, Geometrically controlled endothelial tubulogenesis in micropatterned gels. *Tissue Engineering. Part A*, vol.16(7): 2255–2263. http://dx.doi.org/10.1089/ten.TEA.2009.0584
51. Chaturvedi R R, Stevens K R, Solorzano R D, *et al*. 2015, Patterning vascular networks *in vivo* for tissue engineering applications. *Tissue Engineering Part C: Methods*, vol.21(5): 509–517. http://dx.doi.org/10.1089/ten.TEC.2014.0258
52. Aubin H, Nichol J W, Hutson C B, *et al*. 2010, Directed

3D cell alignment and elongation in microengineered hydrogels. *Biomaterials*, vol.31(27): 6941–6951. http://dx.doi.org/10.1016/j.biomaterials.2010.05.056

53. Nikkhah M, Eshak N, Zorlutuna P, *et al*. 2012, Directed endothelial cell morphogenesis in micropatterned gelatin methacrylate hydrogels. *Biomaterials*, vol.33(35): 9009–018. http://dx.doi.org/10.1016/j.biomaterials.2012.08.068
54. van der Meer A D, Orlova V V, ten Dijke P, *et al*. 2013, Three-dimensional co-cultures of human endothelial cells and embryonic stem cell-derived pericytes inside a microfluidic device. *Lab on a Chip*, vol.13(18): 3562–3568. http://dx.doi.org/10.1039/c3lc50435b
55. Leslie-Barbick J E, Shen C, Chen C, *et al*. 2011, Micron-scale spatially patterned, covalently immobilized vascular endothelial growth factor on hydrogels accelerates endothelial tubulogenesis and increases cellular angiogenic responses. *Tissue Engineering. Part A*, vol.17(1–2): 221–229. http://dx.doi.org/10.1089/ten.TEA.2010.0202
56. Nichol J W, Koshy S T, Bae H, *et al*. 2010, Cell-laden microengineered gelatin methacrylate hydrogels. *Biomaterials*, vol.31(21): 5536–5544. http://dx.doi.org/10.1016/j.biomaterials.2010.03.064
57. Park J H, Chung B G, Lee W G, *et al*. 2010, Microporous cell-laden hydrogels for engineered tissue constructs. *Biotechnology and Bioengineering*, vol.106(1): 138–148. http://dx.doi.org/10.1002/bit.22667
58. Yao L, de Ruiter G C W, Wang H, *et al*. 2010, Controlling dispersion of axonal regeneration using a multichannel collagen nerve conduit. *Biomaterials*, vol.31(22): 5789–5797. http://dx.doi.org/10.1016/j.biomaterials.2010.03.081
59. Chrobak K M, Potter D R and Tien J, 2006, Formation of perfused, functional microvascular tubes *in vitro*. *Microvascular Research*, vol.71(3): 185–196. http://dx.doi.org/10.1016/j.mvr.2006.02.005
60. Sadr N, Zhu M, Osaki T, *et al*. 2011, SAM-based cell transfer to photopatterned hydrogels for microengineering vascular-like structures. *Biomaterials*, vol. 32(30): 7479–7490. http://dx.doi.org/10.1016/j.biomaterials.2011.06.034
61. Yoshida H, Matsusaki M and Akashi M, 2013, Multilayered blood capillary analogs in biodegradable hydrogels for *in vitro* drug permeability assays. *Advanced Functional Materials*, vol.23(14): 1736–1742. http://dx.doi.org/10.1002/adfm.201370069
62. Price G M, Wong K H K, Truslow J G, *et al*. 2010, Effect of mechanical factors on the function of engineered human blood microvessels in microfluidic collagen gels. *Biomaterials*, vol.31(24): 6182–6189. http://dx.doi.org/10.1016/j.biomaterials.2010.04.041
63. Nishida K, Yamato M, Hayashida Y, *et al*. 2004, Functional bioengineered corneal epithelial sheet grafts from corneal stem cells expanded *ex vivo* on a temperature-responsive cell culture surface. *Transplantation*, vol.77(3): 379–385. http://dx.doi.org/10.1097/01.TP.0000110320.45678.30
64. Yamato M, Utsumi M, Kushida A, *et al*. 2001, Thermo-responsive culture dishes allow the intact harvest of multilayered keratinocyte sheets without dispase by reducing temperature. *Tissue Engineering*, vol.7(4): 473–480. http://dx.doi.org/10.1089/10763270152436517
65. Shimizu T, Yamato M, Kikuchi A, *et al*. 2003, Cell sheet engineering for myocardial tissue reconstruction. *Biomaterials*, vol.24(13): 2309–2316. http://dx.doi.org/10.1016/S0142-9612(03)00110-8
66. Asakawa N, Shimizu T, Tsuda Y, *et al*. 2010, Pre-vascularization of *in vitro* three-dimensional tissues created by cell sheet engineering. *Biomaterials*, vol.31(14): 3903–3909. http://dx.doi.org/10.1016/j.biomaterials.2010.01.105
67. Muraoka M, Shimizu T, Itoga K, *et al*. 2013, Control of the formation of vascular networks in 3D tissue engineered constructs. *Biomaterials*, vol.34(3): 696–703. http://dx.doi.org/10.1016/j.biomaterials.2012.10.009
68. Shimizu T, Sekine H, Yang J, *et al*. 2006, Polysurgery of cell sheet grafts overcomes diffusion limits to produce thick, vascularized myocardial tissues. *The FASEB Journal*, vol.20(6): 1–20. http://dx.doi.org/10.1096/fj.05-4715fje
69. Sakaguchi K, Shimizu T, Horaguchi S, *et al*. 2013, *In vitro* engineering of vascularized tissue surrogates. *Scientific Reports*, vol.3: 1316. http://dx.doi.org/10.1038/srep01316
70. Sekine H, Shimizu T, Hobo K, *et al*. 2008, Endothelial cell coculture within tissue-engineered cardiomyocyte sheets enhances neovascularization and improves cardiac function of ischemic hearts. *Circulation*, vol.118(14 Suppl): 145–153. http://dx.doi.org/10.1161/CIRCULATIONAHA.107.757286
71. Wong H K, Ivan Lam C R, Wen F, *et al*. 2016, Novel method to improve vascularization of tissue engineered constructs with biodegradable fibers. *Biofabrication*, vol.8(1): 15004. http://dx.doi.org/10.1088/1758-5090/8/1/015004
72. Nishiguchi A, Yoshida H, Matsusaki M, *et al*. 2011, Rapid construction of three-dimensional multilayered tissues with endothelial tube networks by the cell-accumulation technique. *Advanced Materials*, vol.23(31): 3506–3510. http://dx.doi.org/10.1002/adma.201101787

REVIEW ARTICLE

Digital biomanufacturing supporting vascularization in 3D bioprinting

William Whitford[1*] and James B. Hoying[2]

[1] BioProcess, GE Healthcare Life Sciences, 925 West 1800 South, Logan, UT 84321, USA

[2] Advanced Solutions Life Sciences, 1901 Nelson Miller Parkway, Louisville, KY 40223, USA

Abstract: Synergies in bioprinting are appearing from individual researchers focusing on divergent aspects of the technology. Many are now evolving from simple mono-dimensional operations to model-controlled multi-material, interpenetrating networks using multi-modal deposition techniques. Bioinks are being designed to address numerous critical process parameters. Both the cellular constructs and architectural design for the necessary vascular component in digitally biomanufactured tissue constructs are being addressed. Advances are occurring from the topology of the circuits to the source of the of the biological microvessel components. Instruments monitoring and control of these activates are becoming interconnected. More and higher quality data are being collected and analysis is becoming richer. Information management and model generation is now describing a "process network." This is promising; more efficient use of both locally and imported raw data supporting accelerated strategic as well as tactical decision making. This allows real time optimization of the immediate bioprinting bioprocess based on such high value criteria as instantaneous progress assessment and comparison to previous activities. Finally, operations up- and down-stream of the deposition are being included in a supervisory enterprise control.

Keywords: digital, biomanufacturing, bioprinting, vasculogenesis, microvasculatures, bioinks

*Correspondence to: William Whitford, BioProcess, GE Healthcare Life Sciences, 925 West 1800 South, Logan, UT 84321, USA; Email: bill.whitford@ge.com

Received: November 15, 2016; **Accepted:** November 30, 2016; **Published Online:** January 25, 2017

Citation: Whitford W and Hoying J B, 2017, Digital biomanufacturing supporting vascularization in 3D bioprinting. *International Journal of Bioprinting*, vol.3(1): 18–26. http://dx.doi.org/10.18063/IJB.2017.01.002.

1. Introduction

1.1 Digital Manufacturing

Digital manufacturing promises to increase productivity and robustness in existing processes and facilities, as well as enable the efficient development of difficult, previously unmanageable products or processes[1,2]. It relies upon the comprehensive and real-time controlled interfacing of human and machine sourced information through a centralized system. More than SCADA (supervisory control and data acquisition), it is an embedded interconnection of real-time access to divergent sources of information, and a provider of deep analysis, predictions and process control. Digital manufacturing is a resident and on-line source for continuous optimization of process performance, based on both information available from current operations as well as from previous batches (or time windows). For example, GE's application of the Predix™ cloud-based platform enables powerful handling of rich-data to better support advanced manufacturing platforms (www.ge.com/digital/predix).

2. Digital Biomanufacturing

Digital biomanufacturing is similarly seen as promoting improvements in the manufacturing of biologicals through such initiatives as computer aided design,

Digital biomanufacturing supporting vascularization in 3D bioprinting © 2017 William Whitford and James B. Hoying. This is an Open Access article distributed under the terms of the Creative Commons Attribution-NonCommercial 4.0 International License (http://creativecommons.org/licenses/by-nc/4.0/), permitting all non-commercial use, distribution, and reproduction in any medium, provided the original work is properly cited.

enterprise control, and verification[3,4]. Digital biomanufacturing (DB) is part of an evolution, one further step in the application of *Industrial Internet of Things* (IIoT). It refers to instruments becoming interconnected, but more than that — it denotes high levels of data analysis, information management and process control being implemented into a "process network". DB promises such value as real-time optimization of the manufacturing process based on such highly valuable criteria as projected product quality and batch profitability.

2.1 Terminology

It is desirable to use a distinct term here to distinguish it because, as in the terms *bioproduction and biopharmacology*, DB addresses the many unique aspects of biologically-based activities. For example, the term digital biomanufacturing may be used to describe the advanced manufacturing practices of many biopharmaceutical entities or vaccines. It is not to be confused with direct digital biomanufacturing processes, such as employed in, e.g., some synthetic biology and 3D bioprinting applications[5]. 3-dimensional bioprinting (3DBP) can therefore be conceived of as one implementation of direct digital biomanufacturing or additive biomanufacturing. 3DBP and bioplotting are also now employing other elements of DB. One example of this is software to support the management of imported digital analytics and imaging files, as well as programs to design, visualize, simulate, and analyze 3D computer models of printed structures[6]. Others include the emerging applications of distributed, closed loop and supervisory control technology to bioprinting. As 3DBP operations move towards the promise of therapeutic applications, these factors will enable more efficient, reproducible and self-adaptive processes.

2.2 Bioinks

As fluids are deposited during 3DBP, the composition of bioinks are very important to the outcome of the printing[7,8]. Precise and universal definitions of most terms in biomedical applications of additive manufacturing are rare[9]. Generally, the term "bioink" refers to a fluid containing living cells (or cell assemblies) and many low and high molecular weight components to be employed in 3DBP. However, there are other usages — some refer to cell-free fluids as a type of bioink. For example, bioinks deposited for ancillary buttressing of the primary product (support bioinks), fluids to be removed after leaving a void (sacrificial or fugitive bioinks) and even cell-free matrix solutions intended to be immediately populated with cells post-printing (printed scaffold bioinks). Also, there are printing technologies that either employ optimized de-cellularized natural matrices[10,11], print into polymerization-initiation chemical baths (direct-writing)[12] or whose cell-laden bioinks do not require a scaffold component at all[13].

2.3 Supported Printing Parameters

Therefore, depending upon the specific reference, a bioink must variously support the mechanical and chemical aspects of the particular printing technology(s) employed, structure of the printed assembly, health of the particular cell types employed and post-printing functions[14]. Their specific design and formulation is becoming even more important as the industry is adopting such advances as multi-component bioinks in multi-step 3D printing process and anisotropic matrices[15]. Currently, researchers and printed construct sponsors in 3DBP must develop their own inks. Until quite recently, all the structural material components of bioinks were adopted from other applications. However, some characterized products and bioprinting qualified materials are now becoming commercially available[16,17]. The cell-culture components have been supplied by commercialized culture media formulations and most-often include serum. As applications mature, demand is growing for optimized, serum-free bioinks, and 3DBP-related cell culture media, of consistent quality manufactured in regulated facilities.

2.4 Tunable Fluid Characteristics

Bioinks must provide many distinct features that can be considered as elements of tunable solutions enabling a digital biomanufacturing technology. In 3DBP, this is accomplished by (i) specifically supporting a particular printing technology; (ii) providing a matrix, scaffold or extra-cellular matrix (ECM) for the immediate structural integrity of the printed construct; (iii) supporting the immediate stable culture and robust performance of the living cells within the printed construct (e.g., nutrition, factor and mass-transfer); (iv) enabling required scaffold assembly or polymerization; (v) supporting post-printing cell-attachment, migration or phenotypic progression; (vi) accommodating any required subsequent matrix remodeling, interaction or absorption; and (vii) pro-

viding any product application-specific quality, regulatory or functional requirements.

2.5 Printing Technology

Many technologies supporting digital biomanufacturing are in use today. Chief among them for 3DBP are the laser-assisted, ink-jet, and extrusion (or micro-extrusion) approaches[8]. However, there are other, very creative approaches being explored such as magnetic-based techniques[18]. While there are many overall similarities with these processes, there are some very distinct chemical or mechanical requirements to the bioinks for each. One distinction can be in required physico-mechanical characteristics of the solution — such as its surface tension, conductivity, viscosity, flow characteristics, and any non-Newtonian behavior. Other distinctions pertain to the biologicals, such as consequences of the technique-specific printing pressures, shear or fluid volumes, required cell concentrations, and biocompatibility. A bioink must support both the mechanical and biological requirements of the printing approach adopted.

2.6 Matrix, Scaffold or ECM

Beyond the rheological requirements for the ink in the printing process itself, the post-printing structural characteristics of the bioink are an important aspect of 3DBP. As can be seen from **Table 1**, many HMW natural and synthetic polymers are employed in 3DBP. Each has unique physical, chemical, and biological properties. Furthermore, the means of controlling their state or and stiffness can have effects on other characteristics of the bioink. The first criteria for such thickening agents or structural elements are that they be "biocompatible". However, this term has different connotations depending upon the application. Characteristics included in various concepts of the term include lack of immunoactivity, cellular toxicity, cell lineage differentiation activity, apoptosis induction, up-or down gene regulation/induction and more. Through the application of cross-linking reagents, light, heat or modulation of supramolecular chemistry, active aspects of a bioink — the viscosity, strength, stiffness, visco-elastic plastic, surface and other characteristics imparted by many matrix components — can be varied. Just what is included in the concept of biocompatibility depends a lot upon the type of cells employed and the final application of the construct. Neither innate nor adaptive immune system activity may be very important in a printed construct to be employed in an *in vitro* assay. On the other hand, a printed construct that will be matured by a process including immediate removal/exchange of the printed support matrix post-printing may not require much attention to a minor cytotoxicity in the ink. The means of polymerizing the matrix monomer can be significant. These ranges from temperature; to UV, blue or green light; to chemical activators and their effect must be thoroughly examined.

Table 1. Lists of common bioink and 3DBP culture media component ingredients[7,19,20]

Structural matrix elements	Cell culture elements
Agarose	Animal sera
Alginate	Sera fractions
Carrageenan	Hydrolysates
Cellulose	Cell and tissue extracts
Chitosan	Amino acids, nucleotides
Collagen	(poly) peptides
Chondroitin Sulfate	Defined proteins
Decellularized ECM[1]	Non-protein nitrogens
Dextran	Sugars, carbohydrates
Elastin	Sterol and acyl lipids
Fibrin	A, B, C, and E Vitamins
Gelatin	Enzyme activities
Gellan Gum	Metals (trace elements)
HAMA[2]	Cytokines, factors
Matrigel	Peptide hormones
Methacrylated CS[3]	Steroid hormones
Methylcellulose	Transport agents
PPF[4]	Detoxifying agents
PHEM[5]	Antiapoptotics
PEGDA[6]	Protease inhibitors
PEG / PEO[7]	Shear-force reducers
PGLCS[8], PVA[9], Pluronics	Antibiotics
PLA[10], PGLRA[11], PGLYA[12]	Antimycotics
Polyacrylamide	Acid/base/buffers
Polycaprolactone	Antibiotics
Silk fibroin	Shear protectants
HMW structures of above	Viscosity enhancers

1. ECM: Extra cellular matrix
2. HAMA: Hyaluronic acid methacrylate
3. CS: Chondroitin Sulfate
4. PPF: Polypropylene fumarate
5. PHEM: Polyhydroxyethylmethacrylate
6. PEGDA: Polyethylene glycol diacrylate
7. PEG/PEO: Polyethylene glycol/oxide
8. PGLCS: Polyglycerol sebacate
9. PVA: Polyvinyl alcohol
10. PLA: Polylactic acid
11. PGLRA: Polyglycerolic acid
12. PGLYA: Polyglycolic acid

3. Accommodating Newest Approaches

Newer methods being promoted today include the use of hybrid multicomponent bioinks, deposited in a multi-step and even multi-mode 3D printing process. This will obviously demand a higher level of process monitoring, equipment integration, and process control. Co-deposition of two or more bioink streams can integrate desirable physical properties from each constituent component and exhibit complex phase behavior[15]. It is notable that both the effect of the matrix upon a cell type or implantation environment as well as the inclusion of high complements of cells upon the properties of the gel or matrix itself must be considered. Surprisingly, the exact nature of the reticulation of many matrix monomers (actually homo- or hetero-oligomeric complexes), as well the matrices' effects upon the biological nature of the printed construct, are only becoming understood. For example, the "functionalization" of substrate components, including the introduction of soluble cell-binding inducers to matrix components has demonstrated enhanced cell adhesion and spreading[17]. Peptide gels with simple composition and tunable physical properties have been developed to facilitate targeted differentiation[21]. Post printing perfusion with growth or differentiation factors can drive multipotent cells to a desired lineage[22]. Immediate nutrient mass-transport has been facilitated by both anisotropic matrix environments guiding cellular alignment and microchannel architectures as well as the engineering of inherently high isotropic matrix porosity[23]. Finally, issues have arisen in the application of even elegantly designed approaches — such as the observation of an inverse relationship between printed cell density and robust functionality in immediate scaffold development. Generally, therefore, each application must be studied on its own.

3.1 Cultured Cell-support

When cells are included in a printing operation, maintenance of their viability and state must be considered. Suspensions of robust eukaryotic cells can survive for short periods of time in poorly controlled environments in simple buffered salt solutions. However, for optimized performance and in extended pre- or post-printing incubations, many of the common ingredients of modern cell culture media must be supplied either within the bioink formulation, or made available immediately post printing. Thus, while there are mechanical properties to be considered (such as in protecting from shear-stress and/or establishing cellular orientation) in cell-support, the biomolecular characteristics are also important.

3.2 Maintaining Robust Viability

All printing processes involve an ink being formulated, stored for significantly variable periods of time before or during the printing process, pumped through a nozzle or applied to a dispensing or culture plate, and followed by the actual integration into the progressing construct. There, the cells remain in the media, buffer or bioink until at least the remainder of the construct is completed. From that point onwards, the ambient environment of cells in the nascent construct may or may not be altered during a post-printing "maturation". Throughout these stages the cell needs must be supported, and any of these activities can affect the cells viability, differentiation, adhesion, state, functionality and up-or down regulation such as specifically inducing apoptosis.

4. Major Considerations

When cells are included in a printing operation, maintenance of their viability and state of health must be considered. Suspensions of robust eukaryotic cells can survive for short periods of time in poorly controlled environments in simple buffered salt solutions. However, for optimized performance, especially over extended print periods including pre- or post- printing staging operations, many factors must be considered (**Table 2**).

4.1 Biomolecular Characteristics

First, while there are mechanical properties to be considered in cell-support (such as protecting from shear-stress and/or establishing cellular orientation), the biomolecular characteristics are also important. Many of the common ingredients of modern cell culture media must be supplied either within the bioink formulation, or made available immediately post printing. Furthermore, most nascent constructs may be altered during a post-printing "maturation" operation. Characteristics of the cells ambient fluid media throughout this are important.

4.2 Environmental Parameters

Second, depending upon the cells, bioink formulation and printing style, it can be critical to control environmental parameters during these steps. These can

Table 2. Considerations in the development of a bioink and 3DBP culture media

- Cell-specific metabolites/factors
- Printing-specific rheology values
- Application-specific matrix elements
- Specifically control or inhibit apoptosis
- Support or inhibit further differentiation
- Co-culturing and tissue environment effects
- Address altered cell metabolism rates and flux
  - Existing media formulations are optimized for
    - rapidly dividing cultures
    - low-density culture
  - There may be complex gradients
    - moving from culture expansion to printing
    - moving from 3D culture to *in vivo* placement
- Material sourcing, qualification, QA and regulatory
- Unique matrix and matrix-active component effects
  - ECM / glycans / saccharides / polyesters / poloxamers
  - Supramolecular chemistry support / control
  - Spontaneous intra- and inter-molecular self-assembly
    - Concentration, ion types, pH
  - Involve multiple linkage types
    - hydrophobic, SS/disulfide bridge
    - Can be assisted
    - Hofmeister series
  - Can be inhibited
    - HAPs DTT, carbonate
    - Must be protected
    - bonds are reversible
  - Reported factor sequestration/binding
- Active and passive rheology effects
  - Additives modulating osmolality and density
  - Additives modulating viscosity and surface tension
  - Deposition in plastic flow, rapid elastic response
  - Consequences of flow rates, nozzle size and hydrodynamic forces
- Print matrix-specific stresses
  - Unusual light, temperatures and pressures
  - Unusual gelling agents, polymerizers, crosslinkers
- Serum-free, xeno-free and protein-free ideal
  - Can consider FBS and animal protein-based formula
  - Regulatory, risk, cost and consistency considerations
- Heightened buffering/antioxidant demands
  - Variable mass-transfer rates & environment
  - Often at high air interface-to-medium ratios
- High plastic mass-to-medium volume ratio
  - Sorption of lipophilic vitamins/lipids/sterols
  - Heightened leachable and particulates concerns

also affect the cell's viability, differentiation, adhesion, state, functionality and up- or down-gene regulation. One way of providing some degree of environmental control is in specifically engineered dedicated housing immediately surrounding the printer (Advanced Solutions, www.advancedsolutionsonline.com). Another approach is to house the entire printing assembly inside a modular isolator that actively controls such environmental parameters as temperature, CO_2 and humidity. Such equipment also prevents contamination from both exogenous microbes and aerosols generated during the printing process. Randy Yerden, CEO, BioSpherix (www.biospherix.com) recently observed, "Modern cytocentric isolators can aseptically and safely accommodate bioprinters of any dimension, as well as ancillary equipment — plus control critical cell parameters at optimum CO_2 and O_2 levels during printing".

4.3 Many Cellular Requirements

Bioinks may be required to support (for various durations) the stable culture of stem cells, co-culture of diverse differentiated cells, vasculogenesis or other cellular or tissue functions. The cellular requirements can include primary metabolites/factors optimized to the cell populations being printed or unique requirements due to the nature of the (pre- and post-) printing environment. In some applications, a formulation may be required to support 3D high-density culture in a specialized environment achieved post-printing. This includes post-deposition matrix crosslinking or polymerization forces or chemistries. The type and level of cell growth, attachment and other culture factors may be adjusted to accommodate the different demands or function placed upon the cells post-printing, or due to the factor-sequestration by some printing matrices. An increased or different buffering pH chemistry may be required due to the pre- and intra-printing ambient gas mixture. Accommodation of such printing-specific stresses as hydrodynamic or dehydration forces are especially important as the process progresses from the common product development-supporting serum-containing media to a more regulatory-friendly serum-free formulation. As the types of stresses induced by the printing process are known to induce apoptosis or differentiation in some process cell complements, ingredients known to inhibit these undesired responses may be included. As the concept of 4D bioprinting progresses, formulations to either promote or inhibit post-printing differentiation will likely be more strongly considered. Finally, due to the nature of the disposable bioink storage and print-

ing materials, accommodating (or ameliorating) heightened leachables contamination as well as sorption of lipophilic vitamins or lipids may be considered.

4.4 Application-specific Factors

Depending upon the application, a number of additional manufacturing aspects may need to be considered. For tissues, tissue-mimics or other structures related to either cell and tissue therapies or in IVD applications, the quality and regulatory implications of the bioink must be examined, as has been begun for printed medical devices[24]. For these applications especially, the nature and number of particulates from the disposable components of the printing path could be significant. The composition of biopapers, or a matrix upon which the ink is applied during printing, is another consideration in some applications. An interesting new development for applications employing human pluripotent stem cells is the announcement by GE Healthcare that a serum-derived protein supplement in a completely defined, xeno-free medium can support stable culture of human pluripotent stem cells on untreated matrix[25].

4.5 Vascularization

The importance of including a vascular component in digitally biomanufactured tissue constructs as both a means to provide perfusion to a tissue and impart relevant functionality (as the vasculature also contributes to tissue function) is well appreciated. The ability to establish and maintain a functional microcirculation *in vitro* significantly impacts a broad array of biomedical arenas[21,22]. In virtually every discussion concerning the building of tissue replacements, the critical importance of having a microvasculature integrated into the tissue construct is stressed[23–25]. In cellular assay platforms, the presence of a perfused vasculature in combination with the target parenchyma cell is considered to improve the utility of the assay beyond having just parenchyma cells[26]. Significantly, the smaller elements of the vasculature, the microvasculature, pose unique challenges in a biomanufacturing process. A stereotypical microvessel is comprised of multiple cell types (endothelial cells, smooth muscle/contractile cells, perivascular mesenchymal cells, and immune cells) assembled in a very structured way critical to the microvessel's function[26]. In addition, many individual microvessels are needed (perhaps thousands in some applications) to assemble and effective perfusion circuit. Finally, the organization or topology of the microvessels in the perfusion network impacts overall performance[27]. Thus, the incorporation of a vascular supply into a manufactured tissue construct must address the formation of each of the numerous, complex individual microvessels and their integration into a perfusion circuit[28] matched to the needs of the tissue parenchyma.

4.6 Angiogenesis and Vasculogenesis

New microvessels arise from either angiogenic sprouts of existing, parent microvessels or the *de novo* assembly of vascular cells into the microvessels called vasculogenesis[27]. A variety of cell types and strategies have been employed to derive microvessels. These include the use of endothelial cells, both macrovascular and microvascular, endothelial progenitor cells (EPCs), perivascular cell precursors, mesenchymal and hematopoietic stem cells (MSCs and HSCs), and smooth muscle cells incorporated into the construct either alone or in combination. Adipose stromal vascular fraction (SVF) cells show particularly robust vasculogenic activity, perhaps because all of the cell types necessary to forming microvasculatures are present within the isolate[20,29]. Angiogenesis-based strategies include pre-packaging endothelial cells in clusters or aggregates, from which neovessels sprout[30], or the use of intact microvessel fragments as a source of parent microvessels from which neovessels arise via angiogenesis[28].

4.7 Post Printing Cues

In all cases, the newly formed microvessels (or neovessels) are immature in form and function, requiring hemodynamic cues to drive subsequent maturation[31]. This vascular maturation, of both the individual neovessels and network, depends on substantial remodeling and adaptation activities, as the neovessels specify into arterioles, capillaries, and venules and integrate into a contiguous network. Therefore, consideration of bioinks amenable to successful fabrication of vasculatures in a digital biomanufacturing process should support not only vascular cell viability, but also promote individual neovessel assembly and permit adaptation to a mature microvasculature.

5. Vascular Compatible Bioinks

Nearly all the bioinks used with non-vascular cells will also support vascular cells. Furthermore, leveraging the potent self-assembly capabilities intrinsic to vascular cells, these bioinks readily enable formation

of neovessels, whether by angiogenesis or vasculogenesis. This is true of those materials in which vascular cells are incorporated at the time of fabrication (i.e., a hydrogel) or rigid scaffolds that are made and subsequently seeded with vascular cells or vascular elements[32,33]. Moreover, many of the native matrices used as bioinks have intrinsic pro-angiogenic activity such as tumor matrix and hyaluronic acid gels[34,35]. Of course, many strategies have doped bioinks with angiogenic factors either to drive vasculogenesis/angiogenesis from embedded vascular precursors and/or recruit vessel ingrowth into the construct via angiogenesis. The different materials used promote vascular adaptation to different degrees with softer, native matrices being the most favored. Rigid scaffolds do support vascular adaptation, however, this relies on the spaces between the rigid elements, where the neovessels reside, being filled with a softer material.

5.1 Synthetic Channels

An alternate approach to incorporating a perfusion supply involves creating channels through a matrix within which vascular cells (usually endothelial cells) are seeded onto the channel walls, thereby fabricating a simple vessel-like element. Connecting the channels to each other results in a perfusable network of endothelial cell-lined channels serving to provide a means fluid flow through the construct. The endothelial cell lining adds a biological dynamic to the channels by functionalizing the fluid-tissue interface as a regulated exchange barrier. However, adaptation into more native-like microvasculatures is limited as the channel topology is fixed and vascular remodeling, even with the addition of other vascular cells is constrained. Cellularized channel systems are usually made either by soft photolithographic methods or 3D bioprinted sacrificial reverse molds[36].

5.2 Combining Approaches

The latest efforts at establishing a microcirculation *in vitro* seeks to combine the microfluidic endothelial cell-lined channel platform with a native, derived microvasculature. Here, the channels serve as a perfusion source which, when contiguously connected to a neighboring microvasculature, help to drive the formation of a microcirculation. Often, vascular cells are used to form the initial, native microvasculature to be connected to the channel system[37]. In contrast, Advanced Solutions Life Sciences is using isolated microvessels to form the native microcirculation[36].

5.3 Biomanufacture of Vascularized Systems

With the promise of these *in vitro* microcirculations, exciting new opportunities arise for building more native-like tissue models and mimics for use in the laboratory (and eventually tissue replacement). However, these vascularization advances raise new biomanufacturing challenges as the complexity of the systems rise. For example, individual cell types within systems such as endothelial cells, other vascular cells, targeted parenchymal cells (e.g., hepatocytes, tumor cells), and tissue-specific stromal cells all have unique media and microenvironmental requirements that must be coordinated to support the construct as a whole. Also, new biofabrication strategies addressing when and how to integrate vasculatures with parenchyma cells and other cells types, including staged incubation steps, need to be developed. While 3D bioprinting is a key fabrication approach, the successful strategies in the future will undoubtedly include other fabrication methods. Related to this, organizing manufacturing workflows becomes paramount as different fabrication steps are staged through the entire manufacturing process. While these practices are common to non-biological manufacturing programs, their applications to biomanufacturing have yet to be comprehensively implemented (**Figure 1**). However, new tools enabling these broader biomanufacturing activities with living systems are emerging[36] and groups are beginning to develop the concepts and methods needed to build complex tissues.

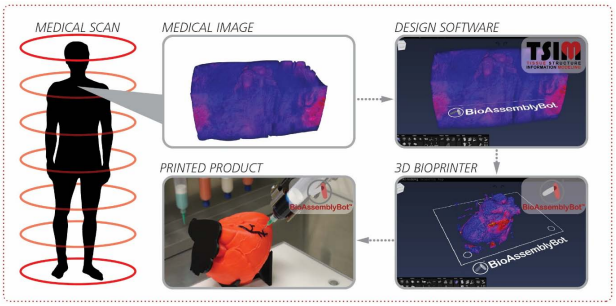

Figure 1. Example work flow (arrows) for digital biomanufacturing. A medical scan of a patient (an MRI of the chest) is imported directly into a commercially available prototyping software (TSIM®, Advanced Solutions Life Science). The biological content (i.e., the structure to be fabricated) is extracted from the image set to produce a 3D digital prototype which is then used to print the physical version in a contour-printing capable robotic arm printer (BioAssembly Bot®, Advanced Solutions Life Science). The process entails a spectrum of technologies including image processing, *in silico* model generation, biology, clinical data, 3D prototyping, robotics, biomaterials, and cell biology.

6. Conclusion

Bioprinting of vascularized tissues has demanded a harmonization of diverse technologies, equipment and materials[38]. Multi-matrix material bioinks are being developed meeting each structural, biologic and regulatory requirement[39]. Multimodal printers can deposit with high speed, mass and resolution[40]. Novel algorithms and software package guide the deposition of neovessels of various sources printed into synthetic networks designed to mature into a contiguous network of arterioles, capillaries, and venules. Digital biomanufacturing promises continuity and optimization of tissue printing operations by insuring real-time access to the required information through high-demand calculations upon rich, timely data.

Conflict of Interest and Funding

No conflict of interest was reported by all authors.

References

1. Rouse M, 2016, *Definition: digital manufacturing*, TechTarget, viewed November 3, 2016, <http://searchmanufacturingerp.Techtarget.Com/definition/digital-manufacturing>
2. Todorovic MH, Datta R, Stevanovic L, *et al*,. 2016, *Proceedings of PCIM Europe 2016; International Exhibition and Conference for Power Electronics, Intelligent Motion, Renewable Energy and Energy Management, May 10–12, 2016: Design and testing of a modular SiC based power block*. Nuremberg, Germany. pp. 1–4. <http://ieeexplore.ieee.org/abstract/document/7499578/>
3. Fan H and Scott C, 2015, *From chips to CHO cells: IT advances in upstream bioprocessing*, BioProcess International, viewed November 11, 2016, <http://www.Bioprocessintl.Com/manufacturing/information-technology/from-chips-to-cho-cells-it-advances-in-upstream-bioprocessing/>
4. National Science Foundation, 2013, *NSF workshop report – advanced biomanufacturing*, viewed November 5, 2016, <http://www.nsf.gov/eng/cbet/documents/adv_biomanufacturing.pdf>
5. Stackpole B, 2016, *3D printing a key piece of digital manufacturing puzzle*, TechTarget, viewed November 13, 2016, <http://searchmanufacturingerp.techtarget.com/feature/3D-printing-a-key-piece-of-digital-manufacturing-puzzle>
6. *TSIM® software*, n.d., viewed November 12, 2016, <http://www.lifesciences.solutions/tsim-software.html>
7. Jose R R, Rodriguez M J, Dixon T A, *et al*., 2016, Evolution of bioinks and additive manufacturing technologies for 3D bioprinting. *ACS Biomaterials Science and Engineering*, vol.2(10): 1662–1678. http://dx.doi.org/10.1021/acsbiomaterials.6b00088
8. Sundaramurthi D, Rauf S, and Hauser C, 2016, 3D bioprinting technology for regenerative medicine applications. *International Journal of Bioprinting*, vol.2(2): 9–26. http://ijb.whioce.com/index.php/int-j-bioprinting/article/view/78
9. Whitford W G and Hoying J B, 2016, A bioink by any other name: Terms, concepts and constructions related to 3D bioprinting. *Future Science OA*, vol.2(3): FSO133. http://dx.doi.org/10.4155/fsoa-2016-0044
10. Jang J, Kim T G, Kim B S, *et al*., 2016, Tailoring mechanical properties of decellularized extracellular matrix bioink by vitamin B2-induced photo-crosslinking. *Acta Biomaterialia*, vol.33: 88–95. https://doi.org/10.1016/j.actbio.2016.01.013
11. Pati F, Jang J, Ha D H, *et al*., 2014, Printing three-dimensional tissue analogues with decellularized extracellular matrix bioink. *Nature Communications*, vol.5: 3935. https://doi.org/10.1038/ncomms4935
12. Ghosh S, Parker S T, Wang X, *et al*., 2008, Direct-write assembly of microperiodic silk fibroin scaffolds for tissue engineering applications. *Advanced Functional Materials*, vol.18(13): 1883–1889. http://dx.doi.org/10.1002/adfm.200800040
13. Organovo Holdings Inc., 2016, *Science and technology*, viewed November 14, 2016, <http://organovo.com/science-technology/>
14. Whitford W G, 2016, *Conference of Bioprinting and 3D Printing in the Life Sciences, July 21–22, 2016: Bioinks supporting angiogenic potential in organ printing*. <https://selectbiosciences.Com/conferences/agendaabstracts.Aspx?Conf=bio3d&abstractid=11535>
15. Armstrong J P K, Burke M, Carter B M, *et al*., 2016, 3D bioprinting using a templated porous bioink. *Advanced Healthcare Materials*, vol.5(14): 1724–1730. http://dx.doi.org/10.1002/adhm.201600022
16. Alakpa E V, Jayawarna V, Lampel A, *et al*., 2016, Tunable supramolecular hydrogels for selection of lineage-guiding metabolites in stem cell cultures. *Chem*, vol.1(2): 298–319. https://doi.org/10.1016/j.chempr.2016.07.001
17. Patel P, 2016, The path to printed body parts — scientists are making steady progress toward 3-D printed tissues and organs. *ACS Central Science*, vol.2(9): 581–583. https://doi.org/10.1021/acscentsci.6b00269
18. Advanced Solutions Inc., n.d., *BioAssemblyBot™*, viewed November 1, 2016, <http://www.lifesciences.solutions/bioprinters.html#more>
19. Zorlutuna P, Annabi N, Camci-Unal G, *et al*., 2012, Microfabricated biomaterials for engineering 3D tissues. *Advanced Materials*, vol.24(14): 1782–1804. https://doi.org/10.1002/adma.201104631

20. Vanderburgh J, Sterling J A, Guelcher S A, 2016, 3D printing of tissue engineered constructs for *in vitro* modeling of disease progression and drug screening. *Annals of Biomedical Engineering*, 1–16. (In Press). https://doi.org/10.1007/s10439-016-1640-4
21. Lokmic Z, Mitchell G M, 2008, Engineering the microcirculation. *Tissue Engineering Part B: Reviews*, vol. 14(1): 87–103. https://dx.doi.org/10.1089/teb.2007.0299
22. LeBlanc A J, Krishnan L, Sullivan C J, *et al*., 2012, Microvascular repair: post-angiogenesis vascular dynamics. *Microcirculation*, vol.19(8): 676–695. https://doi.org/10.1111/j.1549-8719.2012.00207.x
23. Hoying J B, Utzinger U, Weiss J A, 2014, Formation of microvascular networks: role of stromal interactions directing angiogenic growth. *Microcirculation*, vol.21(4): 278–289. https://doi.org/10.1111/micc.12115
24. Muscari C, Giordano E, Bonafè F, *et al*., 2014, Strategies affording prevascularized cell-based constructs for myocardial tissue engineering. *Stem Cells International*, vol.2014: 434169. https://doi.org/10.1155/2014/434169
25. Visconti R P, Kasyanov V, Gentile C, *et al*., 2010, Towards organ printing: engineering an intra-organ branched vascular tree. *Expert Opinion on Biological Therapy*, vol.10(3): 409–420. http://dx.doi.org/10.1517/14712590903563352
26. Moya M L, Hsu Y H, Lee A P, *et al*., 2013, *In vitro* perfused human capillary networks. *Tissue Engineering Part C: Methods*, vol.19(9): 730–737. http://dx.doi.org/10.1089/ten.tec.2012.0430.
27. Carmeliet P, 2005, Angiogenesis in life, disease and medicine. *Nature*, vol.438(7070): 932–936. https://dx.doi.org/10.1038/nature04478
28. Shepherd B R, Chen H Y S, Smith C M, *et al*., 2004, Rapid perfusion and network remodeling in a microvascular construct after implantation. *Arteriosclerosis, Thrombosis and Vascular Biology*, vol.24: 898–904. https://doi.org/10.1161/01.ATV.0000124103.86943.1e
29. Nunes S S, Maijub J G, Krishnan L, *et al*., 2013, Generation of a functional liver tissue mimic using adipose stromal vascular fraction cell-derived vasculatures. *Scientific Reports*, vol.3: 2141. https://doi.org/10.1038/srep02141
30. Laib A M, Bartol A, Alajati A, *et al*., 2009, Spheroid-based human endothelial cell microvessel formation *in vivo*. *Nature Protocols*, vol.4: 1202–1215. https://doi.org/10.1038/nprot.2009.96
31. Pries A R, Reglin B and Secomb T W, 2005, Remodeling of blood vessels: responses of diameter and wall thickness to hemodynamic and metabolic stimuli. *Hypertension*, vol.46: 725-731. https://doi.org/10.1161/01.HYP.0000184428.16429.be
32. Lee V K, Lanzi A M, Haygan N, *et al*., 2014, Generation of multi-scale vascular network system within 3D hydrogel using 3D bio-printing technology. *Cellular and Molecular Bioengineering*, vol.7(3): 460-472 https://doi.org/10.1007/s12195-014-0340-0
33. Laschke M W, Kleer S, Schuler S, *et al*., 2012, Vascularisation of porous scaffolds is improved by incorporation of adipose tissue-derived microvascular fragments. *European Cells & Materials*, vol.24: 266–277. https://doi.org/10.22203/eCM.v024a19
34. Montanez E, Casaroli-Marano R P, Vilaro S, *et al*., 2002, Comparative study of tube assembly in three-dimensional collagen matrix and on Matrigel coats. *Angiogenesis*, vol.5(3): 167–172. https://doi.org/10.1023/A:1023837821062
35. Hemshekhar M, Thushara R M, Chandranayaka S, *et al*., 2016, Emerging roles of hyaluronic acid bioscaffolds in tissue engineering and regenerative medicine. *International Journal of Biological Macromolecules*, vol.86: 917–928. https://doi.org/10.1016/j.ijbiomac.2016.02.032
36. Zheng Y, Chen J, Craven M, *et al*., 2012, *In vitro* microvessels for the study of angiogenesis and thrombosis. *Proceedings of the National Academy of Sciences of the United States of America*, vol.109(24): 9342–9347. https://doi.org/10.1073/pnas.1201240109
37. Moya M L, Hsu Y H, Lee A P, *et al*., 2013, *In vitro* perfused human capillary networks. *Tissue Engineering. Part C: Methods*, vol.19(9): 730–737. https://doi.org/10.1089/ten.TEC.2012.0430
38. Zorlutuna P, Annabi N, Camci-Unal G, *et al*., 2012, Microfabricated biomaterials for engineering 3D tissues. *Advanced Materials*, vol.24(14): 1782–1804. https://doi.org/10.1002/adma.201104631
39. Jose R R, Rodriguez M J, Dixon T A, *et al*., 2016, Evolution of bioinks and additive manufacturing technologies for 3D bioprinting. *ACS Biomaterials Science & Engineering*, vol.2(10): 1662–1678. https://doi.org/10.1021/acsbiomaterials.6b00088
40. Vanderburgh J, Sterling J A and Guelcher S A, 2017, 3D printing of tissue engineered constructs for *in vitro* modeling of disease progression and drug screening. *Annals of Biomedical Engineering*, vol.45(1): 164–179. https://doi.org/10.1007/s10439-016-1640-4

REVIEW ARTICLE

Recent cell printing systems for tissue engineering

Hyeong-jin Lee[1,a], Young Won Koo[1,a], Miji Yeo[1,a], Su Hon Kim[2] and Geun Hyung Kim[1*]

[1] Department of Biomechatronic Engineering, College of Biotechnology and Bioengineering, Sungkyunkwan University (SKKU), Suwon, 16419, Korea

[2] Department of Mechanical Engineering, College of Engineering, Virginia Tech, Blacksburg, Virginia, VA 24061, USA

[a] These authors contributed equally to this work.

Abstract: Three-dimensional (3D) printing in tissue engineering has been studied for the bio mimicry of the structures of human tissues and organs. Now, it is being applied to 3D cell printing, which can position cells and biomaterials, such as growth factors, at desired positions in the 3D space. However, there are some challenges of 3D cell printing, such as cell damage during the printing process and the inability to produce a porous 3D shape owing to the embedding of cells in the hydrogel-based printing ink, which should be biocompatible, biodegradable, and non-toxic, etc. Therefore, researchers have been studying ways to balance or enhance the post-print cell viability and the print-ability of 3D cell printing technologies by accommodating several mechanical, electrical, and chemical based systems. In this mini-review, several common 3D cell printing methods and their modified applications are introduced for overcoming deficiencies of the cell printing process.

Keywords: bioink, cell-printing, tissue engineering

*Correspondence to: Geun Hyung Kim, Department of Biomechatronic Engineering, College of Biotechnology and Bioengineering, Sungkyunkwan University (SKKU), Suwon, Korea; E-mail: gkimbme@skku.edu

Received: November 10, 2016; **Accepted:** November 30, 2016; **Published Online:** January 5, 2017

Citation: Lee H, Koo Y, Yeo M, *et al*., 2017, Recent cell printing systems for tissue Engineering. *International Journal of Bioprinting*, vol.3(1): 27–41. http://dx.doi.org/10.18063/IJB.2017.01.004.

1. Introduction

Since the stereolithographic 3D printer (SLA) was invented by Chuck Hull (the co-founder of 3D Systems Co.), 3D printing has been applied to various fields of industry, including tissue engineering application, namely, 3D bioprinting technique[1]. This technique involves printing bioink, which consisted of various biomaterials with and without live cells, in a layer-by-layer fabrication for human tissue regeneration[2–6]. One of the bioprinting processes, the cell printing system, which can position cells in a desired region, has been accomplished via numerous studies of 3D structure fabrication using natural and synthetic hydrogel polymers. Recently, W. Sun proposed computer-aided tissue engineering; the concept involves printing of 3D interconnected porous structures of anatomically modeled patient tissues and organs from CT or MRI image data[7]. Based on this concept, printing of artificial tissues, such as the ear, blood vessels, skin, bladder[8–12], and organs like the heart or liver will be expected soon.

The conventional 3D printing technology has printed porous tissue-engineered scaffolds with natural or synthetic polymers, which are biocompatible and biodegradable, and seeded cells on the designed structures. However, this technique has been quite passive owing to its dependence on the cell viability of the scaffolds, while the new 3D cell printing method can be more active by controlling the amount and position of various cell-types within the scaffolds. This process was well introduced in the work of Wilson and Boland[13]. They succeeded in printing bioinks that contained live cells instead of the conservative

Recent cell printing systems for tissue engineering © 2017 Hyeong-jin Lee. This is an Open Access article distributed under the terms of the Creative Commons Attribution-NonCommercial 4.0 International License (http://creativecommons.org/licenses/by-nc/4.0/), permitting all non-commercial use, distribution, and reproduction in any medium, provided the original work is properly cited.

printing materials at a size of 50 μm using an ink-jet printer. The printed cell-laden bioinks showed self-assembling characteristics between the cell-aggregates and formed tissue-like structures during culturing time. The results provided the basis for the fabrication of desired tissues or organs by printing and culturing cells at the required sites.

Owing to the strengths of 3D cell printing technology for tissue regeneration, many studies have been devoted to developing the technology using numerous trials and innovative methods. Primarily, they have been modified from conventional 3D-printing methods, and adapting them for cell culture. The 3D cell printing techniques are mainly classified into three techniques: (1) laser-assisted, (2) inkjet, and (3) extrusion cell printing[14–16]. However, unfortunately, the current cell printing processes have not successfully designed or fabricated 3D porous cell-laden structures (**Table 1**).

Table 1. Advantages and disadvantages of basic 3D cell printing techniques.

Techniques	Laser-assisted	Inkjet	Microextrusion
Advantages	Single cell manipulation Nozzle free Usage of high viscosity bioink High resolution High accuracy High gelation speed	High cell viability Noncontact nozzle Printed cell patterns using different cell types Multicell heterogeneous constructs High throughput High gelation speed	High mechanical properties Short fabrication time Printing of various types and viscosities of bioink Wide range of biocompatible materials
Disadvantages	Low mechanical properties Long fabrication time Damage cells due to heat generated from laser energy Aggregate in the final tissue construct	Low mechanical and structural integrity Long fabrication time Low upper limit for viscosity of bioink Low reproducibility Cell aggregation Clogging of the nozzle orifice	Low cell viability due to nozzle wall shear stress and mechanical stress Low accuracy Cell death due to changes in dispensing pressure and bioink concentration
References	[18–21]	[23–27]	[29–33]

In this mini-review, we present the basic cell printing technologies and show several modified cell printing systems, which can overcome the limitations of the current cell printing processes, with a focus on a mechanically modified 3D cell printing process (**Table 2**). In addition, since, in many cases, modified cell printing systems are closely related to hydrogel-based bioinks, we mention various bioinks.

2. Basic Techniques of 3D Cell Printing

2.1 Laser-assisted 3D Cell Printing Technique

Laser-assisted cell printing is a 3D printing method to pattern and assemble bioinks by direct writing using laser. It has been rise to be an automated system that prints the cell-laden bioinks with a high resolution, accuracy, and precision[17]. As the lasers is beamed on the absorbing layer, the bioink is deposited in micro-sizes by controlling scanning mirrors and focusing lens in x and y-axis (**Figure 1a**)[18–21]. This nozzle-free fabrication prevents cell or material clogging often found in extrusion-based 3D cell printing techniques[16]. However, despite of these advantages, it is difficult to print macroscale 3D porous structures using laser-assisted cell printing. Owing to a relatively low flow rate, the vaporization of cell-laden bioink and possibility of cell contamination can significantly increase if a scaffold is built in larger scale. In addition, the potential cell damages caused by the thermal energy of the laser is another factor to be concerned[17,22]. Therefore, the integration of techniques, such as fast gelation of droplets or bio-papers, are actively attempted to overcome the existing limitations.

2.2 Inkjet 3D Cell Printing Technique

In the early generation of 3D cell printing, the inkjet cell printing technique was devised to print biomaterials in a 3D structure by remodeling the existing inkjet printers. Inkjet cell printers were designed to use three general methods: thermal, piezoelectric, and acoustic inkjet printers using heat, piezoelectric, and acoustic wave actuators, respectively, to dispense cell-embedded microdroplets (**Figure 1b**)[23–27]. This technique is widely used for its high cell viability and resolution in microscale structures. In addition, it is easily accessible and inexpensive. However, the inkjet printers can only use comparatively low viscosity materials with a low cell density. This is a critical drawback for a stable 3D cell printing process[25,27]. To overcome this problem, many approaches, such as developing a crosslinking method, are being studied and examined. Although inkjet 3D cell printing has

Table 2. Modified 3D cell printing processes

Modified cell printing	Methods		Bioink materials	Crosslinking conditions	Cell types	Cell viability	Geometry of printed structures	Pros and Cons	References
3D cell printing with modified crosslinking process	Aerosol crosslinking		3.5 wt% alginate + 0.5 wt% $CaCl_2$ mixture (7:3)	1. aerosol: 2~10 wt% $CaCl_2$ (fuming rate: 14.5 ml/min) 2. 2nd cross-linking: 1~3 wt% $CaCl_2$ (immersion for 1 min)	MC3T3-E1 (mouse pre-osteoblasts)	Compatible (~86%)	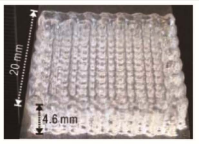	Enhancement of 3D printability and coherence between struts Use of high viscid bioink Possible cell damage by cross-slinking	[36–38]
	Sub-merged crossly-nking (d-rop-on-d emand)	Inkjet	2.3% alginate + 0.1% gelatin	0.25M $CaCl_2$	Mouse endothelial cells	Compatible	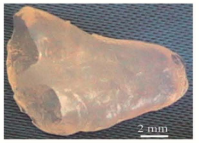	High 3D printability with low viscid bioink Low porosity, mechanical properties	[39,40]
		La-ser-assisted	2% (w/v) alginate	1~2 wt% $CaCl_2$	NIH 3T3 mouse fibroblasts	Low (63~71%)	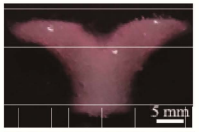	High 3D printability with low viscid bioink Low porosity, mechanical properties, and cell viability	[41]
		Extrusion	2 wt% alginate	50~200 mM $CaCl_2$	ATDC5 mouse teratocarcinoma cells Primary chick chondrocytes	Compatible (76~84%)	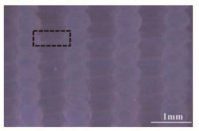	Higher 3D printability (sideway porosity) Low coherence between layers Need for additional surface treatment	[42]
		Extrusion with core/shell nozzle	2-5% (w/v) alginate	2-5% (w/v) $CaCl_2$	L929 mouse fibroblasts	Compatible (67~93%)	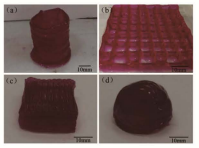	Printability of micro-size hollow structure with use of core/shell nozzle Need of hysiological analysis of nutrient delivery	[44]
	Absorption crosslinking		3~5 wt% alginate	0.8~1.4 wt% $CaCl_2$	MC3T3-E1 (mouse pre-osteoblasts) Human adipose stem cells (hASCs)	High (92.3~93%)	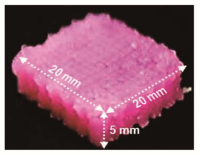	High 3D printability and coherence of layers Simple modification of printing stage Need of core/shell nozzle (non-adaptable to inkjet/laser-assisted printing)	[46]
Temperature-controlled 3D cell printing	High-temperature stage		3 wt% dECM mixed with pepsin (10:1) in 0.5 M acetic acid solution	Incubation at 37 °C for 30 min	Human adipose-derived stem cells (hASCs) Human inferioir turbinate-tissue derived mesenchymal stromal cells (hTMSCs)	High (90~95%)	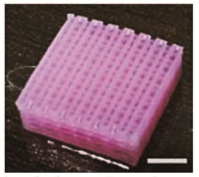 (scale bar = 2 mm)	Capability of printing hASCs or hTMSCs with adequate cell viability and proliferation Enhanced structural maturation of myoblasts with dECM Further applications *in vivo* drug administrations are expected	[48]

Contiued

Modified cell printing	Methods	Bioink materials	Crosslinking conditions	Cell types	Cell viability	Geometry of printed structures	Pros and Cons	References
		10 wt% type I collagen dissolved in 0.05 M acetic acid (pH 3.2) + 10 enriched DMEM in deionized water (1:1)	-	Human primary skin cells (keratinocyte and fibroblast)	Compatible (~85%)	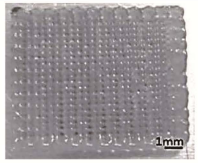	Outstanding biocompatibility and scaffold's structure mimicking native human skin Lower stiffness preventing from commercializing as an engineered skin substitute (ESS)	[49]
	Low-temperature stage	3 wt% alginate + 0.5 wt% $CaCl_2$ mixture (7:3)	0.5 wt% $CaCl_2$ (aerosol) for dispensing with tentative aerosol cross-linking method (DTCM)	Osteoblast-like cell (MG63) Mesenchymal stem cell (MSC)	Compatible (~84%)	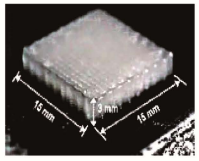	Highly porous cell-laden alginate scaffolds with a thickness over 7 mm Homogeneous pore size and 100% pore interconnectivity Relatively low initial cell viability of MSCs (about 70%)	[50]
Electric field assisted 3D cell printing	Electrohydrodynamic jet (EHDJ)	2 wt% alginate + 2 wt% poly(ethylene oxide) + 0.7 wt% lecithin	5 wt% CaCl2 in phosphate buffer saline (PBS) (aerosol) 2.5 wt% CaCl2 in PBS (secondary crosslinking)	Osteoblast-like cells (MG63)	Compatible (~80%)	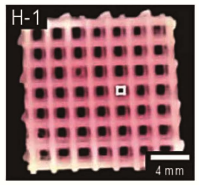	Homogenous cell distribution Improved mechanical properties Need on *in-vivo* test Need on osteogenic test	[51]
	Extrusion-based	4 wt% alginate + 0.5 wt% $CaCl^2$ mixture (7:3)	5% (w/v) $CaCl_2$ in tris-buffered saline (TBS) (aerosol) 2% (w/v) $CaCl_2$ (secondary crosslinking)	Osteoblast-like cells (MG63) Human adipose stem cells (hASCs)	Compatible (~87%)	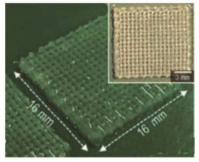	Enhanced printing stability and resolution Increased coherence between layers Potential cell damages by electric field (voltage limitation: 2 kV)	[52]
Hybrid 3D cell printing	Conventional 3D printing (melt-plotting) + 3D cell printing (extrusion/ aerosol crosslinking)	PCL (M_W 70,000-90,000) for melt-plotting 4 wt% alginate, alginate and $CaCl_2$, collagen/ BMP-2, or gelatin/alginate mixture for cell printing	$CaCl_2$ (100mM) + NaCl (145mM) solution 2.5 wt% $CaCl_2$ (aerosol crosslinking) 2 wt% $CaCl_2$ solution (post-print crosslinking)	Human chondrocytes Osteoblast-like cells (MG63) MC3T3-E1 (mouse pre-osteoblasts) Mesenchymal dental pulp derived stem cells (DPSCs)	High (85~99%)	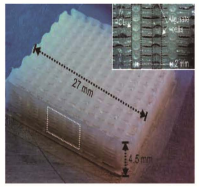	Highly improvement of 3D printability and mechanical properties with high cell viability Need of use of non-natural material and dual-nozzle Potential cell damages by melted polymer while printing	[53,54]
	Conventional 3D printing (melt-plotting, electrospinning) + 3D cell printing (extrusion)	10% of PCL (M_W 90,000) in MC/DMF solution for electrospinning PCL (M_W 45,000) for melt-plotting 3 wt% alginate and 2 wt% PEO (M_W 90,000) in PBS were mixed with 0.05% $CaCl_2$ at a 7:3 ratio	–	C2C12 myoblasts	High (94~96%)	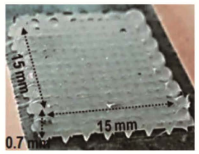	Enhanced formation of myotubes evaluated by MHC expression and the expression levels of various myogenic genes Complicating process to build multi-layer structures (3 methods in one printing process)	[56]

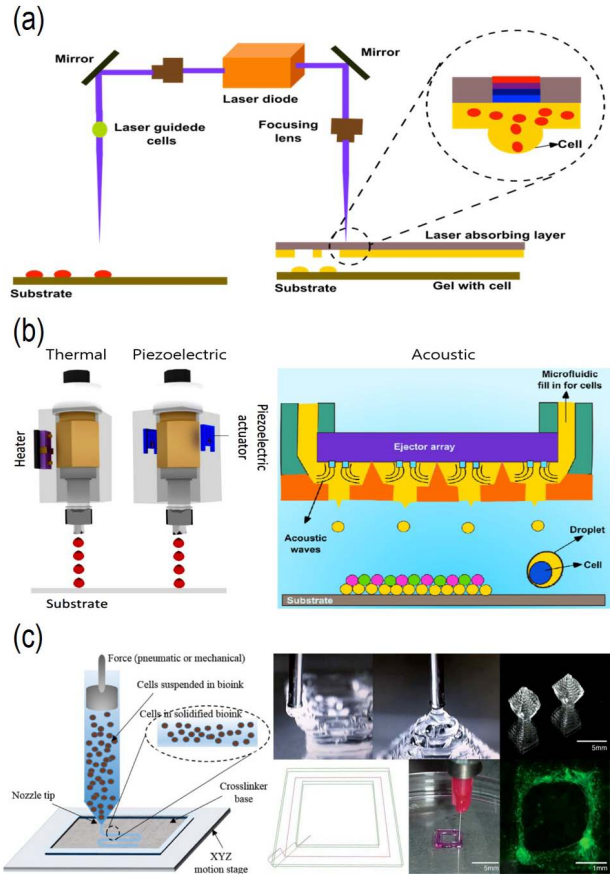

Figure 1. Basic techniques of 3D cell printing, (a) laser-assisted 3D cell printing techniques with and without an absorbing layer,[17,22] (b) thermal, piezoelectric, and acoustic inkjet 3D cell printing systems,[22,28] and (c) microextrusion 3D cell printing systems and products[14,35].

unsolved issues, it is expected to be a versatile tool in broad tissue engineering application[22,28].

2.3 Microextrusion-based Cell Printing

Cell-embedded 3D printing with microextrusion includes a dispensing system that uses pneumatic or mechanical forces to extrude bioink in a line (**Figure 1c**)[29–33]. It is one of the most common cell printing methods owing to its accessibility and versatility in printing 3D structures. Microextrusion can be performed using various bioinks with a broad property range, and especially the viscosity of the bioink in microextrusion is usually much higher than in other 3D cell printing methods. This allows for the fabrication of a complicated 3D structure. Another main advantage of the microextrusion process is its capacity for loading cells at a high density. Using dense cells in the 3D structure can be more effective in the formation of engineered tissues. However, this process also has limitations, such as a relatively low printing resolution owing to the microsized extruding nozzle and comparatively low cell viability caused by severe wall shear stresses within the nozzle using viscous bioink. Therefore, researchers using microextrusion-printing systems are striving for an advanced microextrusion printing technology that creates a precise print with a high cell viability[14,16,34,35].

3. Modified Cell Printing Processes

3.1 3D Cell Printing with Modified Crosslinking Processes

The 3D cell printing process with natural-polymer-based bioink usually contains a crosslinking process owing to low mechanical properties or low viscosity of the bioink. In this section, a few applications of modified crosslinking processes during printing are introduced.

In recent, Ahn *et al.*[36–38] developed a modified 3D cell printing technology with an aerosol crosslinking process (**Figure 2a**) that finely sprayed the crosslinked solution creating a coagulation of the bioink to fabricate the desired form and structure. They reported that the fabrication of a 3D cell-laden porous mesh structure using an alginate bioink can produce adequate cell growth, and it was successfully achieved by spraying aerosols of calcium chloride ($CaCl_2$) solution during the printing process. Spraying the aerosol cross-linked solution induced a high printability of the bioink owing to the hardening of the structure surfaces during the crosslinking process and increased the coherence between the printed cell-laden struts. Throughout the process, the amount and position of the cells were controlled within the scaffold.

The submerged-in-crosslinker cell printing process, referred to as drop-on-demand printing, has been applied to the inkjet[39,40], laser-assisted[41], and extrusion-based[42,43] cell printing processes to build 3D structures with relatively low-viscosity bioinks. Xu *et al.*[39] and Boland *et al.*[40] built the drop-on-demand printing apparatus shown in **Figure 2b**, which uses a layer-by-layer-sinking plate in the crosslinker-filled chamber, and the alginate-based bioink was printed on the surface of the crosslinking liquid. Through their modified method, they overcame one of the limitations of the inkjet printing process, the low 3D printability, and fabricated a 3D structure with a height of approximately 12 mm[40]. In 2015, Xiong *et al.*[41]

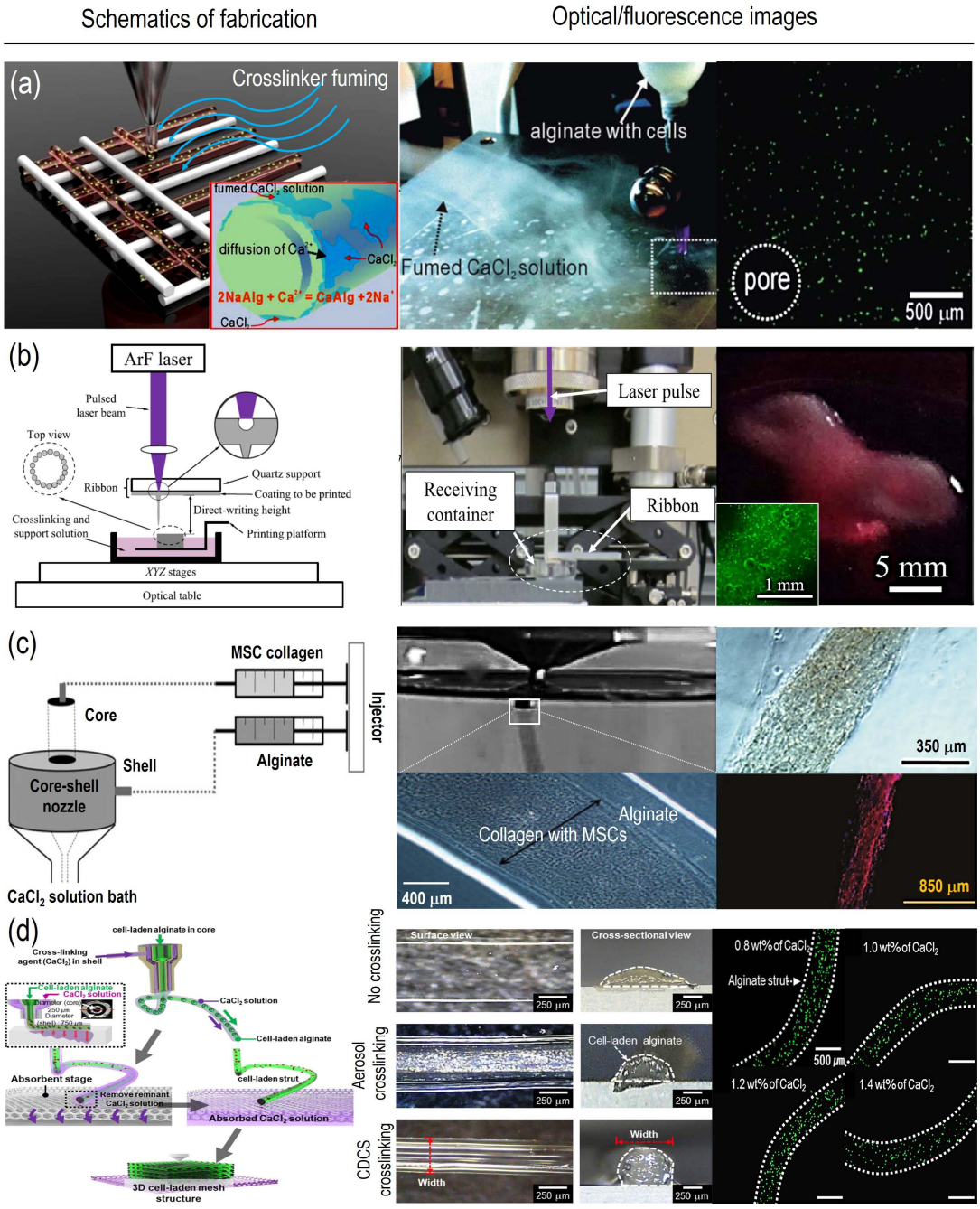

Figure 2. 3D cell printing with modified crosslinking processes, (a) aerosol crosslinking process with calcium chloride using an alginate-based bioink[36–38], (b) drop-on-demand (submerged) crosslinking with a laser-assisted printing process[41], (c) submerged printing with a core (MSC-laden collagen) /shell (2–5 wt% alginate) nozzle[44], and (d) cell printing process with a crosslinked solution and absorbing stage using a core (3 wt% alginate-based cell-laden bioink)/shell (1.2 wt% $CaCl_2$)[46].

applied a similar method to the laser-assisted cell printing process, which contains the same limitations in printing 3D structures, and they were able to fabricate a 3D structure with a height of 9.5 mm. Conversely, You *et al.*[42] fabricated a 3D lattice structure with cell-laden alginate hydrogel via an extrusion-based cell printing process with submerged crosslinking. They coated the surface of a printing plate, instead of using a lifting stage, and printed the bioink in a $CaCl_2$ solution to build a biaxially porous 3D scaffold, which created pores between the deposited layers. Gao *et al.*[43] modified the submerged crosslinking cell print-

ing process using a core/shell nozzle. They extruded the crosslinked solution through the core and the bioink through the shell to create a hollow tube-shaped 3D structure. By applying the drop-on-demand printing method, they were also able to fabricate various 3D cell-laden structures.

For applications in extrusion-based cell printing, a dual or core/shell nozzle is occasionally used as an alternative crosslinking method, as in the study described above[43–46]. The core/shell fibrous collagen–alginate hydrogel was proposed by Perez *et al.*[44] (**Figure 2c**). They placed mesenchymal stem cells (MSCs) into the inner cell-collagen encapsulated with a 2 ~ 5 wt% alginate (the outer portion). The collagen–alginate hydrogel was extruded into a bath filled with a 50-mM $CaCl_2$ solution, and the outer alginate contacted the $CaCl_2$ solution for 5 min and crosslinked. Using this process, sufficient stability of the collagen–alginate hydrogel was maintained and represented by storage moduli as 30 kPa, 40 kPa, and 50 kPa at 2 wt%, 3 wt%, and 5 wt% alginate, respectively. The cell viability was approximately 70 to 80% for the collagen–alginate (3 wt%) sample and pure collagen sample. In addition, Ahn *et al.*[46] developed a simple and innovative cell printing method using a core/shell nozzle and an absorbing printing stage (**Figure 2d**). In their process, the alginate-based bioink was extruded through the core nozzle, and the $CaCl_2$ solution was extruded through the shell nozzle to crosslink the printed bioink simultaneously. The crosslinking solution then immediately absorbed into the absorbing stage to prevent the crosslinked solution from ruining the 3D shape of the alginate struts. On a non-absorbing stage, the crosslinked structure can collapse during printing owing to the weakened coherence between struts by the remaining crosslinked material. The surfaces of the struts can be constantly indurated, and the stability of the scaffold increases through the continuous crosslinking of the previously printed layers. This method formed a 3D structure easy and more consistently than the submerged crosslinking technique, since the submerged process contained a high possibility of the bioink floating in the crosslinking solution during the printing process and required additional treatment, such as polyethylenimine (PEI) surface coating[42,47] or a layer-by-layer interactively moving stage[39–41,43].

3.2 Temperature-controlled 3D Cell Printing Process

For the scaffold printed with formless materials, the temperature was controlled to enhance printability in the 3D structure while the damage to cells was minimized. The rheological property of dECM (decellularized extracellular matrix) bioink was controlled by increasing the temperature to construct a 3D structure (**Figure 3a**)[48]. As the temperature increased beyond 15°C, the storage modulus was increased, and a crosslinked gel was observed at 37°C. In this process, increasing temperature is prerequisite to retain 3D structure, which subsequently makes storage modulus greater than loss modulus at the certain temperature. A high cell viability (> 90%) was maintained over 14 days of culture for the *in vitro* and *in vivo* tests. Furthermore, Yoon *et al.*[49] varied temperature for optimizing the fabrication of a collagen scaffold. In this study, the stage containing a circulating pump, water chamber, and temperature controller was used to maintain the cell-printing plate from 25°C to 60°C. The collagen struts were adequately fabricated between 36°C to 39°C with a cell viability of 85%. Conversely, the strut formation was rather amorphous and not applicable below 35°C or over 42°C, with a significant decrease in cell viability. This phenomenon suggests that the temperature and collagen gelation/crosslinking are correlated, and controlling the temperature allows the 3D structure to be formed by rapid gelation of the bioink. However, the printed collagen scaffold lacks sufficient strength and stiffness (0.01 ± 0.001 kPa of Young's modulus); therefore, further exploration of a non-toxic chemical reagent or crosslinking process is required.

Low-temperature cell printing is a printing method that plots struts by instantly freezing the bioink extruded from the nozzle (**Figure 3b**). The conventional 3D cell printing has revealed the conversion of dispensed nearby struts, which eventually disturbs the layer-by-layer stacking process. To overcome this problem, Ahn *et al.*[50] applied a low temperature from −2°C to−40 °C to fabricate the biaxially porous 3D lattice scaffold in solid structure. Throughout the cell printing process, the alginate bioink with cells was maintained at 4°C to minimize the cell damage by a rapid decrease in temperature. As the temperature was close to 0°C, the cell viability increased up to 84%, but the shaping ability decreased. Conversely, as the temperature decreased to −40°C, the cell viability dropped below 10%, but the shaping ability was enhanced with high fabricating efficiency of 85%. The scaffolds were printed at 487°C with the reasonable initial cell viability (70~84%) and high

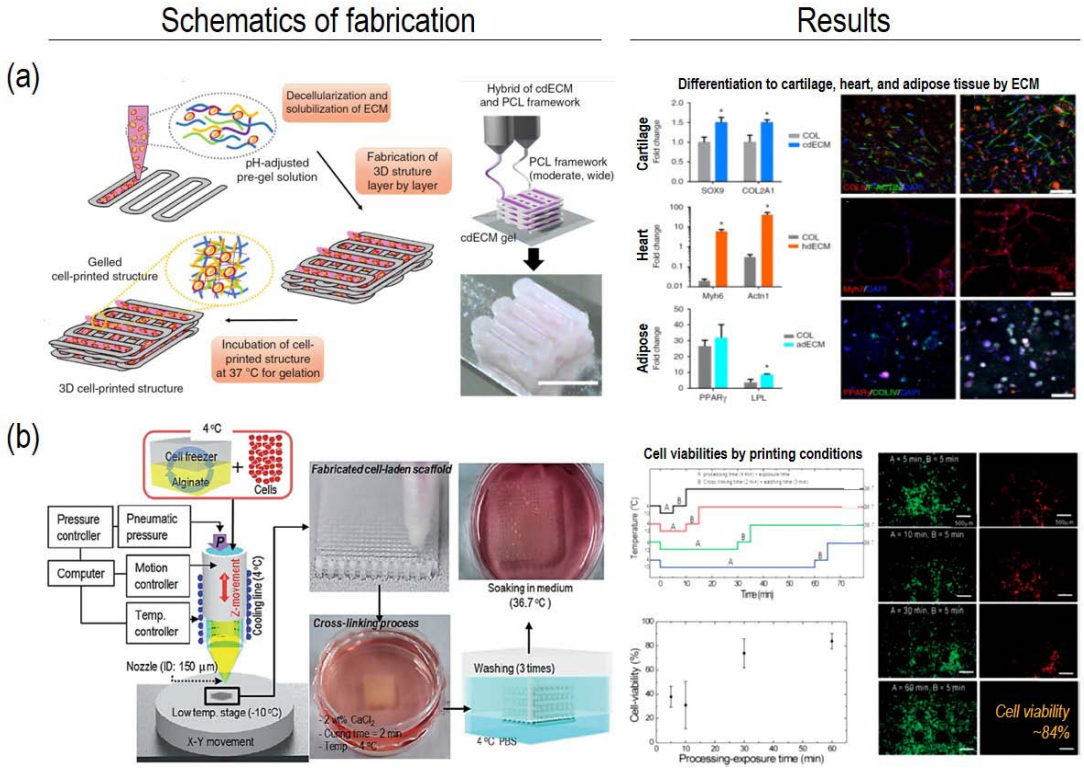

Figure 3. Temperature-controlled 3D cell printing process, (a) increasing temperature-controlled (from 4 to 37°C) printing using ECM-based bioinks [48, 49] and (b) low-temperature (−10°C) cell printing process [50].

shaping ability. It also revealed the successful fabrication of multi-layered scaffold with significantly enhanced mechanical properties (10 ± 2.2 MPa of Young's modulus). For further development, initial cell viability can be improved, and various types of bioink can be used for low-temperature cell printing.

3.3 Electric-field Assisted 3D Cell Printing

Recently, the application of an electric field in cell printing was proposed. Yeo *et al.*[51] combined electric-filed assisted 3D cell printing and aerosol cross-slinking process to fabricate a 3D hybrid cell-laden scaffold. The osteoblast-like cell-laden fibers were deposited with 0.16 kV on 3D lattice PCL struts (**Figure 4a**). The initial cell viability was reasonable (above 80%), and the cells could proliferate for prolonged culture period. The fibers maintained their shape without dispersion on the hybrid scaffold with a significant increase in tensile modulus (4.9 ± 0.6 MPa) compared to alginate mat. Also, Yeo *et al.*[51] applied an electric field to the extrusion-based cell p rinting that pneumatically printed alginate-based bioink with human adipose stem cells with the electrical field (**Figure 4b**). This reduced the wall shear stress in the nozzle and reduced the damage of the cells in the printed bioink[52]. Moreover, the electric field enhanced the printing stability and resolution of the dispensed struts since the electric force pulled down the bioink and resulted in an increase in the coherence between the layers and a decreased strut size. However, there was potential cell damage when the high electric field was used, and they reported that the limitation of the applied voltage with their experimental conditions was less than 2 kV.

3.4 Hybrid Systems for Mechanically Stable 3D Cell-laden Structures

As the 3D cell printing was derived from the conventional 3D printing technology, some researchers have tried to apply the conventional 3D printing methods to the 3D cell printing process. Several papers reported that the melt-plotting method, one of the most common methods among non-cell printing processes, was combined with the cell printing techniques to fabricate and strengthen a ce ll-laden 3D structure by providing a firm frame or support for the soft cell-laden bioinks[48,53–56]. In 2012, Shim *et al.*[53] used the melt-plotting method with a s ynthetic polymer, poly (ε-

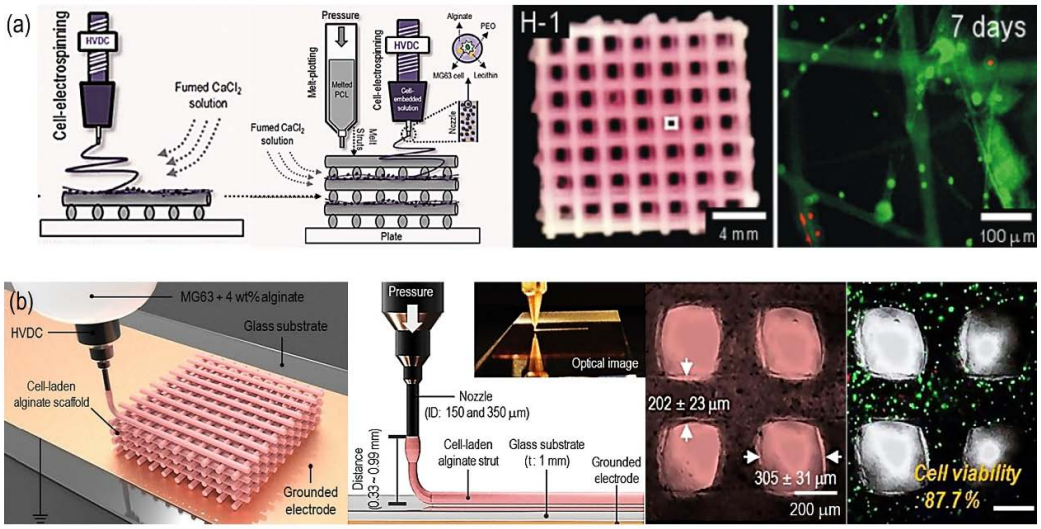

Figure 4. (a) Electrically operated cell printing modification supplemented with the aerosol crosslinking process[51] and (b) extrusion-based cell printing with an electric field (1 to 3 kV in 0.33 to 0.99 mm)[52].

caprolactone) (PCL), to fabricate a frame wall for hydrogel fillings extruded with air pressure between the synthetic polymer walls (**Figure 5a**). Their method enabled the printing of multi-type cells on the desired locations in the 3D spaces. However, the fabricated structures showed necrosis of encapsulated cells in the center of the hydrogel owing to the lack of pores.

In an attempt to overcome this limitation, Lee *et al.*[54] suggested a hybrid 3D cell printing method combined with a crosslinking aerosol process and melt-plotting method to fabricate a highly porous 3D cell-laden structure (**Figure 5b**). This hybrid scaffold was fabricated by printing bioink between the synthetic polymer struts to overcome the low mechanical properties of the struts owing to the low viscosity of the bioink. This printing system contained a high coherence between the strut layers since the two different types of struts had the same diameter and interval. In addition, because of the release of cells inside the bioink struts, the structure contained a uniform cell distribution and a good supply of nutrients to the cells, and it secured the cell transfer, which is important for cell growth. Moreover, hybrid fabrication of the synthetic polymer with high mechanical properties and

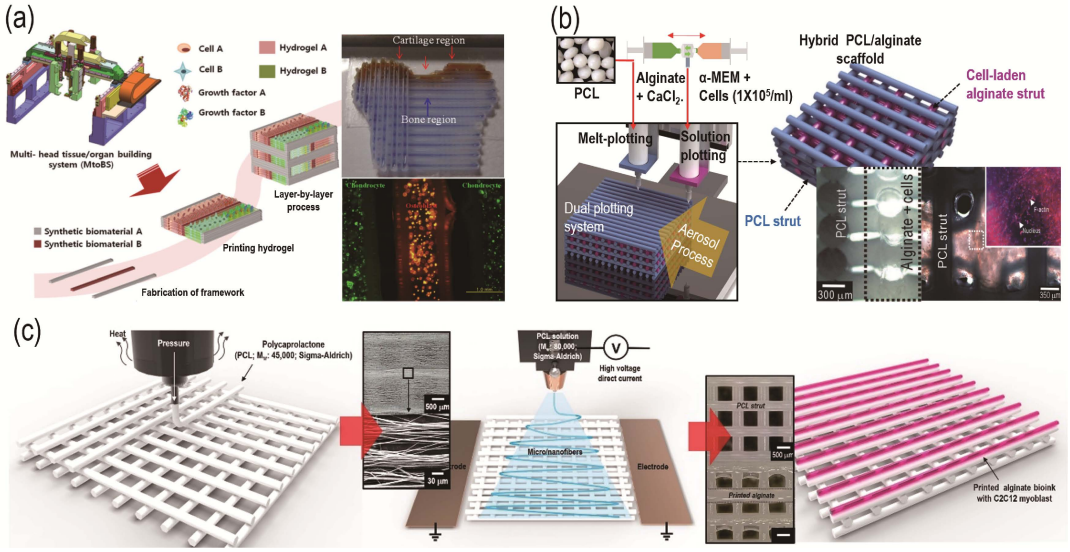

Figure 5. Hybrid modifications of the 3D cell printing process with (a, b) a multi-nozzle system using natural and synthetic polymers ((a) Shim *et al.*[53], (b) Lee *et al.*[54]) and (c) an additional electrospinning process for surface alignment (Yeo *et al.*[56]).

cell-laden bioink enables the production of accurate 3D shapes and can be applied to the regeneration of tissues demanding high mechanical strength because the enhanced mechanical properties and high cellular activity of the structure. Most importantly, a 3D structure like the natural tissue structure can be designed by placing bioink with different cells on each layer of the structure. However, the cells that contacted the PCL struts showed dramatically low viability owing to the hot temperature of the melted PCL during printing. This remains an issue to overcome.

In an additional hybrid application, Yeo *et al*.[22,57] developed a hybrid fabrication of a hierarchical scaffold using an electrospinning method to align fine PCL nano-fibers on the micro-sized PCL struts created from a melt-plotting process as shown in (**Figure 5c**)[56]. Then, they printed alginate-based bioink with myoblasts on the electrospun fibers to examine the alignment and stretching of the myoblast cells. Using this method, they successfully fabricated muscle mimetic scaffold with sufficient mechanical properties. In addition, the myoblasts in the scaffold were well aligned on the nano-fibers as the aspect ratio of F-actin with aligned fibers was over 2 folds of the aspect ratio with random fibers or without fibers, which indicates the elongation of the cell in one direction. These results showed that the fabricated scaffold was suitable and applicable for the regeneration of muscle tissues.

4. Bioink

4.1 Definition of Bioink

In cell printing, hydrogels made of natural and synthetic polymer materials are mainly used in the fabrication of a 3D cell structure. The bioink is defined as a mixture of hydrogel and live cells and is the most important requisite for the successful production of an artificial tissue. The bioink requires several characteristics: (1) 3D printability with uniform viscosity, (2) physical and chemical crosslink ability that enables 3D shape maintenance after printing, (3) cyto-compatibility that supports favorable cell viability and assists cell proliferation and differentiation, and (4) biodegradability after transplantation into a host for the emission of decomposed wastes[58,59]. Currently, the most widely used bioink materials in cell printing are alginate, collagen, hyaluronic acid, gelatin, pluronic F127, polyethylene glycol dimethacrylate[60–62], etc.

4.2 Bioink Viscosity and Crosslink Ability

One of the important variables in producing bioinks with the materials above is viscosity. Viscosity is defined by the concentration of the materials, and the printability and print resolution can be enhanced as the viscosity of the bioink increases. However, it is reported that cell viability can decrease from the severe nozzle wall shear stress generated in a narrow nozzle by high pressure, and this is required to print high-viscosity bioink[63]. In addition, it is known that the ability to crosslink effects the strength and stiffness of the scaffolds and the oxygen and nutrient supply for the cells. However, excessive cross-linking can reduce the cell viability and disturb the formation of new tissue[36]. Therefore, it is essential to develop a biodynamic bioink with appropriate viscosity and crosslink-ability that can be printed in a 3D layered structure with sufficient printing resolution.

4.3 Applications of Bioink in 3D Cell Printing Techniques

The studies of bioink focus on the process conditions to control the viscosity and the bioink's ability to crosslink depending on the compositions of the materials. The printability in 3D printing is an important factor as well as good biocompatibility that promotes and maintains high initial cell viability over 90%, cell proliferation, and differentiation. Therefore, investigations in bi oink composed of different hydrogels have been actively performed and applied to regenerate various cells with 3D cell printing techniques (**Table 3**). For laser assisted 3D cell printing and inkjet 3D cell printing, fibrin bioink is widely used because of its degradability, enhancement of cellular activities, and, most importantly, high printability by fast-gelling and tunable viscosity[64]. In addition, the fibrin bioink can be easily obtained from blood by purification and provides binding affinities that help initial cell attachment[64,65]. For micro-extrusion based 3D cell printing, alginate is the most widely used material because it is inexpensive, and its viscosity can be easily controlled[17,44,46]. In addition, it contains excellent biocompatibility, low toxicity, and a stable 3D structure by simply mixing with the carboxyl of L-guluronic acid in a ca lcium ion solution[66,67]. De spite those advantages, alginate itself lacks bioactive factors inducing cell attachment or activities. There-

fore, collagen bioink has been investigated to improve the 3D cell printing process. To date, the development of collagen bioink has been hindered because of its unstable 3D structure and low process ability; however, modified 3D cell printing techniques, such as aerosol system and crosslinking reagents, are being actively investigated to apply collagen bioink into the 3D cell printing process.

Table 3. Studies and endeavors for the development of bioink in 3D cell printing

Techniques	Materials	Cell types	Crosslinking reagents	References
Laser-assisted 3D cell printing	Fibrin	Endothelial cell/Mesenchymal stem cell	-	[68]
		Smooth muscle cell	-	[69]
Inkjet 3D cell printing	Fibrin	Muscle-derived stem cell	-	[65]
		Mesenchymal fibroblast/Myoblast	-	[70]
		Neuronal precursor cell/Cortical cell	Proteolytic	[64]
		Neural stem cells	-	[71]
	Collagen	Epidermal keratinocyte/Dermal fibro blast	Sodium bicarbonate	[72]
Microextrusion based 3D cell printing	Hyaluronic acid	Aortic valve interstitial cell	Methacrylated gelatin	[73]
	Gelatin/Alginate	Aortic root sinus smooth muscle cell	$CaCl_2$	[74]
	RGD-modified alginate	Cardiomyocyte progenitor cell	$CaCl_2$	[75]
	Alginate/PEO	Myoblast	$CaCl_2$	[56]
		Osteoblast-like cell	$CaCl_2$	[76]
	Alginate	Bone marrow stromal cell	-	[77]
	Fibrin	Endothelial cell	$CaCl_2$	[78]
	Agarose	Smooth muscle cell/Fibroblast	-	[79]
		Schwann cell	-	[80]
	Collagen	Cardiac cell/Endothelial cell	-	[81]
		Adipose stem cell	$CaCl_2$	[82]

5. Conclusion

Since the introduction of 3D cell printing technologies, studies and applications of 3D cell printing have been focused on or striving for the fabrication of 3D tissue-engineered structures that can firmly replace or repair damaged tissues in the human body in a short period of time. If this is possible, 3D cell printing technology may provide patients an instant medical treatment individually by rapidly manufacturing customized tissue-engineered constructs, and, therefore, creating a totally new medical course. This integrated medical course may include the scanning of injured parts, extracting a patient's cells, culturing and printing the cells through 3D cell printing, and implanting the engineered scaffold into the patient's body. However, to implement this new generation of clinical practices several challenges, such as low mechanical properties of natural polymer scaffolds; improvement of crosslink ability without cell damage; materialization of complex 3D structures; development of 3D multi-culturing; and joint works with material sciences, mechatronics, computer engineering, or medicine; etc., need to be surmounted. Especially the fabrication and culturing of 3D multicellular complex organ structure are indispensable steps to achieve the ultimate goal of tissue engineering. This can be reached, however, when the former steps are accomplished, such as the generation of 3D vascular structures in bigger multicell-printed tissue or organ structure. The major challenges of the realization and vascularization of multicellular structure would be the complexity and exquisiteness of the natural tissues and organs that we are striving to mimic. Despite these assignments ahead, we believe that the completion of whole-organ fabrication technology can be occurred in the nearer future than expected, as the studies and collaborations for tissue engineering is now being actively performed.

Conflict of Interest and Funding

There is no conflict of interest. This study was par-

tially supported by a grant from the National Research Foundation of Korea grant funded by the Ministry of Education, Science, and Technology (MEST) (Grant no. NRF- 2015R1A2A1A15055305) and also a grant from the Korea Healthcare Technology R&D Project, Ministry for Health, Welfare and Family Affairs, Republic of Korea (Grant no. HI15C3000).

References

1. Whitaker M, 2014, The history of 3D printing in healthcare, *Annals of The Royal College of Surgeons of England Bulletin*, vol.96: 228 229. https://doi.org/10.1308/147363514X13990346756481
2. Griffith LG, Naughton G, 2002, Tissue engineering Current challenges and expanding opportunities, *Science*, vol.295(5557): 1009 1014. https://doi.org/10.1126/ science.1069210
3. Hollister SJ, 2005, Porous scaffold design for tissue engineering, *Nature Materials*, vol.4(7): 518 524. https://doi.org/10.1038/nmat1421
4. Whitford WG, 2016, Bioinks for 3D Bioprinting: A development parameters review, *Immunome Research*, vol.12(S2): 24. https://doi.org/10.4172/1745-7580.c1.004
5. Loo Y, Lakshmanan A, Ni M, *et al.* 2015, Peptide bioink: self-assembling nanofibrous scaffolds for t hree-dimensional organotypic cultures, *Nano Letters*, vol.15(10): 6919 6925. https://doi.org/10.1021/acs.nanolett.5b02859
6. Mironov V, Reis N, Derby B, 2006, Bioprinting: A beginning, *Tissue Engineering*, vol.12: 4. https://doi.org/10.1089/ten.2006.12.631
7. Sun W, Lal P, 2002, Recent development on computer aided tissue engineering a review, *Computer Methods and Programs in Biomedicine*, vol.67(2): 85 103. https://doi.org/10.1016/S0169-2607(01)00116-X
8. Sachlos E, Czernuszka JT, 2003, Making tissue engineering scaffolds work. Review: the application of solid freeform fabrication technology to the production of t issue engineering scaffolds, *European Cells & Materials*, vol.5: 29 39. https://doi.org/10.22203/eCM.v005a03
9. Hutmacher DW, Sittinger M, Risbud MV, 2004, Scaffold-based tissue engineering: rationale for computer-aided design and solid free-form fabrication systems, *Trends in Biotechnology*, vol.22(7): 354 362. https://doi.org/10.1016/j.tibtech.2004.05.005
10. Fedorovich NE, Schuurman W, Wijnberg HM, *et al*. 2012, Biofabrication of osteochondral tissue equivalents by printing topologically defined, cell-laden hydrogel scaffolds, *Tissue Engineering Part C: M ethods*, vol.18(1): 33 44. https://doi.org/10.1089/ten.tec.2011.0060
11. Guillotin B, Guillemot F, Cell patterning technologies for organotypic tissue fabrication, *Trends in Biotechnology*, vol.29(4): 183 190. https://doi.org/10.1016/j.tibtech.2010.12.008
12. Seol YJ, Kang HW, Lee SJ, *et al*. 2014, Bioprinting technology and its applications, *European Journal Cardio-Thoracic Surgery*, vol.46(3): 342 348. https://doi.org/10.1093/ejcts/ezu148
13. Wilson WC, Boland T, 2003, Cell and organ printing 1: Protein and cell printers, *The Anatomical Record Part A*, 272A: 491 496. https://doi.org/10.1002/ar.a.10057
14. Dababneh AB, Ozbolat IT, 2014, Bioprinting technology: current state-of-the-art review, *Journal of Manufacturing Science and Engineering*, vol.136(6): 061016. https://doi.org/10.1115/1.4028512
15. Seol YJ, Kang HW, Lee SJ, *et al*. 2014, Bioprinting technology and its applications, *European Journal of Cardio-Thoracic Surgery*, 1 7, ezu148.
16. Murphy SV, Atala A, 2014, 3D bioprinting of tissues and organs, *Nature Biotechnology*, vol.32(8): 773 785. https://doi.org/10.1038/nbt.2958
17. Guillemot F, Guillotin B, Catros S, *et al.* 2010, High-throughput biological laser printing: droplet ejection mechanism, integration of a dedicated workstation, and bioprinting of cells and biomaterials, *Cell and Organ Printing*, 95 113.
18. Roda A, Guardigli M, Russo C, *et al.* 2000, Protein microdeposition using a conventional ink-jet printer, *Biotechniques*, vol.28(3): 492–496.
19. Barron J, Ringeisen B, Kim H, *et al*. 2004, Application of laser printing to mammalian cells, *Thin Solid Films*, vol.453(383): 383–387. https://doi.org/10.1016/j.tsf.2003.11.161
20. Hon K, Li L, Hutchings I, 2008, Direct writing technology—advances and developments, *CIRP Annals - Manufacturing Technology*, vol.57(2): 601–620.
21. Guillotin B, Souquet A, Catros S, *et al*, 2010, Laser assisted bioprinting of engineered tissue with high cell density and microscale organization, *Biomaterials*, vol.31(28): 7250–7256. https://doi.org/10.1016/j.biomaterials.2010.05.055
22. Krishnan UM, Sethuraman S, 2013, The integration of nanotechnology and biology for cell engineering: promises and challenges, *Nanomaterials and Nanotechnology*, vol.3(Godište 2013): 3 19.
23. Xu T, Gregory A, Molnar P, *et al*. 2006, Viability and electrophysiology of n eural cell structures generated by the inkjet printing method, *Biomaterials*, vol.27(19): 3580–3588. https://doi.org/10.1016/j.biomaterials.2006.01.048
24. Xu T, Jin J, Gregory C, *et al*. 2005, Inkjet printing of via-

ble mammalian cells, *Biomaterials*, vol.26(1): 93–99. https://doi.org/10.1016/j.biomaterials.2004.04.011

25. Moon S, Hasan K, Song S, *et al*. 2010, Layer by layer three-dimensional tissue epitaxy by cell-laden hydrogel droplets, *Tissue Engineering Part C: Methods*, vol.16(1): 157–166. https://doi.org/10.1089/ten.tec.2009.0179
26. Xu T, Zhao W, Zhu J, 2013, Complex heterogeneous tissue constructs containing multiple cell types prepared by inkjet printing technology, *Biomaterials,* vol.34(1): 130–139. https://doi.org/10.1016/j.biomaterials.2012.09.035
27. Calvert P, 2001, Inkjet printing for materials and devices, *Chemistry of Materials*, vol.13(10): 3299–3305. https://doi.org/10.1021/cm0101632
28. Knowlton S, Onal S, Yu CH, *et al*. 2015, Bioprinting for cancer research, *Trends in Biotechnology*, vol.33(9): 504 513. https://doi.org/10.1016/j.tibtech.2015.06.007
29. Ozbolat I, Yu Y, 2013, Bioprinting toward organ fabrication: challenges and future trends, *IEEE Transactions on Biomedical Engineering*, vol.60(3): 691–699. https://doi.org/10.1109/TBME.2013.2243912
30. Nair K, Yan K, Sun W, 2007, A multi-level numerical model for qua tifying cell deformation in encapsulated alginate structures, *Joruanl of Mechanics of Materials and Structures*, vol.2(6): 1121–1139. https://doi.org/10.2140/jomms.2007.2.1121
31. Shim J, Lee J, Kim J, *et al*. 2012, Bioprinting of a mechanically enhanced three-dimensional dual cell-laden construct for os teochondral tissue engineering using a multi-head tissue/organ building system, *Journal of Micromechanics and Microengineering*, vol.22(8): 085014. https://doi.org/10.1088/0960-1317/22/8/085014
32. Yu Y, Zhang, Y, Martin J, *et al*. 2013, Evaluation of cell viability and functionality in vessel-like bioprintable cell-laden tubular channels, *Journal of Biomechanical Engineering*, vol.135(9): 091011. https://doi.org/10.1115/1.4024575
33. Tirella A, Vozzi F, Vozzi G. 2011, PAM2 (Piston Assisted Microsyringe): A new rapid prototyping technique for biofabrication of cell incorporated scaffolds, *Tissue Engineering Part C: Methods*, vol.17(2): 229–237. https://doi.org/10.1089/ten.tec.2010.0195
34. Koo Y, Kim G, 2016, New strategy for enhancing in situ cell viability of cell printing process via piezoelectric transducer-assisted three-dimensional printing, *Biofabrication*, vol.8(2): 025010. https://doi.org/10.1088/1758-5090/8/2/025010
35. Chang CC, Boland ED, Williams SK, *et al*. 2011, Direct-write bioprinting three-dimensional biohybrid systems for fu ture regenerative therapies, *Journal of Biomedical Materials Research Part B: Applied Biomaterials*, vol.98(1): 160 170. https://doi.org/10.1002/jbm.b.31831
36. Ahn S, Lee H, Bonassar LJ, *et al*. 2012, Cells (MC3T3-E1)-laden alginate scaffolds fabricated by a modified solid-freeform fabrication process supplemented with an aerosol spraying, *Biomacromolecules*, vol.13(9): 2997 3003. https://doi.org/10.1021/bm3011352
37. Ahn S, Lee H, Puetzer J, *et al*. 2012, Fabrication of cell-laden three-dimensional alginate-scaffolds with an aerosol cross-linking process, *Journal of Materials Chemistry*, vol.22(36): 18735 18740. https://doi.org/10.1039/c2jm33749e
38. Ahn S, Lee H, Kim G, 2013, Functional cell-laden alginate scaffolds consisting of core/shell struts for tissue regeneration, *Carbohydrate Polymers*, vol.98(1): 936 942. https://doi.org/10.1016/j.carbpol.2013.07.008
39. Xu T, Jalota S, Manley B, *et al*. 2005, Drop-on Demand Printing of Cell and Materials for Designer Hybrid Cardiovascular Biomaterials, *Society for Imaging Science and Technology*, NIP & Digital Fabrication Conference, 178 178.
40. Boland T, Tao X, Damon BJ, *et al*. 2007, Drop-on-demand printing of cells and materials for designer tissue constructs, *Materials Science and E ngineering: C*, vol.27(3): 372 376. https://doi.org/10.1016/j.msec.2006.05.047
41. Xiong R, Zhang Z, Chai W, *et al*. 2015, Freeform drop-on-demand laser printing of 3D alginate and cellular constructs, *Biofabrication*, vol.7(4): 045011. https://doi.org/10.1088/1758-5090/7/4/045011
42. You F, Wu X, Zhu N, *et al*. 2016, 3D printing of porous cell-laden hydrogel constructs for potential application in cartilage tissue engineering, *ACS Biomaterials Science & Engineering*, vol.2(7): 1200 1210. https://doi.org/10.1021/acsbiomaterials.6b00258
43. Gao Q, He Y, Fu J-z, *et al*. 2015, Coaxial nozzle-assisted 3D bioprinting with built-in microchannels for nutrients delivery, *Biomaterials*, vol.61: 203 215. https://doi.org/10.1016/j.biomaterials.2015.05.031
44. Perez RA, Kim M, Kim TH, *et al*. 2013, Utilizing core–shell fibrous collagen-alginate hydrogel cell delivery system for bone tissue engineering, *Tissue Engineering Part A*, vol.20(1 2): 103 114. https://doi.org/10.1089/ten.tea.2013.0198
45. Faulkner-Jones A, Fyfe C, Cornelissen DJ, *et al*. 2015, Bioprinting of human pluripotent stem cells and their directed differentiation into hepatocyte-like cells for the generation of mini-livers in 3D, *Biofabrication*, vol.7(4): 044102. https://doi.org/10.1088/1758-5090/7/4/044102
46. Ahn SH, Lee HJ, Lee JS, *et al*. 2015, A novel cell print-

ing method and its application to hepatogenic differentiation of human adipose stem cell-embedded mesh structures, *Science Reports-UK*, vol.5:13427

47. You F, Wu X, Chen X, 2016, 3D Printing of porous alginate/gelatin hydrogel scaffolds and their mechanical property characterization, *International Journal of Polymeric Materials and Polymeric Biomaterials*, In-Press.
48. Pati F, Jang J, Ha DH, *et al*. 2014, Printing three-dimensional tissue analogues with decellularized extracellular matrix bioink, *Nature Communications*, vol.5: 3935. https://doi.org/10.1038/ncomms4935
49. Yoon H, Lee JS, Yim H, *et al*. 2016, Development of cell-laden 3D scaffolds for efficient engineered skin substitutes by collagen gelation, *RSC Advances*, vol.6(26): 21439 21447. https://doi.org/10.1039/C5RA19532B
50. Ahn S, Lee H, Lee EJ, *et al*. 2014, A direct cell printing supplemented with low-temperature processing method for obtaining highly porous three-dimensional cell-laden scaffolds. *Journal of Materials Chemistry B*, vol.2(18): 2773 2782. https://doi.org/10.1039/c4tb00139g
51. Yeo M, Kim G, 2015, Fabrication of cell-laden electrospun hybrid scaffolds of alginate-based bioink and PCL microstructures for tissue regeneration, *Chemical Engineering Journal*, vol.275: 27 35. https://doi.org/10.1016/j.cej.2015.04.038
52. Yeo M, Ha J, Lee H, *et al*. 2016, Fabrication of hASCs-laden structures using extrusion-based cell printing supplemented with an electric field, *Acta Biomaterialia*, vol.38: 33 43. https://doi.org/10.1016/j.actbio.2016.04.017
53. Shim J-H, Lee J-S, Kim JY, *et al*. 2012, Bioprinting of a mechanically enhanced three-dimensional dual cell-laden construct for osteochondral tissue engineering using a multi-head tissue/organ building system, *Journal of Micromechanics and Microengineering*, vol.22(8): 085014. https://doi.org/10.1088/0960-1317/22/8/085014
54. Lee H, Ahn S, Bonassar LJ, *et al*. 2013, Cell (MC3T3-E1)-Printed Poly (ϵ-caprolactone)/Alginate Hybrid Scaffolds for Tissue Regeneration, *Macromolecular Rapid Communications*, vol.34(2): 142 149. https://doi.org/10.1002/marc.201200524
55. Park JY, Shim JH, Choi SA, *et al*. 2015, 3D printing technology to control BMP-2 and VEGF delivery spatially and temporally to promote large-volume bone regeneration, *Journal of Materials Chemistry B*, vol.3(27): 5415 5425. https://doi.org/10.1039/C5TB00637F
56. Yeo M, Lee H, Kim GH, 2016, Combining a micro/nano-hierarchical scaffold with cell printing of myoblasts induces cell alignment and differentiation favorable to skeletal muscle tissue regeneration, *Biofabrication*, vol.8(3): 035021. https://doi.org/10.1088/1758-5090/8/3/035021
57. Mota C, Puppi D, Chiellini F, *et al*. 2015, Additive manufacturing techniques for the production of tissue engineering constructs, *Journal of Tissue Engineering and Regenerative Medicine*, vol.9(3): 174 190. https://doi.org/10.1002/term.1635
58. Lutolf MP, Gilbert PM, Blau HM, 2009, Designing materials to direct stem-cell fate, *Nature*, vol.462(7272): 433 441. https://doi.org/10.1038/nature08602
59. Chung JH, Naficy S, Yue Z, *et al*. 2013, Bio-ink properties and printability for extrusion printing living cells, *Biomaterials Science*, vol.1(7): 763 773. https://doi.org/10.1039/c3bm00012e
60. Chang CC, Boland ED, Williams SK, *et al*. 2011, Direct-write bioprinting three-dimensional biohybrid systems for future regenerative therapies, *Journal of Biomedical Materials Research Part B: Applied Biomaterials*, vol.98B(1): 160 170. https://doi.org/10.1002/jbm.b.31831
61. Khalil S, Sun W, 2009, Bioprinting endothelial cells with alginate for 3D tissue constructs, *Journal of Biomechanical Engineering*, vol.131(11): 111002 111007. https://doi.org/10.1115/1.3128729
62. Cui XF, Breitenkamp K, Finn MG, *et al*. 2012, Direct human cartilage repair using three-dimensional bioprinting technology, *Tissue Engineering Part A*, vol.18(11 12): 1304 1312. https://doi.org/10.1089/ten.tea.2011.0543
63. Nair K, Gandhi M, Khalil S, *et al*. 2009, Characterization of cell viability during bioprinting processes, *Biotechnology Journal*, vol.4(8): 1168 1177. https://doi.org/10.1002/biot.200900004
64. Xu T, Gregory CA, Molnar P, *et al*. 2006, Viability and electrophysiology of neural cell structures generated by the inkjet printing method, *Biomaterials*, vol.27(19): 3580 3588. https://doi.org/10.1016/j.biomaterials.2006.01.048
65. Phillippi JA, Miller E, Weiss L, *et al*. 2008, Microenvironments engineered by inkjet bioprinting spatially direct adult stem cells toward muscle and bone like subpopulations, *Stem Cells*, vol.26(1): 127 134. https://doi.org/10.1634/stemcells.2007-0520
66. Cohen DL, Lo W, Tsavaris A, *et al*. 2010, Increased mixing improves hydrogel homogeneity and quality of three-dimensional printed constructs, *Tissue Engineering Part C: Methods*, vol.17(2): 239 248. https://doi.org/10.1089/ten.tec.2010.0093
67. Andersen T, Auk-Emblem P, Dornish M, 2015, 3D cell culture in alginate hydrogels, *Microarrays*, vol.4(2): 133 161.

https://doi.org/10.3390/microarrays4020133

68. Gaebel R, Ma N, Liu J, *et al*. 2011, Patterning human stem cells and endothelial cells with laser printing for cardiac regeneration, *Biomaterials*, vol.32(35): 9218 9230. https://doi.org/10.1016/j.biomaterials.2011.08.071
69. Wu P, Ringeisen B, 2010, Development of human umbilical vein endothelial cell (HUVEC) and human umbilical vein smooth muscle cell (HUVSMC) branch/stem structures on hydrogel layers via biological laser printing (BioLP), *Biofabrication*, vol.2(1): 014111. https://doi.org/10.1088/1758-5082/2/1/014111
70. Ker ED, Nain AS, Weiss LE, *et al*. 2011, Bioprinting of growth factors onto aligned sub-micron fibrous scaffolds for simultaneous control of cell differentiation and alignment, *Biomaterials*, vol.32(32): 8097 8107. https://doi.org/10.1016/j.biomaterials.2011.07.025
71. Ilkhanizadeh S, Teixeira AI, Hermanson O, 2007, Inkjet printing of macromolecules on hydrogels to steer neural stem cell differentiation, *Biomaterials*, vol.28(27): 3936 3943. https://doi.org/10.1016/j.biomaterials.2007.05.018
72. Lee W, Debasitis JC, Lee VK, *et al*. 2009, Multi-layered culture of hum an skin fibroblasts and keratinocytes through three-dimensional freeform fabrication, *Biomaterials*, vol.30(8): 1587 1595. https://doi.org/10.1016/j.biomaterials.2008.12.009
73. Duan B, Kapetanovic E, Hockaday LA, *et al*. 2014, Three-dimensional printed trileaflet valve conduits using biological hydrogels and human valve interstitial cells, *Acta Biomaterialia*, vol.10(5): 1836 1846. https://doi.org/10.1016/j.actbio.2013.12.005
74. Duan B, Hockaday LA, Kang KH, *et al*. 2013, 3D bioprinting of heterogeneous aortic valve conduits with alginate/gelatin hydrogels, *Journal of Biomedical Materials Research Part A*, vol.101(5): 1255 1264. https://doi.org/10.1002/jbm.a.34420
75. Gaetani R, Doevendans PA, Metz CH, *et al*. 2012, Cardiac tissue engineering using tissue printing technology and human cardiac progenitor cells, *Biomaterials*, vol.33(6): 1782 1790. https://doi.org/10.1016/j.biomaterials.2011.11.003
76. Lee H, Kim G, 2014, Enhanced cellular activities of polycaprolactone/alginate-based cell-laden hierarchical scaffolds for hard tissue engineering applications, *Journal of Colloid and Interface Science*, vol.430: 315 325. https://doi.org/10.1016/j.jcis.2014.05.065
77. Fedorovich NE, De Wijn JR, Verbout AJ, *et al*. 2008, Three-dimensional fiber deposition of cell-laden, viable, patterned constructs for bone tissue printing, *Tissue Engineering Part A*, vol.14(1): 127 133. https://doi.org/10.1089/ten.a.2007.0158
78. Cui X, Boland T, 2009, Human microvasculature fabrication using thermal inkjet printing technology, *Biomaterials*, vol.30(31): 6221 6227. https://doi.org/10.1016/j.biomaterials.2009.07.056
79. Norotte C, Marga FS, Niklason LE, *et al*. 2009, Scaffold-free vascular tissue engineering using bioprinting, *Biomaterials*, vol.30(30): 5910 5917. https://doi.org/10.1016/j.biomaterials.2009.06.034
80. Marga F, Jakab K, Khatiwala C, *et al*. 2012, Toward engineering functional organ modules by additive manufacturing, *Biofabrication*, vol.4(2): 022001. https://doi.org/10.1088/1758-5082/4/2/022001
81. Jakab K, Norotte C, Damon B, *et al*. 2008, Tissue engineering by self-assembly of cells printed into topologically defined structures, *Tissue Engineering Part A*, vol.14(3): 413 421. https://doi.org/10.1089/tea.2007.0173
82. Lee HJ, Kim YB, Ahn SH, *et al*. 2015, A New Approach for Fabricating Collagen/ECM-Based Bioinks Using Preosteoblasts and Human Adipose Stem Cells, *Advanced Healthcare Materials*, vol.4(9): 1359 1368. https://doi.org/10.1002/adhm.201500193

RESEARCH ARTICLE

Laser-assisted bioprinting at different wavelengths and pulse durations with a metal dynamic release layer: A parametric study

Lothar Koch[1*], Ole Brandt[2], Andrea Deiwick[1] and Boris Chichkov[1,3]

[1] Laser Zentrum Hannover e.V., Nanotechnology Department, Hollerithallee 8, 30419 Hannover, Germany
[2] DeutschesElektronen-Synchrotron (DESY), Notkestraße 85, 22607 Hamburg, Germany
[3] Leibniz Universität Hannover, Institut für Quantenoptik, Welfengarten 1, 30167 Hannover, Germany

Abstract: For more than a decade, living cells and biomaterials (typically hydrogels) are printed via laser-assisted bioprinting. Often, a thin metal layer is applied as laser-absorbing material called dynamic release layer (DRL). This layer is vaporized by focused laser pulses generating vapor pressure that propels forward a coated biomaterial. Different lasers with laser wavelengths from 193 to 1064 nanometer have been used. As a metal DRL gold, silver, or titanium layers have been used. The applied laser pulse durations were usually in the nanosecond range from 1 to 30 ns. In addition, some studies with femtosecond lasers have been published. However, there are no studies on the effect of all these lasers parameters on bioprinting with a metal DRL, and on comparing different wavelengths and pulse durations – except one study comparing 500 femtosecond pulses with 15 ns pulses. In this paper, the effects of laser wavelength (355, 532, and 1064 nm) and laser pulse duration (in the range of 8 to 200 ns) are investigated. Furthermore, the effects of laser pulse energy, intensity, and focal spot size are studied. The printed droplet volume, hydrogel jet velocity, and cell viability are analyzed.

Keywords: bioprinting, laser-assisted bioprinting, laser-induced forward transfer, laser absorption layer, laser parametric study

*Correspondence to: Lothar Koch, Laser Zentrum Hannover e.V., Nanotechnology Department, Hollerithallee 8, 30419 Hannover, Germany; Email: l.koch@lzh.de

Received: October 1, 2016; **Accepted:** November 25, 2016; **Published Online:** January 25, 2017

Citation: Koch L, Brandt O, Deiwick A, *et al*., 2017, Laser-assisted bioprinting at different wavelengths and pulse durations with a metal dynamic release layer: A parametric study. *International Journal of Bioprinting*, vol.3(1): 42–53. http://dx.doi.org/10.18063/IJB.2017.01.001.

1. Introduction

Printing of proteins, living cells and tissue is a rapidly growing scientific field. Different printing techniques are applied, mainly extrusion techniques (also called robotic dispensing or syringe based techniques), ink-jet printing, and laser-assisted bioprinting (also called biological laser printing, laser-induced forward transfer, or matrix-assisted pulsed laser evaporation direct-write (MAPLE-DW)).

For laser-assisted bioprinting (LaBP), a transparent substrate is usually coated with a thin layer of laser-absorbing material and a second thicker layer of biomaterial, typically a hydrogel with embedded cells, to be printed. Laser pulses are focused into the laser-absorbing layer, sometimes called Dynamic-Release-Layer (DRL), which is vaporized in the focal region, generating a vapor bubble (**Figure 1**). This

Laser-assisted bioprinting at different wavelengths and pulse durations with a metal dynamic release layer: A parametric study. © 2017 Lothar Koch, et al. This is an Open Access article distributed under the terms of the Creative Commons Attribution-NonCommercial 4.0 International License (http://creativecommons.org/licenses/by-nc/4.0/), permitting all non-commercial use, distribution, and reproduction in any medium, provided the original work is properly cited.

bubble expands by vapor pressure and propels the adjacent biomaterial forward, which then is deposited as a droplet at a predefined position on a collector slide.

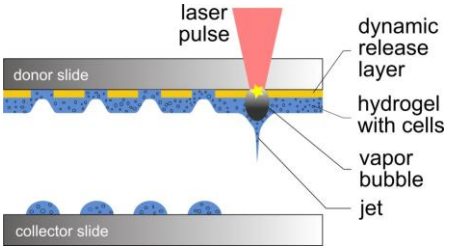

Figure 1. Schematic sketch of the laser-assisted bioprinting technique. The donor slide is coated with a thin laser-absorbing layer and a thicker layer of biomaterial to be transferred, usually a hydrogel with embedded cells. Laser pulses are focused through the donor glass slide into the absorbing layer. The evaporation of this layer in the laser-focused region generates a high vapor pressure that propels the biomaterial underneath towards the collector slide.

As a variant, some groups apply laser printing without dynamic-release layer. Therefore, they use hydrogel (with embedded cells) as the laser-absorbing material; a small part of it is vaporized thereby. Sometimes, they mix the hydrogel with a laser-absorbing material, a matrix material with a high absorption coefficient at the applied laser wavelength, which thereby will also become part of the printed structure. However, DRLs are assumed to enable a printing more softly and gently for the cells with a higher cell vitality after printing.

Several groups in the world have developed self-constructed laser bioprinting setups with different pulsed laser systems. Laser parameters vary in a wide range of wavelengths, pulse durations, pulse energies, and focal spot sizes. For the printing process, lasers with different wavelengths from 193 to 1064 nanometers and different laser pulse durations, mainly in the nanosecond range, are applied (**Figure 2**). They are combined with different DRL materials, including metals (gold, silver, or titanium), polymers (triazene, polyethylene naphthalate, polyimide, or cyanoacrylate), or hydrogels (gelatin). Most groups using LaBP for printing biomaterials apply ultraviolet (UV) lasers with 3 to 30 nanoseconds pulse durations and 193-nm[1,2], 248-nm[3,4], 266-nm[5], 337-nm[6], or 355-nm [7,8] wavelengths.

Alternatively, near-infrared (NIR) lasers with 10 or 30 nanoseconds of pulse duration and 1064-nm[9,10] wavelength are used in combination with metal DRLs (usually gold). Also femtosecond lasers were applied.

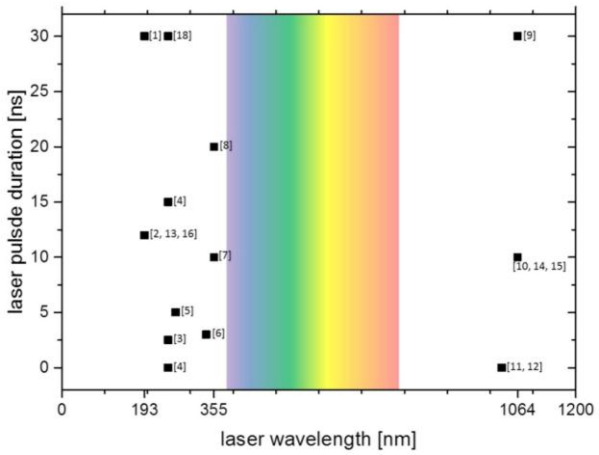

Figure 2. Chart of the laser wavelengths and pulse durations applied for laser-assisted bioprinting by different groups. Numbers in brackets refer to references. Typically, ultraviolet lasers and also some infrared lasers are used, but not lasers in the visible range (*ca.* 380–780 nm, colored background). Most common are pulse durations in the nanosecond range, but also experiments with femtosecond lasers have been conducted. Nanosecond lasers are usually preferred for their compactness and relatively simple maintenance and low costs.

Duocastella *et al.*[11] printed a glycerol-water blend using laser with 1027-nm wavelength and 450-fs pulse duration. Desrus *et al.*[12] printed cell medium and a glycerol-water blend, as well as keratinocytes with cell medium using 1030-nm laser wavelength, and 350-fs and 800-fs pulse durations. Due to the high electro-magnetic forces in the laser focus, these ultra-short pulse lasers are able to induce laser-absorbing plasma in water or hydrogels. Therefore, with laser pulse energy high enough, applying a DRL is not necessary[12].

In spite of this wide range of applied laser parameters, so far, their impact on the transfer process has hardly been analyzed in direct comparison–with the exception of laser pulse energy, laser pulse intensity, and the focal spot size. There is one publication, in which Dinca *et al.*[4] utilized laser-printed proteins and DNA with 500 femtoseconds of pulse duration at 248-nm wavelength and compared the results with those achieved with 15-ns pulse duration.

To narrow this knowledge gap, we studied the dependences of printed droplet volume and cell survival rate on laser wavelength, pulse duration, pulse power, and laser intensity in the focal spot. We applied two different lasers, a Nd:YAG laser with three different wavelengths (1064 nm, 532 nm, and 355 nm) and a Yb:YAG laser with the pulse durations in the range of 8 to 200 nanoseconds at 1064-nm wavelength.

The effect of laser parameters on the printing process depends on the applied laser-absorbing material. Different materials have individual advantages and disadvantages. If no DRL is applied, the process is (strongly) dependent on the optical properties of the matrix material at the applied wavelength; furthermore, cells near to the substrate might be harmed by laser radiation. Metals are good laser-absorbing materials and offer good wettability, enabling a homogeneous distribution of hydrogel layers. However, during laser printing, some metal debris are also transferred into the printed construct which is undesired for printed tissue, even when gold and titanium are inert and biocompatible materials.

Polymers as DRLs are hypothesized to be transformed completely into gaseous phase by laser-induced photo-chemical reactions; however, actually also some polymer debris become part of the printed structure. Even if they are nontoxic, they may have an impact on the cell behavior. Additionally, due to our experience, the distribution of hydrogel layers on some polymers is not as homogeneous and reproducible as on metals such as gold.

Alternatively, Schiele *et al*.[2] used gelatin as a DRL for LaBP at 193-nm laser wavelength. Gelatin is free of growth factors and matrix components that may influence cell behavior. However, the gelatin melted within one hour after printing at 37 °C. This is the typical temperature in human bodies and cell culture. Thus, it is not quite clear if this technique is suitable for 3-D printing, since cell-containing 3-D printed objects would possibly melt before cells could establish intercellular connections to maintain the 3-D cell pattern.

Other groups also applied an absorption layer system that is not completely evaporated, but experience a bulging effect. Lin *et al*.[13] used cyanoacrylate to glue brass foil on a quartz substrate; then they spread cells in medium on the foil. Laser pulses evaporated the cyanoacrylate and the generated bubble rapidly bulged the foil. The cell-medium compound was accelerated thereby and formed a jet. Brown *et al*.[8] used a 7-µm thick layer of polyimide, which was only partially evaporated near the quartz substrate as a confined pocket of gas. The vapor pressure forced the remaining polyimide layer away from the glass as a rapidly expanding blister. Thereby, the polyimide surface remains intact. This bulging or blister effect avoids the contamination of the printed structure with debris. So far, only low-viscosity liquids have been printed and it is not quite clear if also small droplets of hydrogels with higher viscosities can be printed by this way.

In this study, a metal layer is used, since it can be evaporated with all laser wavelengths, while polymer layers usually require UV wavelength below 400 nm. As DRL, we apply 60-nm thick layers of gold sputter-coated onto glass slides.

2. Material and Methods

2.1 The Printing Process and Setup

The laser printing device, in general, consists of the pulsed laser source and two horizontal co-planar glass slides (the upper one hereinafter is called the "donor slide" and the lower one is called the "collector slide"). The distance between the two slides is usually set to about 1 millimeter. The donor slide is coated underneath with a thin layer of laser-absorbing material and a thicker layer of biomaterial to be printed, which can be a hydrogel with embedded cells. Laser pulses are focused through the donor slide on the interface between the donor slide and absorption layer. This layer is evaporated in the focal spot, generating a vapor bubble, which rapidly expands. After a few microseconds, the bubble reaches its peak volume expansion and starts re-collapsing. Due to inertia, the accelerated hydrogel continues its motion and flows as a jet towards the collector slide (**Figure 1**).

The laser focal spot can be moved in x/y direction in the interfacial area between the donor slide and absorption layer. Furthermore, the glass slides can be moved relatively to each other. Thus, any pre-defined two-dimensional pattern and also three-dimensional patterns can be generated layer-by-layer. A more detailed description of the printing process and setup was given by Gruene *et al*.[14]

2.2 The Applied Lasers

Two pulsed lasers have been applied, a Ytterbium: YAG fiber laser (YLPM-1-A4-20-20, IPG Photonics Corp., Oxford, MA, USA) and a Neodym:YAG diode-pumped solid-state laser (Pulselas P-355-100-HP, AlphalasGmbh, Göttingen, Germany). The Yb:YAG fiber laser offers 7 different pulse durations in the nanosecond range (8, 14, 20, 30, 50, 100, 200 ns) at a laser wavelength of 1064 nanometer. The repetition rate can be chosen in the range of 1.6 to 1000 kHz, and the maximum power is 20 watt. The maximum pulse energy depends on the pulse duration and repetition rate. The Nd:YAG laser offers three different wavelengths (1064 nm, 532 nm, 355 nm; fundamental wavelength, second, and third harmonics) at repetition rates in the range of 0.4 to 1 kHz. Laser parameters are listed in **Table 1**.

Table 1. Parameters of the applied lasers

Laser	Nd:YAG[1]			Yb:YAG[2]
Wavelength [nm]	355	532	1064	1064
Pulse duration [ns]	0.5	0.52	0.75	8, 14, 20, 30, 50, 100, 200
Max. pulse energy [µJ]	8	17.5	85	200

[1] PULSELAS-P-355-100-HP, AlphalasGmbh; [2] YLPM-1-A4-20-20, IPG Photonics Corporation

2.3 Cell Culture

For all cell experiments in this study, murine fibroblast cell line NIH-3T3 was used. Asa cell culture medium, Dulbecco's Modified Eagle Medium/F12 supplemented with 10% fetal bovine serum and 1% penicillin/streptomycin (all from PAN Biotech, Aidenbach, Germany) was used and exchanged every third day.

2.4 Preparation of the Donor Layer System

For all presented printing experiments, 1-mm thick glass slides (26×26 mm²) were cleaned with acetone and lens cleaning tissue. The slides were coated with a 60-nm thick gold layer by sputter coating (208 HR, Cressington Scientific Instruments Ltd., Watford, England, UK) with argon. Thickness variation on one slide is low due to a planetary gear turning the glass slides while they are coated. The thickness of the coated layers was controlled with a thickness controller (MTM-20, Cressington Scientific Instruments Ltd., Watford, England, UK). All experiments were conducted with several donor slides with the same layer system to avoid that results are affected by one donor slide with potentially different layer thickness.

Onto this gold layer, a hydrogel layer, usually with embedded cells, was dispersed by blade coating. Here, a blend of 1 part 4 wt% alginate (Sigma-Aldrich), dissolved in a 0.15 M NaCl solution and sterilized by filtration with a 0.8-µm pore size filter, and 1 part EDTA blood plasma was applied. Cells were trypsinized, resuspended in a certain volume of cell medium, and counted with a hemocytometer. They were centrifuged at 500×g for 5 min and the supernatant was removed. The pellet, containing 1.5 million cells, was suspended in 45 µL of the alginate EDTA blood plasma blend. This hydrogel suspension was pipetted onto the gold-coated glass slide and dispersed on the gold surface with a blade coater to form a homogeneous layer of approximately 65-µm thickness.

2.5 Preparation of the Collector Slide

As collector slides, 1-mm thick glass slides (26×26 mm²) were cleaned in an ethanol bath and with acetone using lens cleaning tissue and sterilized by irradiating with UV-C light for 1 hour. For determination of the survival rates of printed cells, the collector slides were coated with 45 µL of 2 wt% alginate hydrogel. Primarily, this hydrogel layer prevents the dying of printed cells by drying-up, but it also cushions the impact of the laser printing process. For analyzing printed droplet sizes, uncoated glass slides were used.

2.6 Measuring Droplet Sizes

For measuring the sizes of printed droplets, the same alginate was always printed on uncoated glass surfaces. Therefore, there is a constant relation between the printed droplet diameter and volume. The volume can be calculated from the diameter by consideration of the contact angle. The contact angle of the applied alginate on glass was measured by the sessile drop method with contact angle measuring device OCA 40Micro (DataPhysics Instruments GmbH, Germany) to be 31° ± 4°. The volume of a spherical segment is $V_{droplet} = \pi/3 \cdot a^3 \cdot (\sin\theta) - 3 \cdot (1 - \cos\theta)^2$. $(2+\cos\theta)$ with radius a of the contact area and contact angle θ. With the contact angle of 31° ± 4°, the volume of the alginate droplets on the glass surface is $V_{droplet} = (0.45 \pm 0.07) \cdot a^3$.

2.7 Characterization of Laser Pulses

The temporal pulse shapes were measured with a photodiode (DET210, ThorlabsGmbh, Dachau, Germany) with a rise time of one nanosecond and an oscilloscope (WaveRunner 62Xi, Teledyne LeCroy GmbH, Heidelberg, Germany). 1000 pulses were averaged for each measurement. The laser pulse energy was determined by measuring the laser power with a laser power meter (Powermax PM10 + Fieldmax II TOP, Coherent Europe BV, Utrecht, The Netherlands) and divided by the laser pulse repetition rate. Spatial pulse shapes were recorded with a beam profiler (Beamstar FX, OphirSpiricon Europe GmbH, Darmstadt, Germany).

2.8 Visualization of the Jetting and Measurement of Jet Velocity

The printing process and the material transfer by formation of a hydrogel jet for some hundred microseconds was visualized and surveyed with an microscopic setup developed in-house with a digital SLR camera

(EOS 450D, Canon, Krefeld, Germany), stroboscopic illumination with a flashlamp (Nanolite KL-M, High-Speed Photo-System, Wedel, Germany) with 11 nanoseconds flash duration, and microscope objective (M Plan Apo NIR 20x, Mitutoyo, Neuss, Germany). A full description of this setup has been published before[15].

2.9 Determination of the Survival Rate

The survival rate of printed cells was determined by rinsing most cells from the donor and collector slides separately after printing, staining the dead cells with Trypan Blue, and counting all cells and dead cells within a hemocytometer. The survival rate was calculated as the percentage of vital cells from the collector slide divided by the percentage of vital cells from the donor slide. Cell survival rates were determined for printing with both, the Yb: YAG laser (at 1064-nm wavelength with 8- and 200-ns pulse duration) and the Nd:YAG laser (wavelength/pulse duration: 1064 nm/750 ps; 532 nm/523 ps; 355 nm/500 ps). The laser pulse energy was adjusted to print about 50% of the cells from the donor to the collector slide.

2.10 Determination of Cell Viability after 24 hours

Cell membrane integrity of printed and non-printed NIH-3T3 cells was assessed by measuring the lactate dehydrogenase (LDH) leakage due to cell membrane damage into the culture medium. The amount of LDH released is proportional to the number of cells damaged or lysed. Briefly, cells were seeded at a density of 5×10^4 cells/well in culture medium into a 24-well culture plate and incubated for 24 hours. Then, the culture medium was removed and the release of LDH into the supernatant was determined by the LDH activity assay according to the online protocol of OPS Diagnostics (Lebanon, NJ, USA). The absorbance was detected at 492-nm wavelength using a microplate reader (Tecan Infinite M200Pro and Tecan i-control™ software, Crailsheim, Germany). Treatment of cells with 1% Triton-X100 served as a 100% positive control of cell damage. The results are given relative to the positive control, in percent. The metabolic activity of living and healthy cells after printing was assayed using Alamar Blue dye (Sigma-Aldrich, Deisenhofen, Germany). Viable cells are able to reduce resazurin (blue) into resorufin (pink) during a specific time span, providing a method for optical detection of cell metabolic activity. Briefly, 20 hours after cell seeding, Alamar Blue dye (resazurin 20 µg/mL culture medium) was added to the cells. After 4 hours of incubation, the absorbance of the solution was measured at 570 nm, with a reference wavelength of 600 nm on a microplate reader.

3. Results

3.1 Wavelength Variation

The dependence of the printed droplet size on laser wavelength and pulse energy was investigated. There are printing thresholds of 12 µJ at 1064-nm, 6 µJ at 532-nm, and 3 µJ at 355-nm wavelengths. Above the threshold, the printed droplet volume increases with the increasing pulse energy, as depicted in **Figure 3.** Applying laser pulses with 1064 nm wavelength at the laser pulse energy of 30 µJ, a maximum droplet volume of about 2.4 ± 0.4 nL is reached. With further growing laser pulse energy the droplet volume increases only slightly. The same droplet volume can be printed with 532-nm wavelength at the lower laser pulse energy of 17.5 µJ, but this droplet volume cannot be reached with 355-nm wavelength due to the limited laser pulse energy, below 8 µJ.

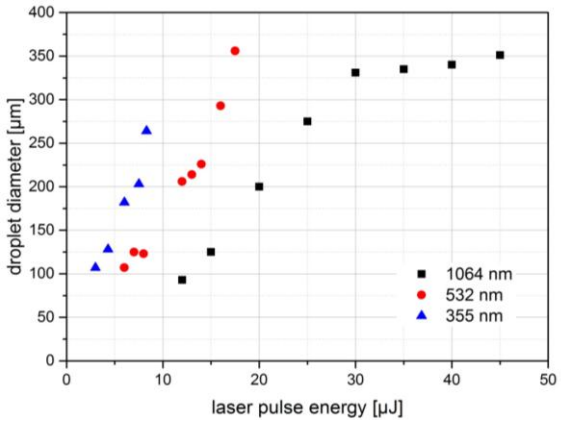

Figure 3. Printed droplet volume dependence on laser wavelength and pulse energy. The size of alginate droplets printed with three different wavelengths and different laser pulse energies. There is an upper droplet size limit (near 350-µm droplet diameter) depending on the hydrogel layer thickness as a limitation of available hydrogel. Since the laser maximum pulse energy for 355 nm (and 532 nm) is much smaller compared to 1064-nm wavelength, the upper droplet size limit has not been reached with 355 nm. Nevertheless, it can be concluded that the achievable droplet size is quite similar for all investigated wavelengths. With 1064 nm, a bit smaller droplets can be printed.

At the same laser pulse energy, but different wavelengths, the printed droplet diameter is about twice as big (the volume is about one order of magnitude higher) at wavelength 355 nm compared to 532 nm,

and at 532 nm compared to 1064 nm. With 1064-nm wavelength, slightly smaller droplets can be printed.

Figure 4A depicts stroboscopic images with defined delay relative to the laser pulse impact for the three different wavelengths with different pulse energies of 20 µJ (1064 nm), 12 µJ (532 nm), and 8 µJ (355 nm), which resulted in the same printed droplet volumes (**Figure 3**). The images are very similar for all wavelengths; with 355-nm wavelength the jet duration is a bit shorter (about 400 µs), while the jet flows for about 500 µs at 532- and 1064-nm wavelengths.

3.2 Pulse Duration Variation

For studying the influence of laser pulse duration on the printing process, it needs to be checked if other laser parameters are changed by varying the pulse duration. Besides the laser pulse energy, this may also affect temporal or spatial pulse shape. **Figure 5A** shows that the temporal shape of laser pulses is not a real flat top profile; the laser power slightly decreases during the pulse duration. However, the rising edge of laser pulses at all pulse durations is similar and longer pulses largely coincide with shorter one at the beginning. Furthermore, pulse energy variations do not substantially change the temporal pulse shape, as can be seen in **Figure 5B** for 200-ns pulses. Therefore, the pulse peak power is proportional to the pulse energy for given pulse duration (**Figure 5C**). The spatial profile of the laser pulse proves to be independent on the pulse duration, as shown for 8- and 200-ns pulses in **Figure 5D**.

Stroboscopic imaging of the printing process depicts that the process and its time scale is independent on different pulse durations from 8 ns to 200 ns (shown in **Figure 4B**) and also for 750 ps (**Figure 4A**).

3.3 Variation of the Biomaterial Layer Thickness at Fixed Laser Pulse Energies for Different Pulse Durations

The images in **Figure 6A** demonstrate that similar droplet volumes (a droplet diameter of 150 µm corresponds to a volume of 190 pL) can be achieved with all applied pulse durations (20 ns is not shown) at different pulse energies and peak powers. To investigate the interrelation between the laser pulse duration, laser pulse energy and biomaterial layer thickness, the laser pulse energies were chosen for 200- and 8-ns pulse durations to transfer the same droplet volume for 65-µm layer thickness (45-µL biomaterial volume). Further printing with these laser pulse energies using different increasing layer thicknesses was conducted. As can be seen in **Figure 6B**, with 80- and 95-µm thickness (55- and 65-µL biomaterial volume) the transferred droplets are quite similar for both pulse durations. However, with biomaterial layer thicknesses of 120 µm (80 µL) and 130 µm (90 µL), there are still

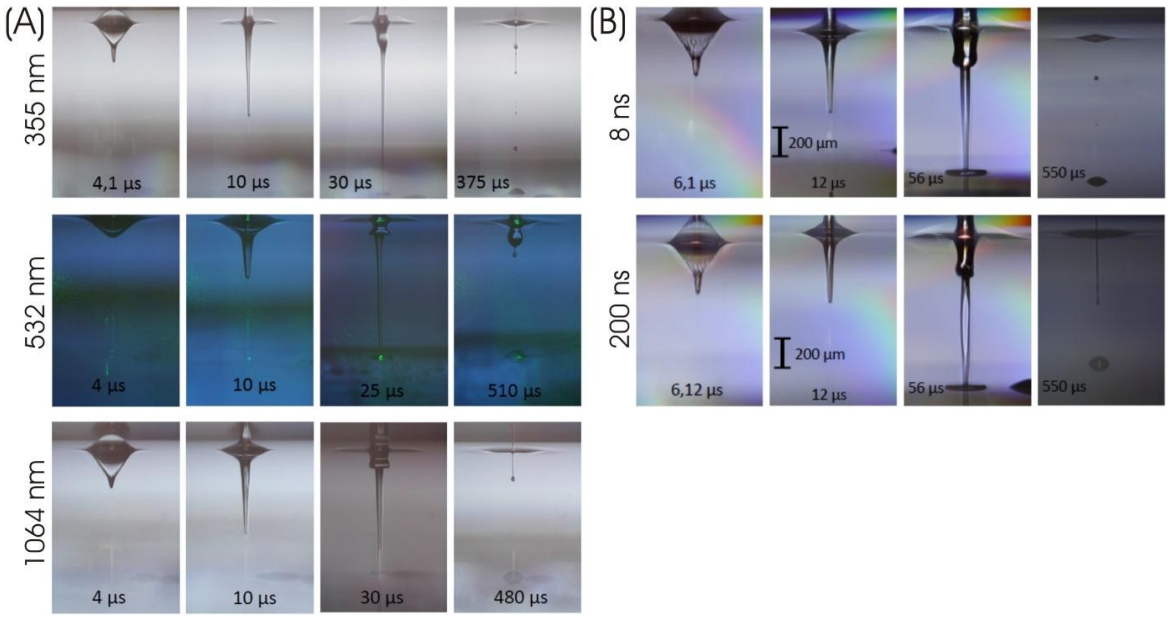

Figure 4. Visualization of the jet dynamics, induced by laser pulses with different (A) wavelengths and (B) pulse durations. Nanosecond stroboscopic illumination was applied to take images at defined delays with respect to the laser pulse impact. There is no substantial dependence of the jet dynamics for metal DRL on laser wavelengths or pulse durations. The process merely is a little bit faster for 355-nm (about 400 µs instead of approximately 500 µs) compared to 532- and 1064-nm wavelengths.

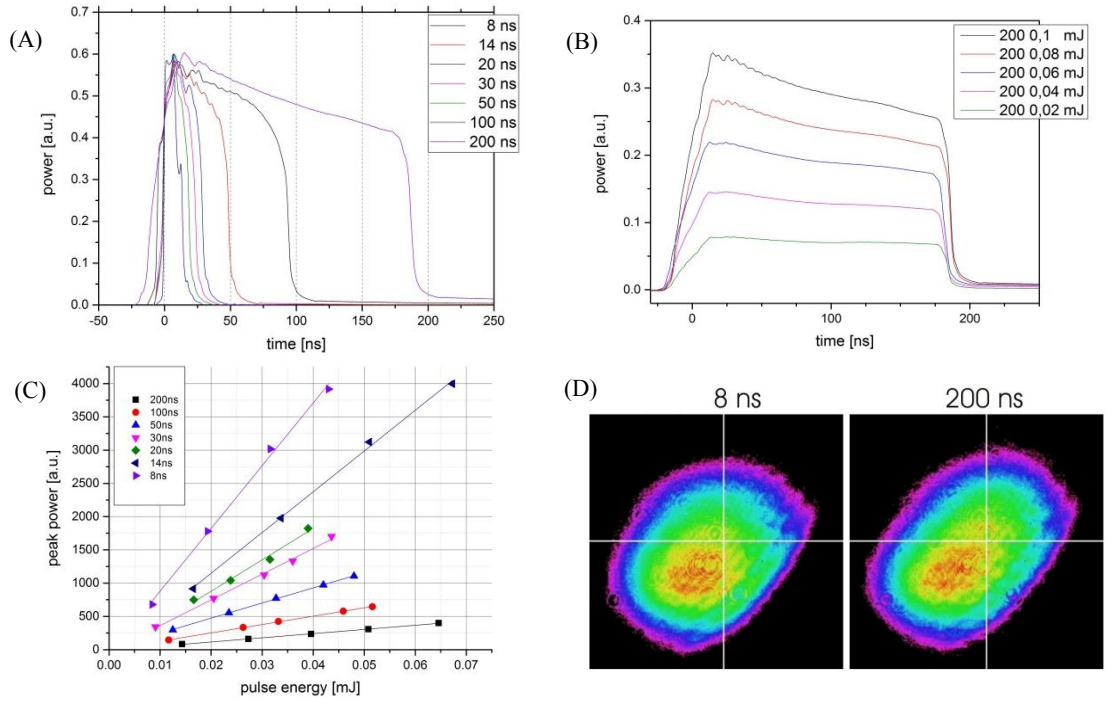

Figure 5. Laser pulse characteristics of the Yb:YAG laser with different:(a, d) pulse durations and (b, c) pulse energies. (A) Pulses with 8- to 200-ns time durations with similar peak power are measured and averaged over 1000 pulses with a photodiode and oscilloscope; (B) The temporal shape of the laser pulses (shown for 200-ns laser pulses) varies only slightly with pulse energies; (C) The relation between the pulse energy and peak power for different pulse durations is nearly proportional; (D) The transversal mode (spatial shape) of the laser pulses is nearly independent on pulse duration (shown for 8 and 200 ns).

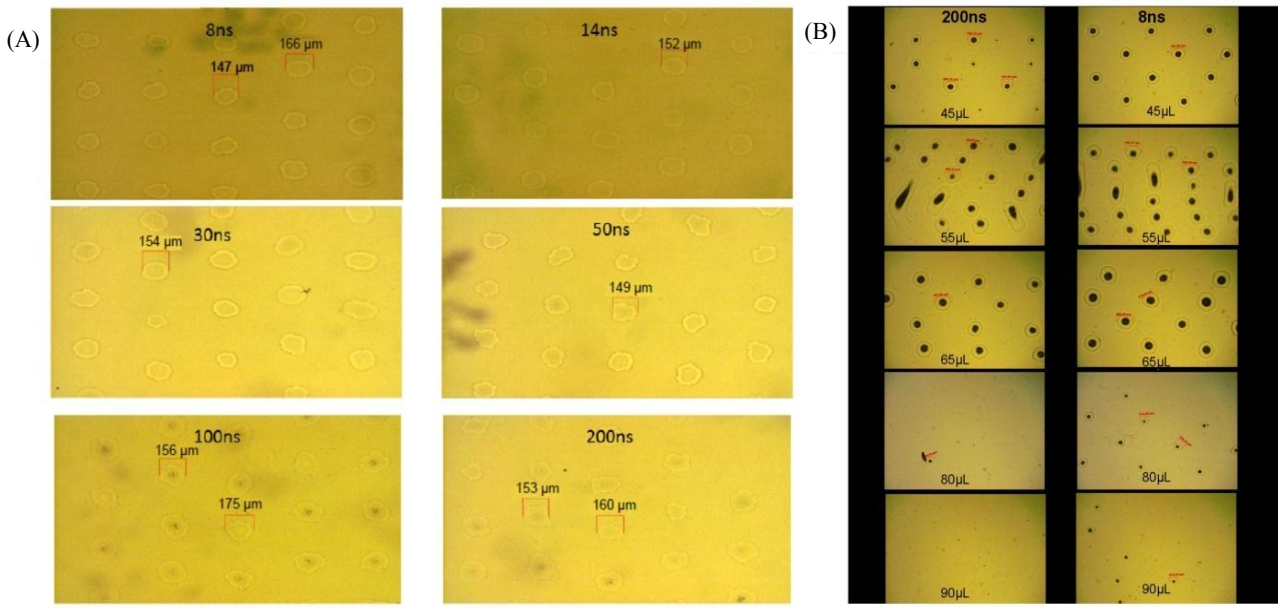

Figure 6. **(A)** Different combinations of pulse duration, energy, and peak power can result in similar printed droplet sizes; here, alginate droplets with about 150–160 µm diameter were printed with different pulse durations and adjusted energy. **(B)** Printing with different pulse durations (200 and 8 ns) and alginate layer thickness; the pulse energies were adjusted for similar printed droplet sizes at 65-µm layer thickness (45-µL alginate). Keeping these two pulse energies constant, printing with different layer thicknesses was tested. The printing result was similar for both pulse durations at 80-µm (55 µL) and 95-µm (65 µL) layer thickness. However, nearly no hydrogel was printed with 200-ns pulses at layer thickness above 115 µm (80 µL and 90 µL), while many droplets were printed with 8-ns pulses.

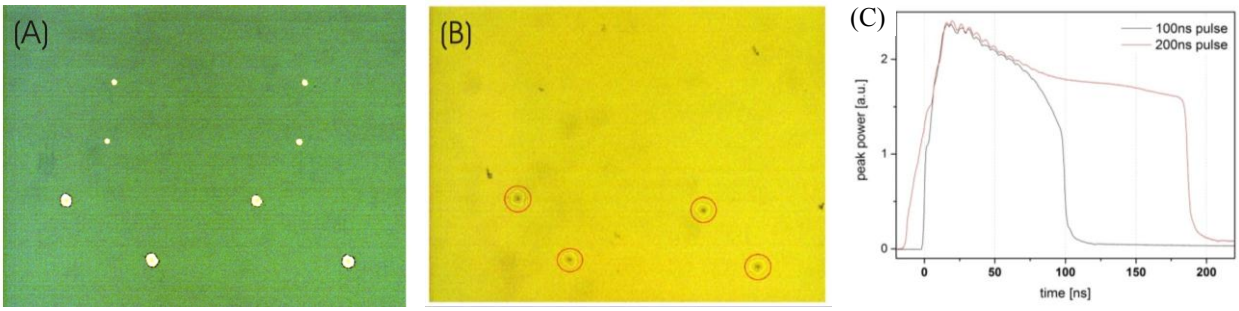

Figure 7. The effect of laser pulse duration at constant peak power. (A) Image of the donor slide after printing: There are eight holes in the gold layer indicating the focal spot position for 100-ns pulses (four smaller holes) and 200-ns pulses (four bigger holes). (B) Image of the collector slide. Four printed hydrogel droplets corresponding to the position of the 200-ns pulses can be seen but no hydrogel droplets printed with 100-ns pulses. (C) Alginate droplets were printed with 100- and 200-ns pulses with the same peak power and similar temporal shapes at the first 80 ns of the laser pulse.

many printed droplets with the shorter pulse duration, but only sporadic (80 µL) or no droplets with 200-ns pulse duration.

Furthermore, it has been studied whether or not long laser pulses still have an impact on the printing process after inducing generation of plasma and an expanding vapor bubble; probably, there could be a limitation in time for pumping the vapor bubble, thus the last part of a longer pulse has no further effect. Therefore, droplets were printed with the two longest pulse durations 200 and 100 ns at the same peak power. It turned out that even after 100 ns, the plasma still absorbs energy from the (200 ns) laser pulse that contributes to the material transfer. For the applied peak power in **Figure 7**, no biomaterial was printed with the 100-ns pulse, whereas droplets were printed with 200-ns pulses – although the shorter pulses induced plasma (and thereby a vapor bubble) as well.

The dependence of the printed droplet volume on pulse duration, pulse energy and peak power is shown in **Figure 8**. Droplets with the same volume can be printed with very different combinations of these laser parameters (depicted as lines). There is a linear dependency but not a proportionality of the laser pulse energy required to print a certain droplet volume and the pulse duration. The required energy E_{pulse} can be described by the formula $E_{pulse} = E_0 + m \cdot \tau_{pulse}$ with τ_{pulse} being the pulse duration. Taken from **Figure 8B**, E_0 is about 20 µJ and m is in the range of 150 to 300 Watt. Since the laser pulses peak power is proportional to the quotient of laser pulse energy and duration, the required peak power can be calculated as $P_{peak} \approx \frac{E_{pulse}}{\tau_{pulse}} + m$. Entering the values 20 µJ for E_0 and 150 to 300 Watt for *m*, the calculated peak power is in good agreement with **Figure 8(C)**.

3.4 Focal Spot Size Variation

Besides laser wavelength, pulse duration, energy, and peak power, the printing process might also be affected by the laser focal spot size. One aspect of the printing process, which is influenced by these parameters, is the velocity of the hydrogel jet that might affect the vitality of printed cells. Zhang *et al.*[16] demonstrated printing with jet velocities down to 10 m/s, while the jet velocities in our study have been about 50 m/s so far. Therefore, printing of alginate droplets with three different focal spot sizes (3000, 4000, and 7500 µm²) and the generated jet velocities have been investigated for different laser pulse energies (**Figure 9A**). As expected, the jet velocity increases with increasing laser pulse energy. The jet velocity is higher for smaller focal spot sizes at fixed laser pulse energy. More interestingly is the dependence of the jet velocity on the laser intensity (**Figure 9B**). At lower intensities, the jet velocity is independent or nearly independent on the focal spot size. By increasing the intensity, the jet velocities for the three different spot sizes separate. Above 1 J/cm² the jet velocity at 7500-µm² spot size is much higher than the velocities at 3000- or 4000-µm² spot sizes, which are still nearly equal. Above 1.4 J/cm² the jet velocity at 4000-µm² spot size is also higher compared to the velocity at 3000-µm² spot size.

3.5 Cell Survival Rates

The cell survival rates are listed in **Figure 10A**. They have been determined as 97 ± 1.5% (1064 nm wavelength/200 ns pulse duration), 95 ± 3.8% (1064 nm/8 ns), 93.5 ± 2.2% (1064 nm/750 ps), 95 ± 4.2%

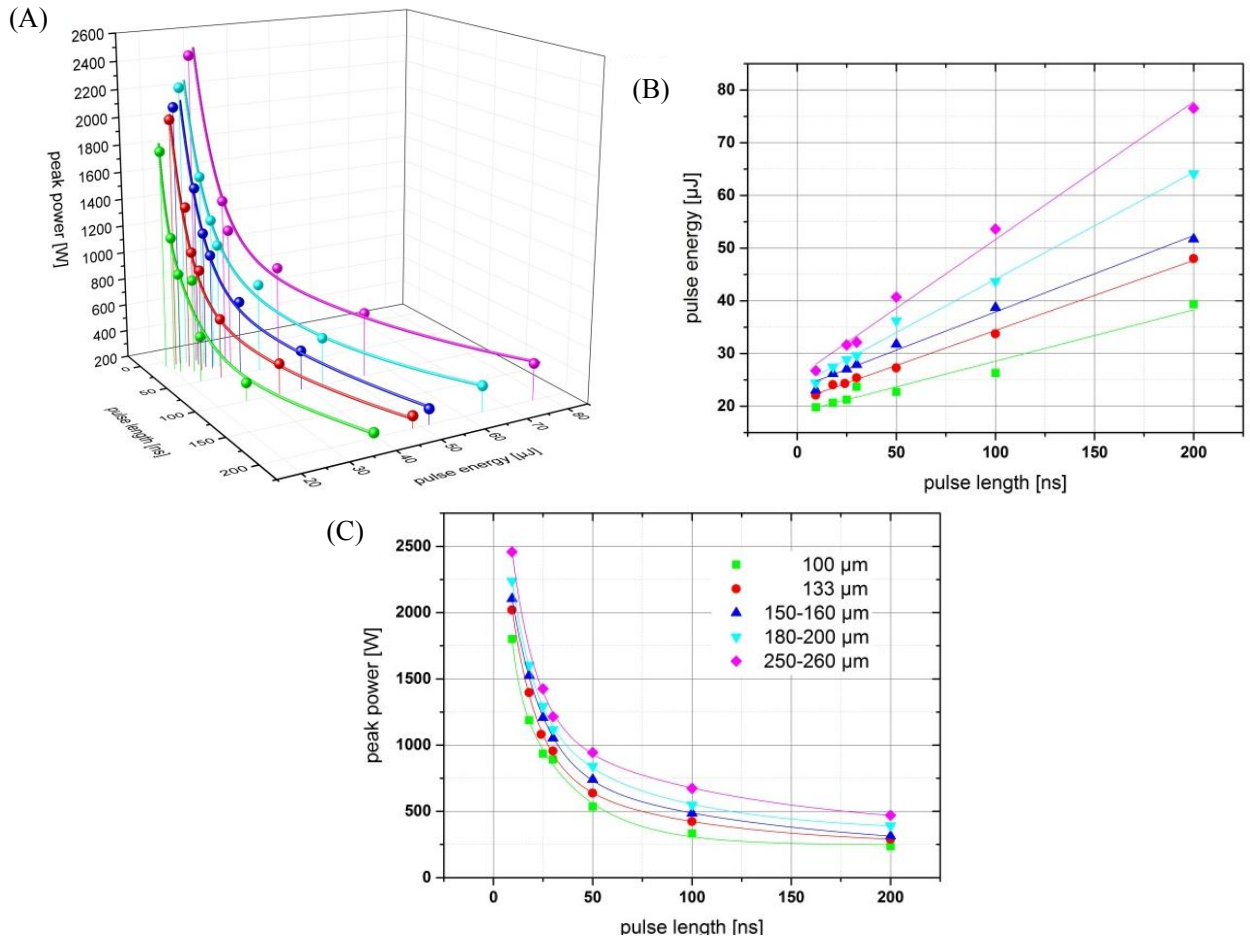

Figure 8. Dependence of the printed droplet size on laser pulse duration, pulse energy, and resulting peak power. Each color represents a different printed droplet size. The measured values are depicted as spheres; the lines represent curves fitted to the measured values. With increasing pulse duration, the required energy increases linear (but not proportional) and the required peak power decreases inversely.

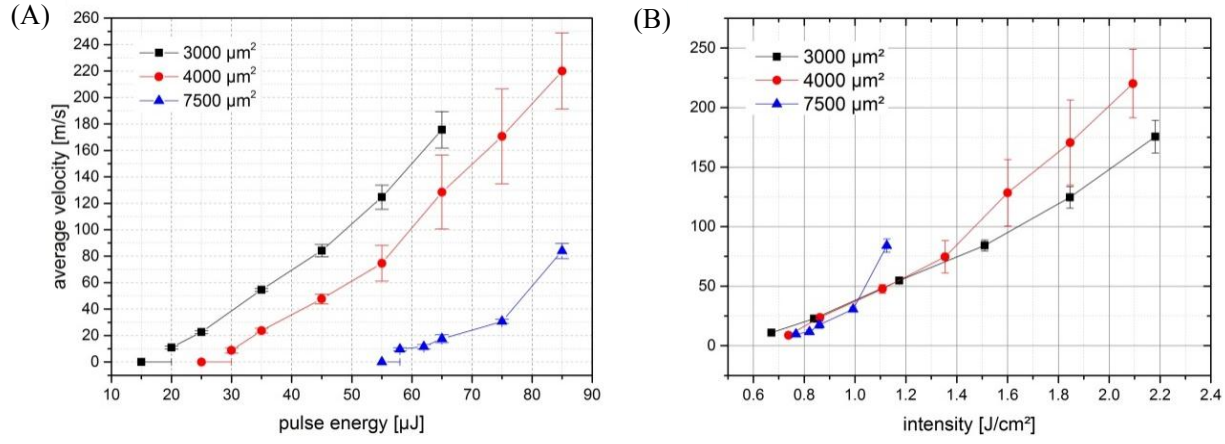

Figure 9. Dependence of the jet velocity on laser pulse energy and intensity. With three different focal spot sizes, the average jet velocity was observed at different pulse energies and intensities. For low energies (and intensities), the jet velocity depends only on the intensity and not on the pulse energy. With increasing intensity, however, pulse energy becomes more important and the jet velocity differs at equal intensity but different focal spot sizes and pulse energy.

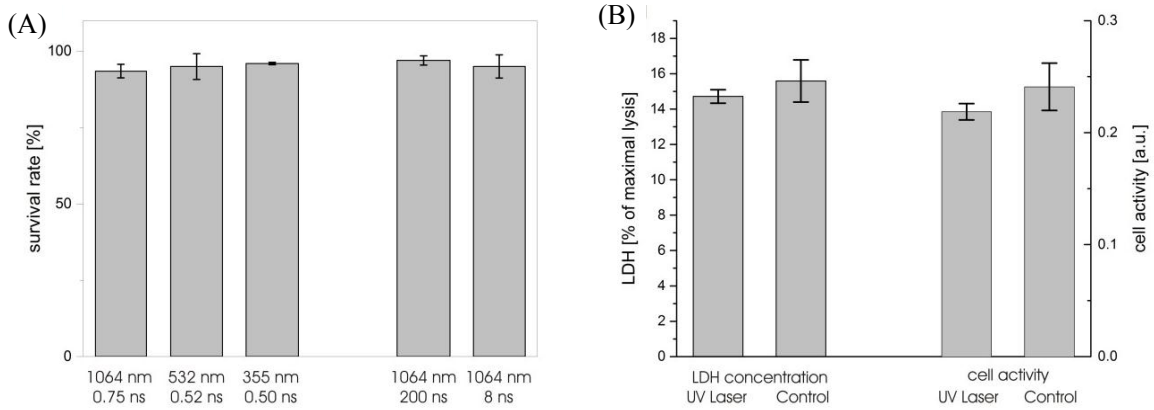

Figure 10. Vitality of fibroblast cells laser-printed with different wavelengths and pulse durations. The survival rate **(A)** was determined one hour after printing by counting vital and dead cells stained with Trypan Blue. The vitality after 24 hours was analyzed by measuring the amount of LDH **(B)** in the cell medium as a measure for dead cells and the transformation of Alamar Blue dye as a measure for the metabolic activity of living and healthy cells after printing.

(532 nm/523 ps), and 96 ± 0.4% (355 nm/500 ps). There is no significant difference ($p > 0.05$) in the cell survival rate at different pulse durations and wavelengths.

To exclude cell damage by UV radiation that might not directly kill cells, additionally a lactate dehydrogenase (LDH) assay was conducted with cells embedded in alginate and printed at 355-nm wavelength, 500-ps pulse duration, and 8-µJ pulse energy. The enzyme LDH, found in most living cells, is released after cell damage. Thus, it can be used as a quantitative measure for cell damage. Therefore, after 24 hours the amount of LDH in the medium was measured. The results are shown in **Figure 10B** on the left side. No significant ($p = 0.50$) difference between the printed and control cells was detected. Additionally, the cell activity was investigated with Alamar Blue assay (**Figure 10B**, right side). There is also no significant difference ($p = 0.34$) in the cell activity between the cells printed with UV laser and control cells.

4. Discussion

To our knowledge, this is the first extensive study on the effect of different laser parameters on laser-assisted bioprinting of hydrogel and cells. Of course, the effect of laser pulse energy and focal geometry has been investigated before. Here we studied the role of laser wavelength, pulse duration (in the nanosecond regime), pulse energy, focal spot size, and laser intensity.

The aim of this study was to investigate the dependence of laser-assisted bioprinting on specific laser parameters and identify optimal parameters. To cover a broad range of different parameters, especially of different pulse durations and laser wavelengths, two different lasers were applied.

First, the influence of laser wavelength was studied with gold DRL. If the laser wavelength was varied at fixed pulse energy, there was a substantial effect on printed droplet volume. With shorter wavelengths, less energy was required to print a certain droplet volume. However, this effect can be compensated by adjusting the laser pulse energy. In combination with well-adapted laser pulse energy, the influence of laser wavelength turned out to be very small. At 1064-nm wavelength, droplets with slightly smaller volume could be printed, and at 355 nm, the jet duration was a bit shorter. Thus, applying a gold absorption layer, there is no evidence for an optimal laser wavelength.

Second, printing with different laser pulse durations was investigated. The volume of the printed droplet depends on both laser pulse energy and peak power. At least up to 200-ns pulse duration, the laser pulse still influences the printing process and laser pulse energy irradiating after more than 100 ns can contribute in inducing the jet dynamic.

To achieve the same droplet volumes with different pulse durations, the required energy increases linearly but not proportional with the pulse duration while the required peak power decreases with an inverse proportional part plus a constant minimum peak power.

At shorter pulse durations, the droplet volume increases faster with increasing laser pulse energy. Therefore, statistical variations of the laser pulse energy have a larger impact on the droplet volumes at shorter pulse durations, although the difference is not big. This indicates that a part of the energy of longer laser pulses (a bigger part compared to shorter

laser pulses) is not transferred into kinetical energy of the printing process. It is probably transferred into thermal energy, since significant thermal conduction occurs within tens of nanoseconds[17].

A further important parameter for the printing process is the focusing geometry with the focal spot size determining the relation between the laser pulse energy and intensity. Here, we investigated to what extent the printing process is dependent on energy or intensity of the laser pulse. Therefore, the formation and velocity of the hydrogel jet were observed with the stroboscopic imaging system; in general, a low jet velocity stands for low shear forces. It turns out that for low intensities above the threshold for printing at about 0.7 J/cm², the jet velocity is dependent only on laser pulse intensity and is independent on the focal spot size (at least above 3000 µm²). With increasing intensity the energy becomes a more relevant parameter. Since the droplet volume increases with the laser pulse energy, bigger droplets can be achieved without increasing shear forces. Therefore, the pulse energy has to be increased at constant intensity by increasing the focal spot size.

The influence of the investigated laser parameters, wavelength and pulse duration, on cell survival and vitality has also been studied. As can be seen in **Figure 10**, the cell survival rate is independent of the applied wavelengths. This might be different if no absorption layer is applied and wavelengths in the deep UV are used. However, studies of other groups demonstrated high survival rates also with such wavelengths.

5. Conclusion

The objective of this study was to investigate the existence of optimal laser parameters for the laser-assisted bioprinting technique and to identify these parameters if indicated. Since an optimum LaBP system should be equipped with a compact and relatively inexpensive laser system, this study is limited to the parameter range of Q-switched solid state lasers with nanosecond and sub-nanosecond pulse durations. Nanosecond lasers are also most commonly applied for laser-assisted bioprinting by other groups. In addition, some studies with femtosecond lasers have been published. However, there are no studies investigating the effect of the usually inalterable laser parameters wavelength and pulse duration on LaBP to an extent that they could serve as a basis for a laser purchase decision. The present study should contribute to remedy of this deficiency.

It turns out that in combination with a metal DRL, a wide range of laser wavelengths and pulse durations can be applied and no optimal parameters really exist. Therefore, other laser parameters can be decisive such as pulse-to-pulse and long-term stability, compactness, or inexpensiveness. However, wavelengths and pulse durations outside the investigated range, especially even longer pulse durations, might be less suitable for LaBP. Furthermore, if other absorption materials such as polymers are used, a significant effect of the applied wavelength would be expected and UV lasers are often preferred. Additionally, investigating the effect of the parameters laser pulse energy, focal spot size, and the resulting pulse intensity also did not identify specific optimal parameters but a complex dependence of droplet volume and jet velocities on focus geometry and pulse energy.

In conclusion, this study does not identify the best laser for LaBP, but demonstrates that a wide variety of lasers can be applied for LaBP with metal DRL.

Conflict of Interest and Funding

No conflict of interest was reported by all authors. The authors acknowledge financial support from Deutsche Forschungsgemeinschaft (DFG), the Cluster of Excellence REBIRTH, and Lower Saxony project Biofabrication for NIFE.

References

1. Palla-Papavlu A, Paraico I, Shaw-Stewart J, *et al*., 2011, Liposome micropatterning based on laser-induced forward transfer. *Applied Physics A*, vol.102(3): 651–659. https://doi.org/10.1007/s00339-010-6114-1
2. Schiele NR, Chrisey DB, and Corr DT, 2011, Gelatin-based laser direct-write technique for the precise spatial patterning of cells. *Tissue Engineering Part C: Methods*, vol.17(3): 289–298. https://doi.org/10.1089/ten.tec.2010.0442
3. Pirlo RK, Wu P, Liu J, *et al*., 2012, PLGA/hydrogel biopapers as a stackable substrate for printing HUVEC networks via BioLP™. *Biotechnology and Bioengineering*, vol.109(1): 262–273. https://doi.org/10.1002/bit.23295
4. Dinca V, Farsari M, Kafetzopoulos D, *et al*., 2008, Patterning parameters for biomolecules microarrays constructed with nanosecond and femtosecond UV lasers. *Thin Solid Films*, vol.516(18): 6504–6511. https://doi.org/10.1016/j.tsf.2008.02.043
5. Othon CM, Wu X, Anders JJ, *et al*., 2008, Single-cell

printing to form three-dimensional lines of olfactory ensheathing cells. *Biomedical Materials*, vol.3(3): 034101.
https://doi.org/10.1088/1748-6041/3/3/034101

6. Horneffer V, Linz N, and Vogel A, 2007, Principles of laser-induced separation and transport of living cells. *Journal of Biomedical Optics*, vol.12(5): 054016.
https://doi.org/10.1117/1.2799194
7. Duocastella M, Fernández-Pradas JM, Morenza JL, *et al*., 2010, Sessile droplet formation in the laser-induced forward transfer of liquids: A time-resolved imaging study. *Thin Solid Films*, vol.518(18): 5321–5325.
https://doi.org/10.1016/j.tsf.2010.03.082
8. Brown MS, Brasz CF, Ventikos Y, *et al*., 2012, Impulsively actuated jets from thin liquid films for high-resolution printing applications. *Journal of Fluid Mechanics*, vol.709: 341–370.
https://doi.org/10.1017/jfm.2012.337
9. Ali M, Pages E, Ducom A, *et al*., 2014, Controlling laser-induced jet formation for bioprinting mesenchymal stem cells with high viability and high resolution. *Biofabrication*, vol.6(4): 045001.
https://doi.org/10.1088/1758-5082/6/4/045001
10. Taidi B, Lebernede G, Koch L, *et al*., 2016, Colony development of laser printed eukaryotic (yeast and microalga) microorganisms in co-culture. *International Journal of Bioprinting*, vol.2(2): 37–43.
https://doi.org/10.18063/IJB.2016.02.001
11. Duocastella M, Patrascioiu A, Fernández-Pradas JM, *et al*., 2010, Film-free laser forward printing of transparent and weakly absorbing liquids. *Optics Express*, vol.18(21): 21815–21825.
https://doi.org/10.1364/OE.18.021815
12. Desrus H, Chassagne B, Catros S, *et al*., 2016, *Proceedings of SPIE 9706—Optical Interactions with Tissues and CellsXXVII,97060O, March 7, 2016: Laser assisted bioprinting using a femtosecond laser with and without a gold transductive layer: A parametric study*. SPIE Digital Library, USA.
https://doi.org/ 10.1117/12.2209087
13. Lin Y, Huang Y, and Chrisey DB, 2011, Metallic foil-assisted laser cell printing. *Journal of Biomechanical Engineering*, vol.133(2): 025001.
https://doi.org/10.1115/1.4003132
14. Gruene M, Unger C, Koch L, *et al*., 2011, Dispensing pico to nanolitre of a natural hydrogel by laser-assisted bioprinting. *Biomedical Engineering Online*, vol. 10: 19.
https://doi.org/10.1186/1475-925X-10-19
15. Unger C, Gruene M, Koch L, *et al*., 2011, Time-resolved imaging of hydrogel printing via laser-induced forward transfer. *Applied Physics A*, vol.103(2): 271–277.
https://doi.org/10.1007/s00339-010-6030-4
16. Zhang Z, Xiong R, Mei R, *et al*., 2015, Time-resolved imaging study of jetting dynamics during laser printing of viscoelastic alginate solutions. *Langmuir*, vol.31(23): 6447− 6456.
https://doi.org/10.1021/acs.langmuir.5b00919
17. Sharma MK, 2013, *Optimization of laser induced forward transfer by finite element modeling*. Master thesis, Royal Institute of Technology-KTH, Stockholm, Sweden, viewed October 2, 2016.
<http://www.diva-portal.org/smash/get/diva2:617570/fulltext01.pdf>
18. Hopp B, Smausz T, Antal Z, *et al*., 2004, Absorbing film assisted laser induced forward transfer of fungi (*Trichoderma conidia*). *Journal of Applied Physics*, vol.96(6): 3478–3481.
https://doi.org/10.1063/1.1782275

RESEARCH ARTICLE

3D bioprinting of stem cells and polymer/bioactive glass composite scaffolds for bone tissue engineering

Caroline Murphy[1,a], Krishna Kolan[1,a*], Wenbin Li[1], Julie Semon[2], Delbert Day[3] and Ming Leu[1]

[1] Department of Mechanical and Aerospace Engineering, Missouri University of Science and Technology, Rolla, MO 65409, USA

[2] Department of Biological Sciences, Missouri University of Science and Technology, Rolla, MO 65409, USA

[3] Department of Materials Science and Engineering, Missouri University of Science and Technology, Rolla, MO 65409, USA

[a] These authors contributed equally to this work.

Abstract: A major limitation of using synthetic scaffolds in tissue engineering applications is insufficient angiogenesis in scaffold interior. Bioactive borate glasses have been shown to promote angiogenesis. There is a need to investigate the biofabrication of polymer composites by incorporating borate glass to increase the angiogenic capacity of the fabricated scaffolds. In this study, we investigated the bioprinting of human adipose stem cells (ASCs) with a polycaprolactone (PCL)/bioactive borate glass composite. Borate glass at the concentration of 10 to 50 weight %, was added to a mixture of PCL and organic solvent to make an extrudable paste. ASCs suspended in Matrigel were ejected as droplets using a second syringe. Scaffolds measuring 10 × 10 × 1 mm^3 in overall dimensions with pore sizes ranging from 100 – 300 μm were fabricated. Degradation of the scaffolds in cell culture medium showed a controlled release of bioactive glass for up to two weeks. The viability of ASCs printed on the scaffold was investigated during the same time period. This 3D bioprinting method shows a high potential to create a bioactive, highly angiogenic three-dimensional environment required for complex and dynamic interactions that govern the cell's behavior *in vivo*.

Keywords: bioprinting, biofabrication, human adipose-derived stem cell, MSCs, bioactive glass, polycaprolactone, scaffold, tissue engineering

*Correspondence to: Krishna Kolan, Department of Mechanical and Aerospace Engineering, Missouri University of Science and Technology, Rolla, MO, USA; E-mail: kolank@mst.edu

Received: November 9, 2016; **Accepted:** December 6, 2016; **Published Online:** January 6, 2017

Citation: Murphy C, Kolan K, Li W, *et al.*, 2017, 3D bioprinting of stem cells and polymer/bioactive glass composite scaffolds for bone tissue engineering. *International Journal of Bioprinting*, vol.3(1): 54–64. http://dx.doi.org/10.18063/IJB.2017.01.005.

1. Introduction

Dysfunctional or reduced blood supply is symptom of many health concerns, including diabetes, wound healing, and bone repair. Diabetes alone affects about 8.5% of the human population and costs the world over $376 billion in medical related expenses each year[1]. Another problem associated with reduced blood supply exists in bone grafts. Bone defects resulting from trauma, cancer, infection, or congenital skeletal abnormalities contribute to major surgeries performed every year. Autologous bone graft is still considered as the gold standard for most applications but creates donor site morbidity[2,3]. Allografts avoid these issues but have limited availability, concerns over immunogenicity, and potential disease transmission[4]. Several materials including biocompatible metals, bioceramics, and biopolymers are currently being investigated as candidates for synthetic grafts. Additive manufacturing

3D bioprinting of stem cells and polymer/bioactive glass composite scaffolds for bone tissue engineering. © 2017 Caroline Murphy, et al. This is an Open Access article distributed under the terms of the Creative Commons Attribution-NonCommercial 4.0 International License (http://creativecommons.org/licenses/by-nc/4.0/), permitting all non-commercial use, distribution, and reproduction in any medium, provided the original work is properly cited.

(AM), or popularly known as 3D printing, is a layer-by-layer material deposition process in which functional parts with complex shapes can be made which are otherwise difficult to manufacture. AM of biomaterials has shown that complex and strong implants can be made to treat different regions of bone, including load-bearing bone[5–7]. However, engineered bone scaffolds have not been as successful as autologous grafts thus far, largely due to insufficient vascularization and reduced biomechanical function[8–9].

The choices of materials and fabrication process are two significant factors that determine the success of engineered scaffolds. Many synthetic polymers and bioceramic materials have been used to make scaffolds for bone tissue engineering based on different AM techniques[10,11]. Since polymers are only biocompatible, attempts have been made to improve their bioactivity by adding different bioceramics to make polymer composites. Typically, such composites are prepared by mixing an inorganic bioceramic material (in particle or fiber form) with a polymer which has been either heat melted or dissolved in an organic solvent[12]. The bioactivity of the eventual composite material not only depends on the choice of bioceramic (including bioactive glass, hydroxyapatite, etc.) but also depends on the method of composite preparation itself. Composite foams and films made by traditional fabrication methods such as solvent casting and particle leaching (SCPL) and thermally induced phase separation (TIPS) have reported improved water absorption and formation of hydroxyapatite[13]. However, it is difficult to control the scaffold porosity and shape using such methods. Scaffolds made with AM techniques such as selective laser sintering and ink-jet printing have also shown improved bioactivity, but incorporating cells during fabrication akin to bioprinting is not feasible due to processing limitations.

3D bioprinting is a process that fabricates a "living" construct in a layer-by-layer fashion using a "bio-ink" (cells suspended in a medium) with or without additional materials. Creation of a 3D environment with spatial arrangement of cells and materials is essential for vascularization and complete implant integration with the surrounding tissue. 3D bioprinting techniques can be broadly classified into three categories: (i) laser-assisted[14,15], (ii) inkjet-based[16], and (iii) extrusion-based printing[17]. Extrusion-based 3D bioprinting is the most successful biofabrication process to date with a range of materials compatible with the process[17,18]. In an extrusion-based bioprinting process, cells, hydrogels, and other materials are deposited using one or multiple syringes with a pressure system. The pressure system consists of either a mechanical piston or a pneumatic pressure source (mostly compressed air) that is computer controlled. The material is extruded through a nozzle tip and the process can deposit hydrogels with high cell density and minimal wastage in comparison to laser-assisted and ink-jet bioprinting techniques. Recent research has focused on creating living or cell-laden grafts for tissues including bone, cartilage, and skeletal muscle[18–20]. In extrusion bioprinting, one syringe is typicallly devoted to melt the polymer and deposit the melt for scaffolding structure. However, research to date has only considered the melt-deposition process to print scaffolding and is limited to low melting point polymers. Therefore, it is essential to investigate alternate approaches for printing other materials in order to develop more promising approaches in 3D bioprinting.

The addition of bioactive glass to a biocompatible polymer transforms the 3D environment with its dissolution products by up-regulating the cell-cell and cell-matrix interactions, which promotes vascularization. In the current study, we use a highly angiogenic bioactive 13-93B3 borate glass because of its osteo stimulatory/conductive nature and anti-microbial properties[21]. In comparison to the more comm.on bioactive silicate glass, such as 45S5 or 13-93 glass, 13-93B3 has a higher reaction rate (5–10 times faster than silicate glasses) and resorbs (60 to 70% wt. loss) in a few days to weeks[9]. Ion release from the borate glass has been linked to the wound healing nature of this glass, with the boron ions in particular leading to the angiogenic effects, which are marginal in the silicate glasses[22]. The borate glass was recently approved by the Food and Drug Administration of the United States for human use with trade name Mirragen™ Advanced Wound Matrix.

Mesenchymal stem/progenitor cells (MSCs) have been used for cell therapy and in tissue engineering because of their ability to differentiate into multiple mesenchymal lineages *in vitro*, immune modulatory effects, and angiogenic capacity[23,24]. MSCs have been isolated from several tissues, including the bone marrow (BMSCs), adipose tissue (ASCs), and skin tissue[25–28]. The frequency of MSCs in adipose tissue is much higher than the more commonly studied source of bone marrow, yielding 100 to 500 times more cells per tissue volume[29–30]. ASCs have similar self-renewal abilities, common surface epitopes, growth ki-

netics, and cytokine expression profiles to BSCs. With the addition of ASCs, the scaffold is expected to improve its biomechanical and biological properties for better repair of the target tissue. In the current study, we investigate the feasibility of scaffold fabrication using a two syringe system with a PCL/borate glass composite dissolved in an organic solvent as a scaffold material, whilst simultaneously printing cells suspended in Matrigel, which is a gelatinous protein mixture representing basement membrane. Included in this study are the effect of borate glass content on the composite paste printability, the scaffold temporal bioactivity, its degradation in culture media, and ASC viability in the scaffold.

2. Materials and Methods

2.1 Preparation of PCL/13-93B3 Borate Glass Composite Material

Polycaprolactone (Sigma-Aldrich, St. Louis, Missouri, USA) was dissolved in chloroform (CF) (Sigma-Aldrich, St. Louis, Misouri, USA) in a covered glass container with the help of a stirrer at ~5 0 °C. The PCL weight to CF volume ratio (grams:mL) was varied from 1:1 to 5:4 to determine the ideal ratio for printing. An appropriate ratio was established by visually inspecting the paste and through filament extrusion using a digital syringe dispenser (Loctite®, Henkel North America, Rocky Hill, Connecticut, USA). Then, 13-93B3 glass (Mo-Sci Corporation, Rolla, Missouri, USA) (nominal composition – 53% B_2O_3, 20% CaO, 12% K_2O, 6% Na_2O, 5% MgO, 4% P_2O_5 in weight percentage) with ~20 μm particle size was added to the PCL:CF mix in five different weight percentages in increments of 10, ranging from 10% to 50%. A magnetic stirrer was used to uniformly mix the composite paste, and no settling of the glass particle precipitate was observed before transferring the paste to a syringe. Each ratio was tested using a digital syringe dispenser at air pressure ranging from 10 to 50 psi and with nozzle tip diameter ranging from 110 to 600 μm (32 G to 20 G).

2.2 Preparation of Bio-ink

Frozen vials of approximately 1×10^6 ASCs were obtained from three separate donors (LaCell, New Orleans, Louisiana, USA). Vials were unthawed, plated on 150 cm^2 culture dishes (Nunc, Rochester, New York, USA) in 25 mL complete culture media (CCM), and incubated at 37 °C with 5% humidified CO_2. The CCM contained 10% fetal bovine serum (Corning, Manassas, Virginia, USA), 1% 100× L-glutamine (GE Life Sciences, Logan, Utah, USA), 2% 100× antibiotic/antimycotic (GE Life Sciences, Logan, Utah, USA, and minimum essential medium alpha modified (α-MEM) (Sigma-Aldrich, St. Louis, Missouri, USA). After 24 hours, the media was removed and adherent, viable cells were washed twice with PBS, harvested with 0.25% trypsin/1 mM EDTA (Gibco, Grand Island, New York, USA), and replated at 100 cells/cm^2 in CCM. The media was changed every 3 to 4 days. For all experiments, sub-confluent cells (⩽70% confluent) between passages 2 and 6 were used. To prepare the bio-ink, ASCs were suspended at a concentration of 10×10^6 cells per mL of Matrigel (Corning, Bedford, Massachusetts, USA) diluted to 9 mg/mL in phosphate buffered saline (PBS). The bio-ink was then transferred to a tap ered nozzle tip (30G) which was stored on ice during the entire non-printing time. The bio-ink was gently pipetted to obtain a uniform distribution of cells just before printing. Matrigel was used in this work as it resembles the complex extra cellular environment found in many tissues.

2.3 Scaffold Fabrication

A square scaffold measuring 10 mm in length was printed with 0°–90° orientation of the filaments in alternate layers. The schematic in **Figure 1A** shows the printing set-up and **Figure 1B** depicts the printing process. A custom modified cartesian 3D printer (Geeetech, Prusa I3 A Pro) with two additional syringes controlled by digital dispensers was used for fabrication. The G-code for nozzle movement was written to print in a 0°–90° pattern to obtain rectangular pores. The printing parameters such as air pressure, filament spacing, layer height, and printing speed were identified based on visual inspection and optical microscopic images after the first and second layer printing for different paste compositions. To determine the printing parameters for Matrigel, an experiment was conducted by varying the nozzle tip distance from the glass slide, droplet dispensing time, and air pressure. Fluorescent images of the droplets were taken and ImageJ software was utilized to quantify the number of cells and cell distribution in each fluorescent image. A tapered nozzle tip (30 G) with 160 μm orifice provided the suitable droplet size (~400 μm) at 10 psi and 0.035 s dispensing time for deposition on the filament. While some droplets fell to the surrounding pores, most of the droplets stayed on the filament before the Matrigel was allowed to cross-link at room temperature. The fabrication experiments were

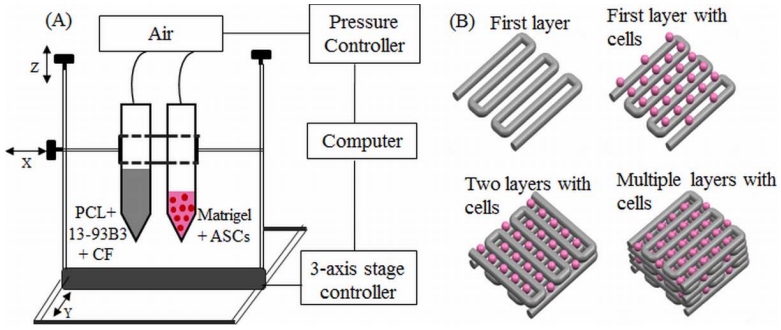

Figure 1. (A) Schematic of the printing set-up. One syringe contained PCL, 13-93B3 glass, and chloroform, while the other syringe contained ASCs suspended in Matrigel. **(B)** The composite layers are printed in 0°–90° pattern using one syringe while a second syringe prints the bio-ink droplets on top of every other layer.

performed at room temperature (64°F) where the variation in relative humidity (58–60%) was not considered to be a major factor.

2.4 Degradation of PCL/13-93B3 Glass Composite

The degradation of the PCL/13-93B3 composite was studied on scaffolds measuring (10×10×1) mm^3. The printed scaffolds were dried at least for one day for complete evaporation of CF. Before immersion, the scaffolds were weighed and 300 mL of α-MEM was used for 1 g of the scaffold for soaking. Scaffolds were immersed in high density polyethylene (HDPE) bottles containing α-MEM and stored in an incubator maintained at 37 °C for different time intervals ranging from 1 day to 14 days. After removal, the scaffold was gently washed with de-ionized (DI) water, and dried overnight. The dried scaffold was weighed to calculate the weight loss percentage. A sample size of three for each time interval was used in the study and the results were reported as mean ± standard deviation.

2.5 Cell Viability and Proliferation

The effect of chloroform evaporation from the scaffold on the viability of the ASCs was studied by depositing bio-ink droplets on the printed composite filaments. For this study, three composite layers were printed on a two-chamber microscope slide (Thermo Fischer Scientific, Rochester, New York, USA) and allowed to dry for ~2 mins before depositing a layer of bio-ink droplets. The Matrigel in bio-ink was allowed to polymerize at room temperature for 20 minutes, then 1 mL of CCM was added. The slides were then incubated at 37 °C with 5% humidified CO_2 for three time intervals of 2 hrs, 1 week, and 2 weeks. The medium was changed every three days. After each time interval, the CCM was removed and the cells were stained using the Live/Dead Cell Imaging Kit (ref. R37601, Eugene, Oregon, USA), incubated for 15 minutes at room temperature and examined under a fluorescent microscope (Olympus IX51, Melville, New York, USA).

2.6 Scaffold Characterization

Optical microscopic images were used to measure the filament width and pore size with at least five measurements and the results were reported as mean ± standard deviation. Samples were sputter coated with gold/palladium (Au/Pd) for 60 s before performing scanning electron microscopy (SEM). SEM (Hitachi S-4700 FESEM, Hitachi Co., Tokyo, Japan) images were taken to evaluate the surface morphology of the scaffolds, internal structure of the filaments, and formation of hydroxyapatite-like material on the scaffold surface. Scans were run from 2θ values ranging from 10° to 80° using Cu Kα radiation (λ = 0.154056 nm) for X-ray diffraction (XRD) analysis (Philips X-Pert, Westborough, MA) on the as-received PCL, as-printed PCL/B3 glass scaffold, and the scaffold after α-MEM immersion to determine the changes in the crystalline/amorphous nature of the material.

3. Results

3.1 Fabrication of PCL/13-93B3 Glass Composite Scaffolds

The initial set of printing tests included depositing single layers using the composite paste with 10 wt. % of 13-93B3 glass. A minimum air pressure of 30 psi was required to extrude the paste through a 260 μm (25G) nozzle tip. Larger tips (>260 μm) resulted in thick filaments which took longer time (>5 min) to dry and smaller tips (<260 μm) consistently caused clogging issues. The roundness of the filament improved with increasing glass content along with the paste

viscosity. The minimum air pressure required to extrude the paste increased when glass content was increased from 10 wt. % to 30 wt. %. At higher glass content (40 wt. % and 50 wt. %), the nozzle clogged during fabrication. Therefore, additional CF (about 1 mL) was added to the paste to reduce the viscosity for clog-free extrusion using the 25G tip. The 13-93B3 glass weight percentage and PCL: CF ratios used to make composite pastes are shown in **Table 1**. The final printing parameters used to fabricate the composite scaffolds containing 50 wt. % 13-93B3 glass content is also provided in **Table 1**.

Table 1. PCL/13-93B3 glass paste compositions and printing parameters

Composite Paste #	13-93B3 Glass (wt. %)	PCL:CF (g to mL)	Final Printing Parameters (using C5 paste)
C1	10	5:3	Printing speed – 8 mm/s
C2	20	5:3	Dwell time – 2 min
C3	30	5:3	Layer height – 0.1 mm
C4	40	5:4	Air pressure – 30 psi
C5	50	5:4	Nozzle tip – 260 µm

A filament width of 397±10 µm was measured for scaffolds printed with the C5 paste while average pore size is dependent on the filament spacing. A filament spacing of 600 µm provided square pores measuring ~160 µm (**Figure 2A**). In comparison, the average pore size was ~350 µm for scaffolds fabricated with 800 µm filament spacing. **Figure 2B** shows scaffolds fabricated with 800 µm filament spacing. Warping was predominant while fabricating scaffolds with C1 and C2 pastes and this led to difficulty in printing after about 8 layers; see warped C1 and C2 scaffolds in **Figure 2B.** The warpage in scaffolds fabricated with C3 paste was less pronounced and a scaffold height of 0.8 mm (10 layers) was obtained. Overall, the best results were achieved for scaffolds fabricated with C5 paste as they were successfully printed to 1 mm height (12 layers). The scaffold fabricated with C5 paste had enough strength to be safely handled for subsequent degradation and *in vitro* assessment.

SEM images of scaffolds fabricated with C5 paste are shown in **Figure 3. Figures 3A** and **3B** show the surface morphology of the filament. Glass particles are conspicuously absent from the surface of filaments. No pores on the filament surface were detected even when observed at a 2000× magnification. **Figures 3C** and **3D** show the filament cross-sectional surface. Glass particles dispersed in the PCL matrix can be seen in the interior. The dissolved PCL in chloroform encloses the glass particles and surface tension effects between the nozzle tip and PCL during extrusion appear to have caused the presence of only PCL on the surface.

3.2 Degradation and Bioactivity of PCL/13-93B3 Glass Composite

Recent studies suggest that cell culture medium can be used as an alternative to simulated body fluid (SBF) to evaluate the bioactivity of the materials, with no significant differences in the formation of hydroxyapatite (HA)[31]. We studied the degradation of the composite by soaking the scaffolds made with C5 paste in α-MEM for 1, 3, 7, and 14 days. The scaffold weight before and after immersion (post drying) was recorded at each time interval. No significant weight loss was observed for 3 days (less than 1%), and the measured weight loss was 10.7±5% at 7 days and 23.2±4% at 14 days. As PCL takes a longer time to degrade, the weight loss measured is due to the ionic dissolution of the 13-93B3 borate glass. Formation of flower like florets, which typically represent HA-like material, was observed on the filament surface as shown in **Figures 4A** and **4B**.

The energy-dispersive X-ray spectroscopy (EDX) analysis indicated the presence of calcium (Ca), phosphorous (P), and oxygen (O) on the reacted

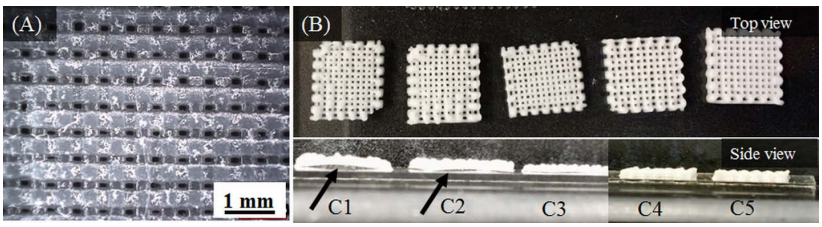

Figure 2. **(A)** Optical microscopic image showing the pores (~160 µm) in a composite scaffold fabricated with C5 paste. **(B)** Scaffolds fabricated with different composite pastes (C1 to C5). The bottom panel shows scaffold warpage with an arrow indicating space between scaffold and slide. Warpage was minimal in C3/C4 scaffolds and completely absent in C5 scaffolds.

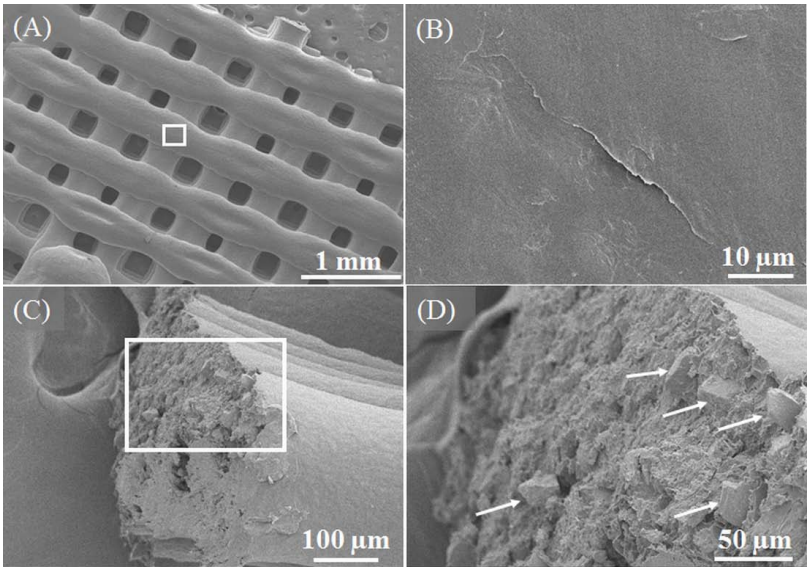

Figure 3. SEM images of the 50:50 PCL/13-93B3 glass scaffold. **(A)** Low magnification (30×) image of scaffold surface showing filaments and pores, **(B)** smooth surface morphology of filament (2000× magnified image of the region marked in **(A)**, **(C)** fractured surface of a broken filament with PCL matrix and glass particles, **(D)** magnified image of the region marked in **(C)** with arrows indicating glass particles present a few microns beneath the surface.

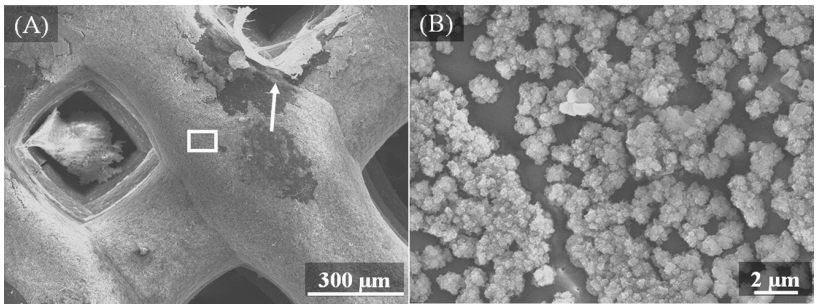

Figure 4. SEM images of the 50:50 PCL/13-93B3 glass scaffold after immersion in α-MEM for 14 days. **(A)** ~1 µm thick layer was formed on the filament surface (a piece of the reacted layer indicated by arrow raised to expose the polymer beneath), **(B)** magnified image (8000×) of the area marked in **(A)** showing the formation of HA-like florets on the filament.

surface of the scaffold after 14-day immersion in α-MEM. **Figure 5A** shows the result of the line scan performed on the surface indicating the changes in elemental composition in atomic weight percentage. In particular, carbon (C), Ca, P, and O are plotted to provide a better comprehension of the reacted surface. Signals of sodium (Na) and magnesium (Mg) were also detected but in very small amounts. All the signals correspond to K series emissions (K_α and K_β). The location of the scan region is shown by an arrow line in **Figure 5B**. The location was selected such that a scan line (~70 µm long) has to start on a reacted surface, pass through the exposed PCL surface, and end on the reacted surface. As signals were recorded, the presence of elements was confirmed. It can be observed that the percentage of Ca and P drops to zero and amount of O decreases as well when scanning the PCL surface (from ~30 µm to ~50 µm in **Figure 5A**). The presence of Ca, P, and O indicates that the glass has reacted and formed HA-like material on the scaffold surface.

3.3 Effect of Chloroform Evaporation on ASC Viability

The viability of ASCs was studied by performing a live/dead assay after incubating the samples for 24 hours, and 1 week. The viability of cells after 24 hours was 70±10% (**Figures 6A** and **6B**). After 1 week, the viability of cells was 58±11% (**Figures 6C** and **6D**).

4. Discussion

A variety of solvents are available to dissolve different

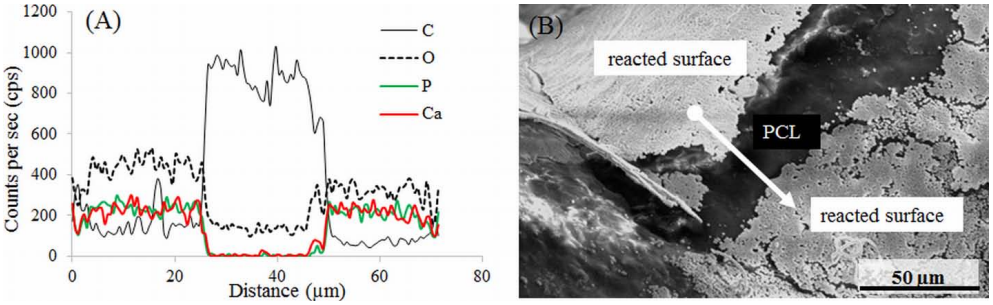

Figure 5. EDX analysis on the surface of the 50:50 PCL/13-93B3 glass scaffold soaked in α-MEM. **(A)** Graph of line scan data showing the variation in Ca, P, O, and C in atomic weight percentages; presence of Ca, P, and O on the reacted surface confirms the glass reaction and formation of HA-like material, **(B)** SEM image with the arrow line indicating the scanned area for EDX analysis.

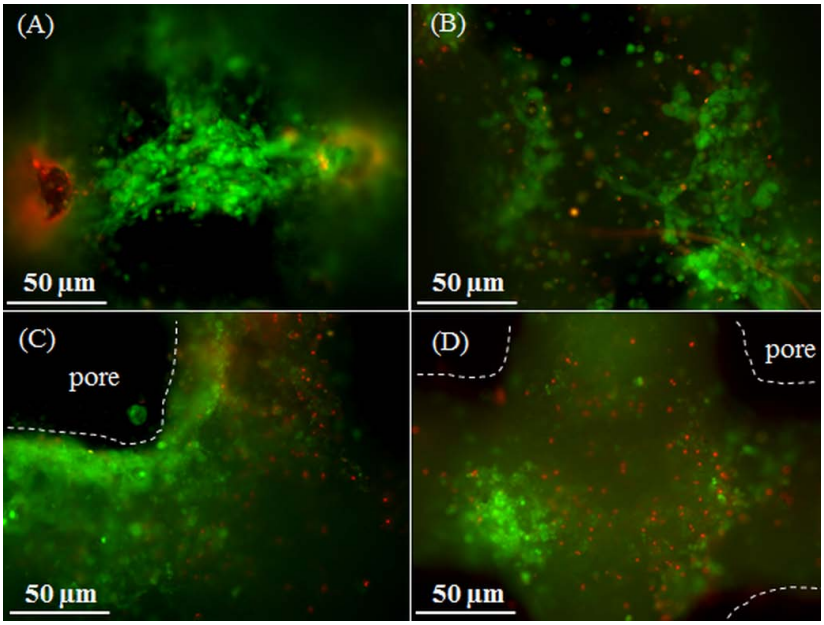

Figure 6. Live/Dead images of ASCs suspended in Matrigel and printed on the 50:50 PCL/13-93B3 glass composite scaffold. Imaged after **(A–B)** 24 hours, and **(C–D)** 1 week. The dotted lines indicate the outline of the filament and dark space indicates the pore.

biopolymers[32]. Extrusion of solvent dissolved polymer and bioactive glass is safe at room temperature and reduces the process complexity since there is no need for temperature control. This method can be adopted by most of the existing open-source 3D printers available in the market. Chloroform (CF) was used in this study because it provides: (i) a high viscosity paste, making it suitable for extrusion-based 3D printing, (ii) fast evaporation (~2 min), making it safe to print ASCs in Matrigel during the fabrication process, (iii) filament porosity for accelerated glass dissolution to the surrounding, and (iv) faster polymer bulk degradation by exposing the interior of filament. To address the issue of safety with the use of CF while depositing bio-ink, we performed cell viability study on scaffolds made with C3 (30% glass) and C5 (50% glass) composite pastes using a live/dead assay. The results showed healthy living ASCs on PCL/13-93B3 glass filaments even after one week of incubation.

An important aspect in extrusion bioprinting is to create a scaffolding structure that supports cells and provides shape and mechanical integrity. Extrusion bioprinters typically have more than one syringe, with one of the syringes devoted to print scaffolding structure. The options utilized for this purpose include melt-deposition of polymer and fused deposition modeling (FDM) with a polymer wire feed. Because of high temperatures involved in many melting biopolymers such as polylactic acid (PLA, with a melting point of 160 °C), PCL has become one of the most widely used polymers owing to its lower melting point of 60 °C. For 3D printing, PCL is an attractive op-

tion because of its good rheological and viscoelastic properties. Despite its slow degradation rate (~2 years depending on the molecular weight), PCL has been widely used to fabricate scaffolds for bone tissue engineering[33]. But for other tissue engineering applications which require faster degrading of scaffolding structure, this may become an impediment. Since FDM fabricated polymer scaffolds are only biocompatible, another issue would be to make the scaffolding structure bioactive by incorporating bioceramic materials. In the past, some researchers made a polymer-bioactive glass wire for use by the FDM process to fabricate polymer-bioactive glass scaffolds[34]. However, no significant improvement in bioactivity and cell growth has been reported, which could be due to inadequate ionic dissolution of the glass into the surrounding environment. This makes the FDM and melt-deposition options unattractive for fabrication of polymer-glass composite scaffolds. In our current study, polymer (PCL) was dissolved in a s olvent (chloroform), mixed with a bioactive glass (13-93B3 glass), and then extruded to fabricate the scaffold. Our weight loss results showed that most of the 13-93B3 glass has reacted in 2 weeks. The schematic in **Figure 7** explains the difference in the glass dissolution from filaments printed using (A) FDM or melt-extrusion process and (B) solvent-based extrusion process. Fine cracks on the filament surface which are a couple of microns wide and up to ten microns or more in length can be observed in **Figure 7C**. Those cracks are believed to aid glass dissolution when the scaffold is immersed in the culture medium.

Our degradation results also show a controlled release of 13-93B3 glass over a period of two weeks into the surrounding solution. In the past, composite thin films have been made using PCL/13-93B3 glass and PCL/45S5 glass with different amount of glass content[35]. The degradation data of such thin films indicate that the entire glass almost completely dissolves in about three days. The graph shown in **Figure 8** compares the weight loss percentage of the PCL/13-93B3 glass thin films (80 µm) with that of the current study. Almost entire 13-93B3 glass was reacted in about 3 da ys from thin films. The faster degradation in composite films could be due to the thickness of the film. The scaffolds in the current study are made by filaments which are about 400 µm in diameter and have no surface pores that explained the very little glass dissolution in three days. However, the water absorbing potential of polymers in general was reportedly found to improve after the addition of bioceramic filler materials such as HA and even bioactive glass[12]. In our study, the glass dissolution increased significantly after 7 and 14 days, which is

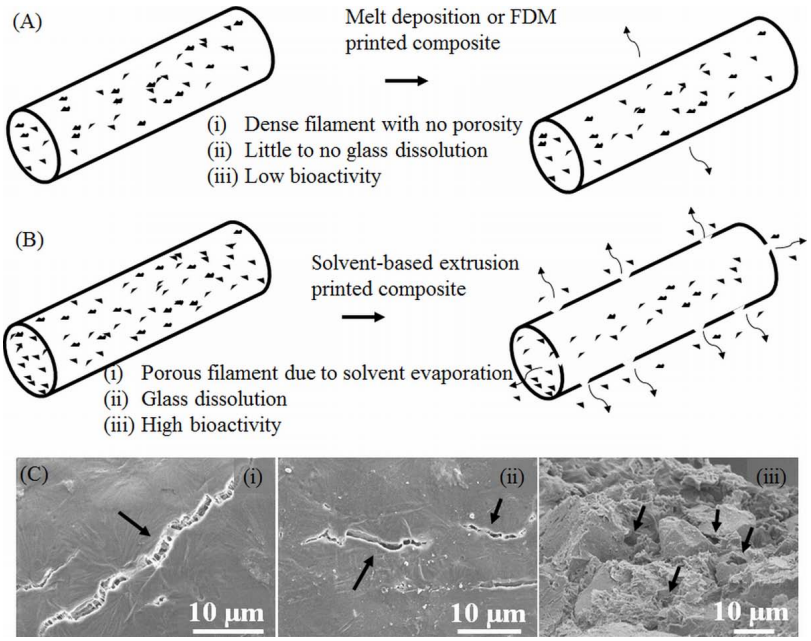

Figure 7. Schematic highlighting the difference in two methods of extrusion printing. **(A)** Melt-deposition of polymer-glass composite resulting in a dense filament and low bioactivity, **(B)** solvent-based extrusion printed composite resulting in a porous filament with high bioactivity, **(C)** SEM images showing surface cracks on the filament indicated by arrows in (i) and (ii), and pores inside the filament measuring less than 10 µm are also indicated by arrows in (iii).

believed to be due to the internal porosity of the filament created after the CF evaporation and also glass dissolution creating more porosity. The entire B_2O_3 present in the borate glass (53 B_2O_3, 20 CaO, 12 K_2O, 6 Na_2O, 5 MgO, 4 P_2O_5 in composition by weight %) completely dissolves into surrounding environment, and the rest oxides with the exception of MgO participate in the formation of HA. By neglecting the weight of HA formed, it can be theoretically calculated that there is about ~35% weight loss for the scaffold, assuming a complete 13-93B3 glass dissolution in 50:50 PCL/13-93B3 composite. In this study, the weight loss for 50:50 PCL/13-93B3 composites-caffold was ~23%, indicating that ~70% of the 13-93B3 glass present in the scaffold had reacted in 14 days. This degradation vs. time characteristic can be used to develop a controlled degradation of 3D scaffold that is beneficial in certain tissue engineering applications, especially in drug delivery.

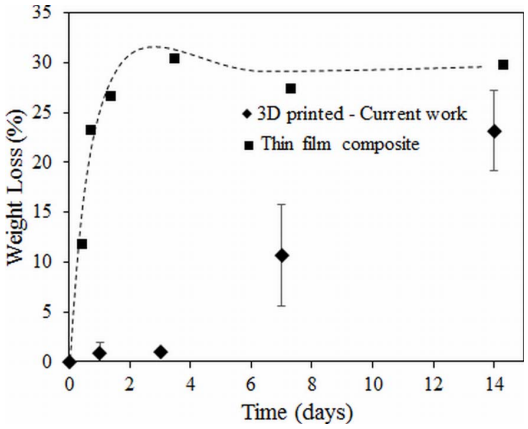

Figure 8. Weight loss percentage comparison of 3D printed 50:50 PCL/13-93B3 glass composite scaffolds vs. thin film composite made using PCL, CF, and 50% 13-93B3 glass[35].

The reacted layer formed on the scaffold surface was ~1 µm thick and not completely uniform (dense collection of florets can be seen in **Figure 4C**). XRD analysis was performed to confirm the presence of crystalline HA but the XRD pattern obtained on a 14 day soaked scaffold could not match the known HA crystalline peak. This is believed to be because of formation of amorphous HA or non-stoichiometric HA, which is not uncommon in such cases. **Figure 9** shows XRD patterns of the as-received 13-93B3 glass, PCL/13-93B3 glass composite scaffold, and the composite scaffold after soaking in α-MEM for 2 weeks. The semi-crystalline nature of the PCL was confirmed with characteristic peaks (marked by *) and amorphous profile of 13-93B3 glass with no sharp peaks and characteristic hump can be observed in the XRD patterns shown in **Figure 9**. There are additional peaks observed for the α-MEM soaked sample which could not be identified to a known material in the database (marked by †). However, the typical amorphous hump seen in glass was not existent in the soaked sample, indicating that most of the 13-93B3 glass in the scaffold has reacted after 14 days.

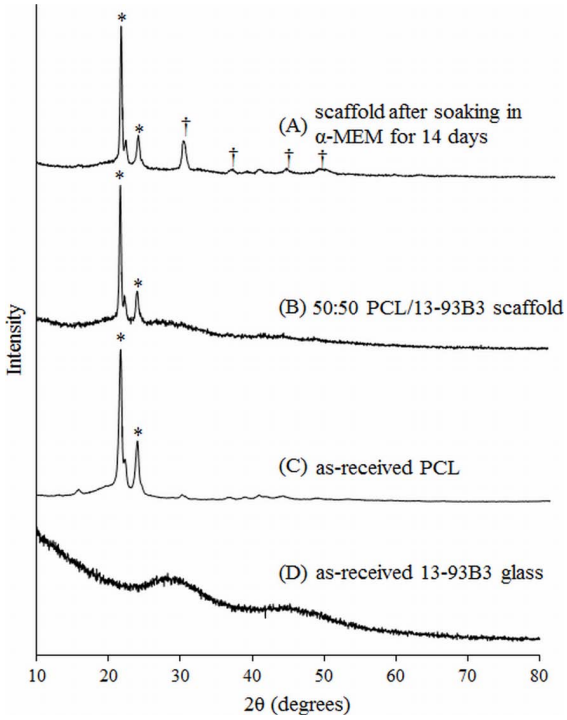

Figure 9. XRD patterns of **(A)** 50:50 PCL/13-93B3 glass composite scaffold soaked in α-MEM for 14 days, **(B)** PCL/13-93B3 glass scaffold, **(C)** as-received PCL showing a semi-crystalline nature with characteristic peaks marked by *, and **(D)** as-received 13-93B3 glass with characteristic amorphous hump (25° to 35° and 40° to 50°).

It is known that pore size is an important parameter of the scaffold that could potentially affect the bone growth after implantation, and it has been reported that pore size in the range of 100 to 300 µm is beneficial for bone growth[9]. The scaffolds we fabricated have pores in this range. Moreover, the ASCs when co-cultured with 2.5 mg of 13-93B3 glass per 1 mL of culture media in standard culture conditions show osteogenic differentiation with no detrimental effects. Therefore, the scaffolds fabricated using solvent-based extrusion 3D bioprinting developed as in the present study have a high potential for non-load-bearing bone repair applications.

5. Conclusion

This study investigated the feasibility of fabricating a scaffold with polycaprolactone/bioactive borate glass composite using a solvent based extrusion 3D printer integrated with printing of human ASCs suspended in Matrigel during the scaffold fabrication process. Printing process parameters were identified for the composite and bio-ink to fabricate a (10×10×1) mm^3 ASC-laden scaffold with pore sizes ranging from 100 to 300 μm suitable for bone tissue engineering. In comparison to the conventional melt-deposition extrusion 3D bioprinting, the degradation of polymer/bioactive glass scaffolds showed a c ontrolled release of bioactive glass with ~23% weight loss in two weeks. Formation of hydroxyapatite-like crystals on the surface of the scaffold after soaking in culture media for up to two weeks shows the strong bioactivity of the fabricated composite scaffold and its high potential for bone repair. The live/dead assay showed more than 60% viable ASCs on the scaffold after 1 week of incubation, with minimal negative effects from chloroform evaporation on the cells. The results of this study show the high potential of the solvent-based extrusion 3D bioprinting process to fabricate a scaffold with cells and polymer composites for tissue engineering applications.

Conflict of Interest and Funding

No conflict of interest was reported by the authors.

Acknowledgment

The glass used in this study was provided by MO-SCI Corporation, Rolla, Missouri, USA. The authors thank Mariahe Long for her assistance during experiments and imaging.

References

1. Zhang P, Zhang X, Brown J B, *et al*., 2010, Economic impact of diabetes. *IDF Diabetes Atlas*.
2. Banwart J C, Asher M A and Hassanein R S, 1995, Iliac crest bone graft harvest donor site morbidity. A statistical evaluation. *Spine (Phila. Pa. 1976)*, vol.20(9): 1055–1060.
https://doi.org/10.1097/00007632-199505000-00012
3. Goulet J A, Senunas L E, DeSilva G L, *et al.*, 1997, Autogenous iliac crest bone graft. Complications and functional assessment. *Clinical Orthophopedics and Related Research*, (339): 76–81.
https://doi.org/10.1097/00003086-199706000-00011
4. Giannoudis P V, Dinopoulos H and Tsiridis E, 2005, Bone substitutes: an update. *Injury*, vol.36(3): S20–S27.
http://dx.doi.org/10.1016/j.injury.2005.07.029
5. Doiphode N D, Huang T, Leu M C, *et al.*, 2011, Freeze extrusion fabrication of 13–93 bioactive glass scaffolds for bone repair. *Journal of Materials Science: Materials in Medicine,* vol.22(3): 515–523.
http://dx.doi.org/10.1007/s10856-011-4236-4
6. Kolan K C R, Leu M C, Hilmas G E, *et al.*, 2012, Effect of material, process parameters, and simulated body fluids on mechanical properties of 13–93 bioactive glass porous constructs made by selective laser sintering. *Journal of Mechanical Behaviour of Biomedical Materials*, vol.13: 14–24.
http://dx.doi.org/10.1016/j.jmbbm.2012.04.001
7. Bartolo P, Kruth J P, Silva J, *et al*., 2012, Biomedical production of implants by additive electro-chemical and physical processes. *CIRP Annals — Manufacturing Technology*, vol.61(2): 635–655.
http://dx.doi.org/10.1016/j.cirp.2012.05.005
8. Temple J P, Hutton D L, Hung B P , *et al.*, 2014, Engineering anatomically shaped vascularized bone grafts with hASCs and 3D-printed PCL scaffolds. *Journal of Biomedical Materials Research Part A*, vol.102(12): 4317–4325.
http://dx.doi.org/10.1002/jbm.a.35107
9. Rahaman M N, Day D E, Sonny Bal B, *et al*., 2011, Bioactive glass in tissue engineering. *Acta Biomaterialia*, vol.7(6): 2355–2373.
http://dx.doi.org/10.1016/j.actbio.2011.03.016
10. Liu X and Ma P X, 2004, Polymeric scaffolds for bone tissue engineering. *Annals Biomedical Engineering*, vol.32(3): 477–486.
http://dx.doi.org/10.1023/B:ABME.0000017544.36001.8e
11. Bose S, Vahabzadeh S and Bandyopadhyay A, 2013, Bone tissue engineering using 3D printing. *Materials Today*, vol.16(12): 496–504.
http://dx.doi.org/10.1016/j.mattod.2013.11.017
12. Puska M, Aha A J and Vallittu P, 2011, Polymer composites for bone reconstruction. *Advances in Composite Materials – Analysis of Natural Man-Made Materials*: 55–72.
http://dx.doi.org/10.5772/20657
13. Rezwan K, Chen Q Z, Blaker J J, *et al*., 2006, Biodegradable and bioactive porous polymer/inorganic composite scaffolds for bone tissue engineering. *Biomaterials*, vol.27(18): 3413–3431.
http://dx.doi.org/10.1016/j.biomaterials.2006.01.039
14. Guillotin B, Souquet A, Catros S, *et al.*, 2010, Laser assisted bioprinting of engineered tissue with high cell density and microscale organization. *Biomaterials*, vol.31(28): 7250–7256.

http://dx.doi.org/10.1016/j.biomaterials.2010.05.055

15. Yan J, Huang Y, Chrisey D B, *et al.*, 2013, Laser-assisted printing of alginate long tubes and annular constructs. *Biofabrication*, vol.5(1): 15002. http://dx.doi.org/10.1088/1758-5082/5/1/015002
16. Chang C C, Boland E D, Williams S K, *et al.*, 2011, Direct-write bioprinting three-dimensional biohybrid systems for future regenerative therapies. *Journal of Biomedical Materials Research Part B: Applied Biomaterials*, vol.98B(1): 160–170. http://dx.doi.org/10.1002/jbm.b.31831
17. Ozbolat I T and Hospodiuk M, 2016, Current advances and future perspectives in extrusion-based bioprinting. *Biomaterials*, vol.76:321–343. http://dx.doi.org/10.1016/j.biomaterials.2015.10.076
18. Murphy S V and Atala A, 2014, 3D bioprinting of tissues and organs. *Nature Biotechnology*, vol.32(8): 773–785. http://dx.doi.org/10.1038/nbt.2958
19. Kang H-W, Lee S J, Ko I K, *et al*., 2015, A 3D bioprinted complex structure for engineering the muscle–tendon unit. *Biofabrication*, vol.7(3): 35003. http://dx.doi.org/10.1088/1758-5090/7/3/035003
20. Wu Z, Su X, Xu Y, *et al*., 2016, Bioprinting three-dimensional cell-laden tissue constructs with controllable degradation. *Science Reports*, vol.6: 24474. http://dx.doi.org/10.1038/srep24474
21. Lin Y, Brown R F, Jung S B, *et al*., 2014, Angiogenic effects of borate glass microfibers in a rodent model. *Journal of Biomedical Materials Research Part A*, vol.102(12): 4491–4499. http://dx.doi.org/10.1002/jbm.a.35120
22. Jung S B and Day D E, 2011, Revolution in wound care? Inexpensive, easy-to-use cotton candy-like glass fibers appear to speed healing in initial venous stasis wound trial. *The American Ceramic Society Bulletin*, vol.90(4): 25–29.
23. Salem H K and Thiemermann C, 2009, Mesenchymal stromal cells: current understanding and clinical status. *Stem Cells*, vol.28(3): 585–596. http://dx.doi.org/10.1002/stem.269
24. Wu Y, Chen L, Scott P G, *et al.*, 2007, Mesenchymal stem cells enhance wound healing through differentiation and angiogenesis. *Stem Cells*, vol.25(10): 2648–2659. http://dx.doi.org/10.1634/stemcells.2007-0226
25. De Ugarte D A, Morizono K, Elbarbary A, *et al.*, 2003, Comparison of multi-lineage cells from human adipose tissue and bone marrow. *Cells Tissues Organs*, vol.174(3): 101–109. http://dx.doi.org/10.1159/000071150
26. Izadpanah R, Trygg C, Patel B, *et al*., 2006, Biologic properties of mesenchymal stem cells derived from bone marrow and adipose tissue. *Journal of Cellular Biochemistry,* vol.99(5): 1285–1297. http://dx.doi.org/10.1002/jcb.20904
27. Wagner W, Wein F, Seckinger A, *et al.*, 2005, Comparative characteristics of mesenchymal stem cells from human bone marrow, adipose tissue, and umbilical cord blood. *Experimental Hematology*, vol.33(11): 1402–1416. http://dx.doi.org/10.1016/j.exphem.2005.07.003
28. Sakaguchi Y, Sekiya I, Yagishita K, *et al.*, 2005, Comparison of human stem cells derived from various mesenchymal tissues: superiority of synovium as a cell source. *Arthritis Rheumatology*, vol.52(8): 2521–2529. http://dx.doi.org/10.1002/art.21212
29. D'Andrea F, De Francesco F, Ferraro G A, *et al.*, 2008, Large-scale production of hum an adipose tissue from stem cells: a new tool for r egenerative medicine and tissue banking. *Tissue Engineering Part C Methods*, vol.14(3): 233–242. http://dx.doi.org/10.1089/ten.tec.2008.0108
30. Casteilla L and Dani C, 2006, Adipose tissue-derived cells: from physiology to regenerative medicine. *Diabetes & Metabolism*, vol.32(5 Pt 1): 393–401. http://dx.doi.org/DM-11-2006-32-5-1262-3636-101019-200519820
31. Lee J T Y, Leng Y, Chow K L, *et al.*, 2011, Cell culture medium as an alternative to conventional simulated body fluid. *Acta Biomaterialia*, vol.7(6): 2615–2622 http://dx.doi.org/10.1016/j.actbio.2011.02.034
32. Miller-Chou B A and Koenig J L, 2003, A review of polymer dissolution. *Progress in Polymer Science*, vol.28(8): 1223–1270. http://dx.doi.org/10.1016/S0079-6700(03)00045-5
33. Woodruff M A and Hutmacher D W, 2010, The return of a forgotten polymer — polycaprolactone in the 21st century. *Progress in Polymer Science*, vol.35(10): 1217–1256. http://dx.doi.org/10.1016/j.progpolymsci.2010.04.002
34. Korpela J, Kokkari A, Korhonen H, *et al.*, 2013, Biodegradable and bioactive porous scaffold structures prepared using fused deposition modeling. *Journal of Biomedical Materials Research Part B: Applied Biomaterials*, vol.101B(4): 610–619. http://dx.doi.org/10.1002/jbm.b.32863
35. Mohammadkhah A, Marquardt L M, Sakiyama-Elbert S E, *et al.*, 2015, Fabrication and characterization of poly-(ε)-caprolactone and bioactive glass composites for tissue engineering applications. *Materials Science and Engineering: C*, vol.49: 632–639. http://dx.doi.org/10.1016/j.msec.2015.01.06

RESEARCH ARTICLE

Fabrication of titanium based biphasic scaffold using selective laser melting and collagen immersion

Swee Leong Sing[1,2], Shuai Wang[2], Shweta Agarwala[2], Florencia Edith Wiria[1,3], Thi Mai Hoa Ha[3] and Wai Yee Yeong[1,2]

[1] SIMTech-NTU Joint Laboratory (3D Additive Manufacturing), Nanyang Technological University, 65A Nanyang Drive, Singapore 637333

[2] Singapore Centre for 3D Printing, School of Mechanical & Aerospace Engineering, Nanyang Technological University, 2A Nanyang Link, Singapore 637372

[3] Singapore Institute of Manufacturing Technology (SIMTech) @ NTU, 73 Nanyang Drive, Singapore 637662

Abstract: Tissue engineering approaches have been adopted to address challenges in osteochondral tissue regeneration. Single phase scaffolds, which consist of only one single material throughout the whole structure, have been used extensively in these tissue engineering approaches. However, a single phase scaffold is insufficient in providing all the properties required for regeneration and repair of osteochondral defects. Biphasic scaffolds with two distinct phases of titanium/type 1 c ollagen and titanium-tantalum/type 1 collagen were developed for the first time using selective laser melting and collagen infiltration. Observation of the biphasic scaffolds demonstrated continuous interface between the two phases and mechanical characterization of the metallic scaffolds support the feasibility of the newly developed scaffolds for tissue engineering in osteochondral defects.

Keywords: selective laser melting, titanium, tantalum, collagen, biphasic scaffolds

*Correspondence to: Wai Yee Yeong, SIMTech-NTU Joint Laboratory (3D Additive Manufacturing), Nanyang Technological University, HW30101, 65A Nanyang Drive, Singapore 637333; Email: wyyeong@ntu.edu.sg

Received: November 22, 2016; **Accepted:** December 21, 2016; **Published Online:** January 24, 2017

Citation: Sing SL, Wang S, Agarwala S, *et al*., 2016, Fabrication of titanium based biphasic scaffold using selective laser melting and collagen immersion. *International Journal of Bioprinting*, vol.3(1): 65–71. http://dx.doi.org/10.18063/IJB.2017.01.007.

1. Introduction

Osteochondral defects refers to any damage in the articular cartilage and underlying bone. These can be caused by either trauma related injuries or natural degradation. In 2008, over 59 million people in America and European Union was estimated to suffer from osteoarthritis which may leads to osteochondral defects[1]. Osteochondral tissue regeneration remains clinical challenging due to its multi-layered structure comprised of multiple tissue segments involving cartilage, bone and the cartilage-bone interface[2, 3]. In the last decade, several tissue engineering approaches have been developed to address this clinical challenge. The aim of tissue engineering is to regenerate functional tissue by combining three key factors, namely, scaffold, functional cells and bioactive molecules such as growth factors[4-6]. Scaffolds, being critical for osteochondral regeneration, should have a rigid osseous structure. This requirement demands good mechanical strength and a porous phase to allow seeding, migrating and extracellular matrix (ECM) remodeling of cells[7, 8].

Additive manufacturing, or 3D printing, presents new opportunities in fabrication of design-dependent scaffolds tailored for maximum osteochondral regeneration. Scaffolds fabrication using different materials have been demonstrated, including polymers[9-11], metals[12-16] and ceramics[17]. In particular, selective laser melting (SLM) is a powder bed fusion additive

Fabrication of titanium based biphasic scaffold using selective laser melting and collagen immersion. © 2017 Swee Leong Sing, et al. This is an Open Access article distributed under the terms of the Creative Commons Attribution-NonCommercial 4.0 International License (http://creativecommons.org/licenses/by-nc/4.0/), permitting all non-commercial use, distribution, and reproduction in any medium, provided the original work is properly cited.

manufacturing technique that fuses metal powders to form functionally parts directly. It uses laser power source to fabricated parts based on computer aided design (CAD) files[15, 18-23]. There are many new research opportunities that emerges due to the capability of SLM in producing parts with complex geometry. One of such areas includes the fabrication of metallic porous structures with controlled porosity and varying designs[12, 14, 16, 24-26]. The interest in this field has also fueled focus on the use of biocompatible materials in SLM. Among them, titanium alloys are of special interest due to their excellent properties. Many studies done on SLM produced titanium alloys such as Ti6Al4V[13, 15, 27-30] and Ti6Al7Nb[16, 31, 32]. The studies have proven their superior properties for biomedical applications. Titanium-tantalum (TiTa) formation by SLM has recently been studied[33] and it has the potential to outperform Ti6Al4V and commercially pure titanium (cpTi) due to its higher strength to modulus ratio and better biocompatibility[34, 35].

Despite the advantages titanium alloys provide, a single phase scaffold alone cannot meet the complex functional demands of bone and cartilage tissues as these have wide differences in their chemical, structural and mechanical properties[36]. Biphasic scaffolds provide the solution by allowing the composition ratio between the two phases to be tailored and altered to cater to individuals and for specific applications. Such biphasic scaffolds have a rigid osseous phase to integrate with the native bone and a porous chondral phase to allow the seeding and proliferation of cells[37]. Zhao *et al.*[38] prepared porous PLGA/titanium biphasic scaffold and evaluated the mechanical properties, microstructure and interface. The analysis showed that the scaffold has good overall integrity and stable interface. Nover *et al.*[39] recently fabricated an osteochondral grafts that consists of bone-like porous titanium and a chondrocyte-seeded hydrogel. The porous titanium is made using SLM with cpTi, and together with the hydrogel, it is able to support robust cartilage growth. As one of the essential component of ECM, type 1 collagen has been widely used as tissue scaffold material[40]. It is biocompatible and provides favorable cellular micro-environment to induce chondrogenesis of mesenchymal stem cells (MSCs) *in vivo*. For example, collagen-glycosaminoglycan phosphate biphasic scaffold were evaluated in caprine femoral condyle and lateral trochlear sulcus osteochondral defects model. After 26 weeks of implantation, both scaffolds provide indications of structural repair[41].

In this paper, SLM is used to fabricate cpTi and TiTa metallic porous structures using a unit cell design that has been proven to be suitable for fabrication using SLM. CpTi is used as a benchmark material for this method of forming biphasic scaffolds as the mechanical properties of these two materials have been evaluated previously[33]. The novel biphasic scaffolds constructs formed using the metallic porous structures and type 1 collagen is studied for the first time to investigate the interface between these materials and type 1 collagen.

2. Experimental details

2.1 Scaffolds design

Design concept of the scaffolds mimics the nature, which involved a porous cpTi or TiTa scaffold base to mimics the osseous bone structure's mechanical strength and a type 1 collagen phase as the cartilage phase. The titanium scaffolds are designed using cubic unit cells of 1 mm × 1 mm × 1 mm, as shown in **Figure 1.**

The unit cell is designed such that the fabricated scaffolds have a porosity of 80.3% with square struts of 0.285 mm and square pore size of 0.715 mm. The fully infiltrated collagen matrix provides micro-environment for cells attachment, migration, proliferation and nutrient transportation. In future study, cells can be encapsulated directly into collagen matrix.

2.2 Biphasic scaffolds formation

All the scaffolds were fabricated using a SLM 250HL machine (SLM Solutions Group AG, Germany). The SLM machine uses a fiber laser with Gaussian beam profile and maximum power of 400 W. The laser has spot size of 80 μm. To prevent oxidation and degradation of materials, all processing occurred in an argon environment with less than 0.05% oxygen[18]. The detailed characteristics of cpTi and TiTa powders have been described previously[33]. In this work, identical processing parameters are used for TiTa and cpTi, and is shown in **Table 1.**

For the hydrogel portion, 2 mg/ml collagen were prepared according to the manufacturer's instruction. Briefly, the required volume of collagen was neutralized with 1 M NaOH in PBS. The biphasic scaffolds were prepared by immersing the scaffolds in degassed collagen solution while shaking gently. Excess collagen solution was removed before gelling at 37 °C. A summary of the process is shown in **Figure 2.**

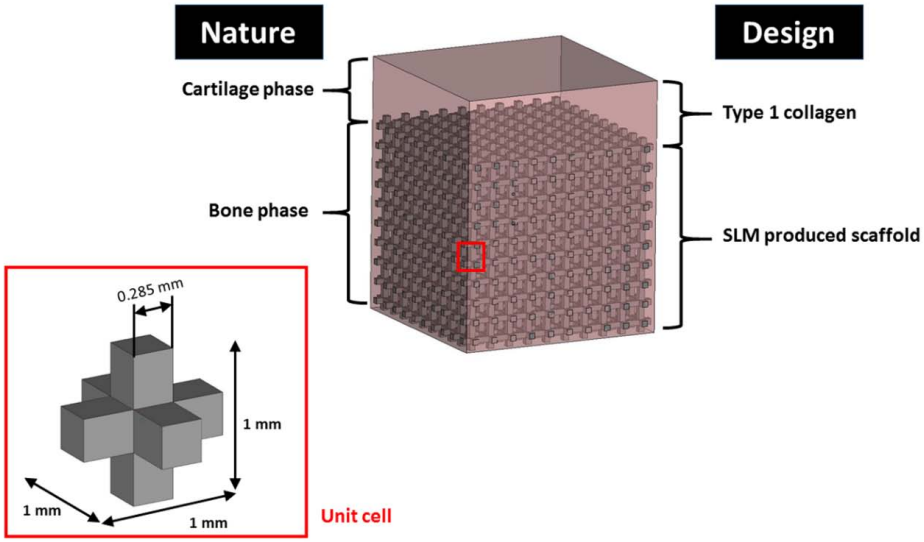

Figure 1. Design concept for biphasic scaffolds

Table 1. SLM processing parameters

Processing Parameters	
Laser Power (W)	100
Laser Scan Speed (mm/s)	500
Hatch Spacing (mm)	0.120
Layer thickness (μm)	30

2.3 Scaffold characterization

2.3.1 Scanning Electron Microscopy

The biphasic scaffolds are characterized using scanning electron microscopy (SEM), using a s canning electron microscope (JEOL JSM-5600LV, Japan). Scaffolds were frozen at –20 °C for two days and lyophilized. All samples were gold-sputtered at 18 mA for 10 sec. Images were taken at an accelerating voltage of 10 kV under high vacuum.

2.3.2 Micro-CT evaluation

The biphasic scaffolds are imaged by microcomputed tomography (μCT) to visualize the internal structures, and the interface between the type 1 collagen and metal scaffolds. Scans were performed using X-ray

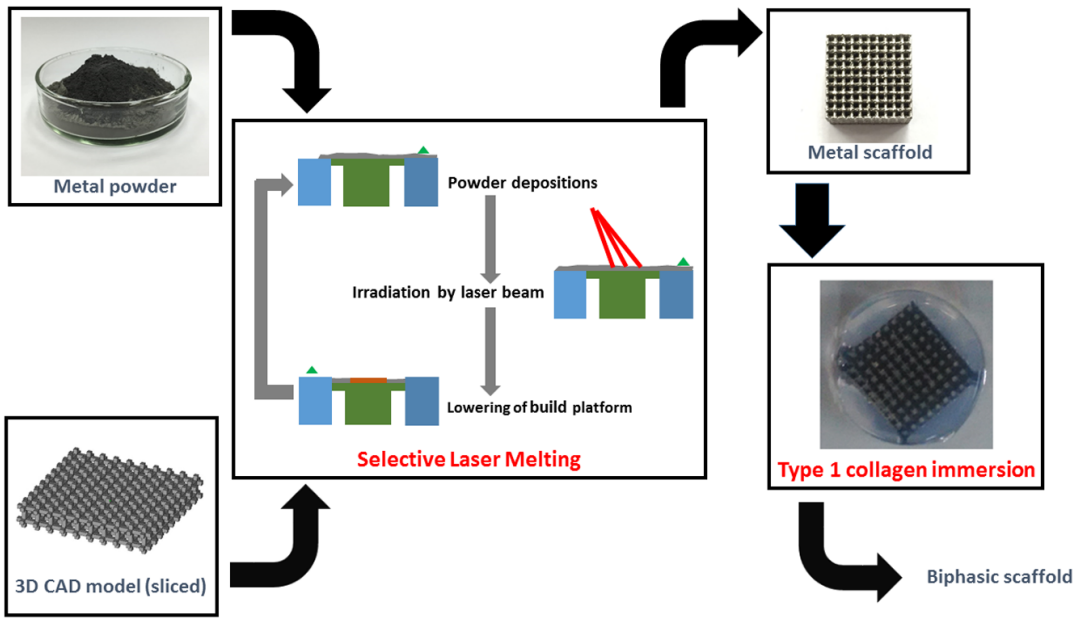

Figure 2. Process flowchart for fabrication of biphasic scaffolds

Imaging Machine (FeinFocus 160.25, United States) at 70 kV and 20 µA with resolution of approximately 15 µm. Three-dimensional renderings and projection planes were made using VGStudio Max software (Volume Graphics GmbH, Germany).

2.3.3 Mechanical characterization

To obtain the compressive properties, the SLM fabricated lattice cubic samples of designed dimensions of 10 mm × 10 mm × 10 mm was tested with 3 replicates, by using Instron Static Tester Series 5569 (Instron, United States) using test conditions recommended by ISO 13314-2011. The tester is equipped with a 50 kN load cell. The compression tests were carried out at room temperature (25 °C). The loading speed was set at 0.6 mm/min for all samples so as to maintain a constant strain rate. This is to minimize the effects of different strain rates in titanium[42-44].

The compression tests were carried out until the samples were fully deformed axially or when the maximum load of 50 kN was reached, whichever came first. The stress-strain curves, yield strengths and elastic constants in compression of the as-fabricated samples were then obtained from the compression tests.

3. Results and Discussion

The fabrication of titanium based scaffolds using SLM has the potential to be a technique for the repair and regeneration of bone via tissue engineering. A skeletal reconstruction scaffolds must have the mechanical properties that can support *in vivo* loads, promote tissue in-growth and be biocompatible.

Micro-CT technique was used to visualize nondestructively the infiltration of type 1 collagen in to the scaffolds, as shown in **Figure 3A** and **Figure 3B**. The actual porosity of the cpTi and TiTa scaffolds are 59.86 ± 0.59% and 59.79 ± 0.68%, respectively. In order to further study the interface between the type 1 collagen and commercial pure titanium or TiTa, SEM was used. Continuous interface was found to exist between the type 1 collagen and metal scaffolds. As shown in **Figure 3**, the type 1 collagen infiltrated the pores of the metal scaffolds without any significant impedance.

From the SEM images (**Figure 3C** and **Figure 3D**), it can be observed that the surface of commercially pure titanium and TiTa scaffolds were rough due to the SLM powder fusion process which can results in powder adhesions on the scaffolds[14]. The top collagen layer was between 200 µm and 500 µm. Infiltration of collagen into the scaffolds was also evident where the type 1 collagen acts as coating over the metal phase of the scaffolds. With type 1 collagen coating, the metallic scaffolds can have enhanced biological response.

The resulting compression elastic constant and yield strength of the as-fabricated lattice structures are shown in **Table 2**. The gradient of the straight-line portion of the stress-strain curve is established to define the elastic constant and the yield strength is taken as the stress at plastic compressive strain of 0.2%. The standard deviation in the elastic constant and yield strength may be due to the laser power fluctuations during SLM resulting in varying amount of powder adhesion on the struts. This in turn affects the compressive properties of the lattice structures.

The resulting elastic constants of both TiTa and cpTi scaffolds are comparable to that of human bones which have wide range of elastic constants, for example, from 1.0 to 25.0 GPa[45, 46]. This shows that with careful design, TiTa and cpTi can serve as load bearing implants while avoiding the adverse "stress shielding" effect[47].

The biphasic scaffolds formed are advantageous for several reasons. Firstly, they can be designed to fit patient specifically using medical imaging such as X-ray. Secondly, they can be designed to cater to specific properties required in different bone regions. Thirdly, the biphasic components can function separately, the hydrogel component can regulate cell differentiation and growth, while promoting bone regeneration and vasculature. The SLM produced scaffold component can act as structural reinforcement and provide the mechanical strength required during the healing process.

Table 2. Compressive properties of SLM produced TiTa and commercially pure titanium samples (n = 5).

Material	Elastic constant (GPa)	Yield strength (MPa)	Strength to elastic constant ratio
TiTa	4.57 ± 0.09	151.93 ± 8.47	3.32×10^{-2}
cpTi	4.29 ± 0.15	121.20 ± 3.67	2.83×10^{-2}

4. Conclusion

Biphasic scaffolds provide bone-like mechanical properties while having the potential to support cartilage growth. The SLM technique offers control over the micro-scale complex design of the bone phase which can be fabricated using biocompatible metals. In this

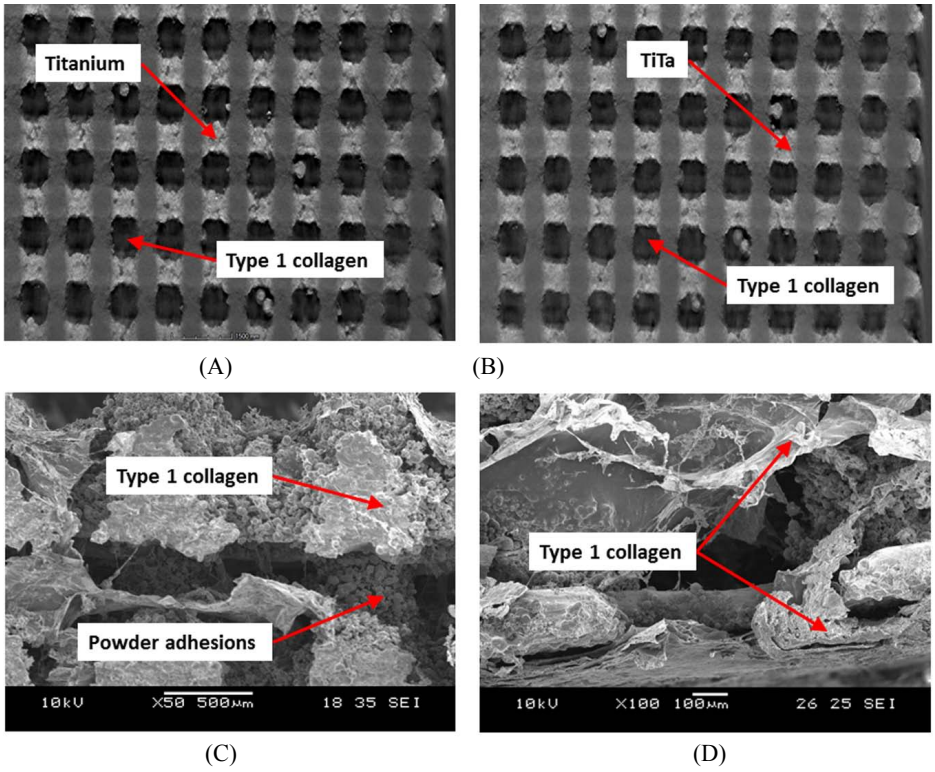

Figure 3. Micro-CT images of biphasic scaffolds (**A**) cpTi (**B**) TiTa, and SEM images of (**C**) cpTi and (**D**) TiTa, showing infiltration of Type 1 collagen into the pores

study, the feasibility of forming cpTi-collagen and TiTa-collagen biphasic scaffolds has been shown. Future studies will aim to optimize the designs and evaluation with *in vitro* cell culture experiment will be carried out. It is anticipated that scaffolds can be tailored to better suit the biochemical and mechanical requirements for osteochondral tissue regeneration.

Conflict of Interest and Funding

The authors declare no conflict of interest.

References

1. Csaki C, Schneider P R A , and Shakibaei M, 2008, Mesenchymal stem cells as a potential pool for cartilage tissue engineering. *Annals of Anatomy-Anatomischer Anzeiger*, vol.190(5): 395 412. https://doi.org/10.1016/j.aanat.2008.07.007
2. Kon E, Filardo G, Di Martino A, *et al*., 2014, Clinical results and MRI evolution of a nano-composite multilayered biomaterial for osteochondral regeneration at 5 years. *American Journal of Sports Medicine*, vol.42(1): 158 165. https://doi.org/10.1177/0363546513505434
3. Panseri S, Russo A, Cunha C, *et al*., 2012, Osteochondral tissue engineering approaches for articular cartilage and subchondral bone regeneration. *Knee Surgery Sports Traumatology Arthroscopy*, vol.20(6): 1182 1191. https://doi.org/10.1007/s00167-011-1655-1
4. Wang S, Taraballi F, Tan L P, *et al*., 2012, Human keratin hydrogels support fibroblast attachment and proliferation in vitro. *Cell and Tissue Research*, vol.347(3): 795 802. https://doi.org/10.1007/s00441-011-1295-2
5. Wang S, Wang Z, Foo S E M, *et al*., 2015, Culturing Fibroblasts in 3D Human Hair Keratin Hydrogels. *ACS Applied Materials & Interfaces*, vol.7(9): 5187 5198. https://doi.org/10.1021/acsami.5b00854
6. Hollister S J, 2005, Porous scaffold design for tissue engineering. *Nature Materials*, vol.4(7): 518 524. https://doi.org/10.1038/nmat1421
7. Duan X, Zhu X, Dong Z, *et al*., 2013, Repair of large osteochondral defects in a beagle model with a novel type I c ollagen/glycosaminoglycan-porous titanium biphasic scaffold. *Materials Science & Engineering C-Materials for Biological Applications*, vol.33(7): 3951 3957. https://doi.org/10.1016/j.msec.2013.05.040
8. Nover A B, Lee S L, Georgescu M S, *et al*., 2015, Porous titanium bases for osteochondral tissue engineering. *Acta Biomaterialia*, vol.27: 286 293. https://doi.org/10.1016/j.actbio.2015.08.045

9. Chua C K, Yeong W Y, and Leong K F, 2005, Rapid prototyping in tissue engineering: A state-of-the-art report. Virtual odeling and Rapid anufacturing, 19 27.
10. Yeong, W Y, Chua C K, Leong K F, *et al*., 2005, Development of s caffolds for t issue engineering using a 3D inkjet model maker. *Virtual Modelling and Rapid Manufacturing-advanced Research in Virtual and Rapid Prototyping*, 115 118.
11. Lee J M, Zhang M, and Yeong W Y, 2016, Characterization and evaluation of 3D printed microfluidic chip for cell processing. *Microfluidics and Nanofluidics*, vol.20 (5). https://doi.org/10.1007/s10404-015-1688-8
12. Cheng X Y, Li S J, Murr L E, *et al*., 2012, Compression deformation behavior of Ti-6A1-4V alloy with cellular structures fabricated by electron beam melting. *Journal of the Mechanical Behavior of Biomedical Materials*, vol 16: 153 162. https://doi.org/10.1016/j.jmbbm.2012.10.005
13. Sallica-Leva E, Jardini A L, and Fogagnolo J B, 2013, Microstructure and mechanical behavior of porous Ti-6Al-4V parts obtained by selective laser melting. *Journal of the Mechanical Behavior of Biomedical Materials*, vol.26: 98 108. https://doi.org/10.1016/j.jmbbm.2013.05.011
14. Sing, S L, Yeong W Y, Wiria F E, *et al*., 2016, Characterization of titanium lattice structures fabricated by selective laser melting using an adapted compressive test method. *Experimental Mechanics*, vol.56: 735 748. https://doi.org/10.1007/s11340-015-0117-y
15. Sun, J F, Yang Y Q, and Wang D, 2013, Mechanical properties of a Ti6Al4V porous structure produced by selective laser melting. *Materials & Design*, vol.49: 545 552. https://doi.org/10.1016/j.matdes.2013.01.038
16. Szymczyk P, Junka A, Ziolkowski G, *et al*., 2013, The ability of S.aureus to form biofilm on the TI-6Al-7Nb scaffolds produced by Selective Laser Melting and subjected to the different types of surface modifications. *Acta of Bioengineering and Biomechanics*, vol.15(1): 69 76.
17. Yeong W Y, Yap C Y, Mapar M, *et al*., 2013, State-of-the-art review on selective laser melting of ceramics. *High Value Manufacturing: Advanced Research in Virtual and Rapid Prototyping*, 65 70.
18. Liu Z H, Zhang D Q, Sing S L, *et al*., 2014, Interfacial characterization of S LM parts in multi-material processing: Metallurgical diffusion between 316L stainless steel and C18400 copper alloy. *Materials Characterization*, vol.94: 116 125. https://doi.org/10.1016/j.matchar.2014.05.001
19. Sing S L, An J, Yeong W Y, *et al*., 2015, Laser and electron-beam powder-bed additive manufacturing of metallic implants: A review on processes, materials and designs. *Journal of Orthopaedic Research*, vol.34(3): 369 385. https://doi.org/10.1002/jor.23075
20. Sing, S L, Yeong W Y, Chua C K, *et al*., 2013, Classical lamination theory applied on parts produced by selective laser melting in High Value Manufacturing: Advanced Research in Virtual and Rapid Prototyping, 77 82.
21. Thijs L, Sistiaga M L M, Wauthle R, *et al*., 2013, Strong morphological and crystallographic texture and resulting yield strength anisotropy in selective laser melted tantalum. *Acta Materialia*, vol.61(12): 4657 4668. https://doi.org/10.1016/j.actamat.2013.04.036
22. Yap C Y, Chua C K, and Dong Z L, 2016, An effective analytical model of selective laser melting. *Virtual and Physical Prototyping*, vol.11(1): 21 26. https://doi.org/10.1080/17452759.2015.1133217
23. Yap C Y, Chua C K, Dong Z L, *et al*., 2015, Review of selective laser melting: Materials and applications. *Applied Physics Reviews*, vol.2(4): 041101. https://doi.org/10.1063/1.4935926
24. Ciocca L, Fantini M, De Crescenzio F, *et al*., 2011, Direct metal laser sintering (DMLS) of a customized titanium mesh for prosthetically guided bone regeneration of atrophic maxillary arches. *Medical & Biological Engineering & Computer*, vol.49(11): 1347 1352. https://doi.org/10.1007/s11517-011-0813-4
25. Li R, Liu J, Shi Y, *et al*., 2010, 316L Stainless steel with gradient porosity fabricated by selective laser melting. *Journal of Materials Engineering and Performance*, vol. 19(5): 666 671. https://doi.org/10.1007/s11665-009-9535-2
26. Yan C, Hao L, Hussein A, *et al*., 2014, Advanced lightweight 316L stainless steel cellular lattice structures fabricated via selective laser melting. *Materials & Design*, vol.55: 533 541. https://doi.org/10.1016/j.matdes.2013.10.027
27. Facchini L, Magalini E, Robotti P, *et al*., 2010, Ductility of a Ti-6Al-4V alloy produced by selective laser melting of prealloyed powders. *Rapid Prototyping Journal*, vol. 16(6): 450 459. https://doi.org/10.1108/13552541011083371
28. Murr L E, Quinones S A, Gaytan S M, *et al*., 2009, Microstructure and mechanical behavior of Ti-6Al-4V produced by rapid-layer manufacturing, for bi omedical applications. *Journal of the Mechanical Behavior of Biomedical Materials*, vol.2(1): 20 32. https://doi.org/10.1016/j.jmbbm.2008.05.004
29. Vrancken B, Thijs L, Kruth J P, *et al*., 2012, Heat treatment of Ti6Al4V produced by selective laser melting: Microstructure and mechanical properties. *Journal of Alloys and Compounds*, vol.541: 177 185.

https://doi.org/10.1016/j.jallcom.2012.07.022

30. Thijs L, Verhaeghe F, Craeghs T, *et al*., 2010, A study of the microstructural evolution during selective laser melting of Ti-6Al-4V. *Acta Materialia*, vol.58(9): 3303 3312. https://doi.org/10.1016/j.actamat.2010.02.004
31. Chlebus E, Kuznicka B, Kurzynowski T, *et al*., 2011, Microstructure and mechanical behaviour of Ti-6Al-7Nb alloy produced by selective laser melting. *Materials Characterization*, vol.62(5): 488 495. https://doi.org/10.1016/j.matchar.2011.03.006
32. Rotaru H, Armencea G, Spirchez D, *et al*., 2013, In vivo behavior of surface modified Ti6Al7Nb alloys used in selective laser melting for custom-made implants. A preliminary study. *Romanian Journal of Morphology and Embryology*, 54(3 SUPPL.): p. 791 796.
33. Sing S L, Yeong W Y, and Wiria F E, 2016, Selective laser melting of titanium alloy with 50 wt% tantalum: Microstructure and mechanical properties. *Journal of Alloys and Compounds*, vol.660: 461 470. https://doi.org/10.1016/j.jallcom.2015.11.141
34. Zhou YL, Niinomi M, and Akahori T, 2004, Effects of Ta content on Young's modulus and tensile properties of binary Ti-Ta alloys for biomedical applications. *Materials Science and Engineering A*, vol.371: 283 290. https://doi.org/10.1016/j.msea.2003.12.011
35. Zhou Y L, Ninomi M, Akahori T, *et al*., 2007, Comparison of various properties between titanium-tantalum alloy and pure titanium for biomedical applications. *Materials Transactions*, vol.48(3): 380 384. https://doi.org/10.2320/matertrans.48.380
36. Yousefi A M, Hoque M E, Prasad R G S V, *et al*., 2015, Current strategies in multiphasic scaffold design for osteochondral tissue engineering: A review. *Journal of Biomedical Materials Research Part A*, vol.103(7): 2460 2481. https://doi.org/10.1002/jbm.a.35356
37. Duan X, Zhu X, Dong X, *et al*., 2013, Repair of large osteochondral defects in a beagle model with a novel type I collagen/glycosaminoglycan-porous titanium biphasic scaffold. *Materials Science and Engineering C*, vol.33: 3951 3957. https://doi.org/10.1016/j.msec.2013.05.040
38. Zhao C, Zhang H, Cai B, *et al*., 2012, Preparation of porous PLGA/Ti biphasic scaffold and osteochondral defect repair. Biomaterials Science, vol.7(1): 703 710. https://doi.org/10.1039/C3BM00199G
39. Nover A B, Lee S L, Georqescu M S, *et al*., 2015, Porous titanium bases for osteochondral tissue engineering. *Acta Biomaterialia*, vol.27: 286 293. https://doi.org/10.1016/j.actbio.2015.08.045
40. Zhao X, He J, Xu F, *et al*., 2016, Electrohydrodynamic printing: a potential tool for high-resolution hydrogel/cell patterning. *Virtual and Physical Prototyping*, vol. 11(1): 57 63. https://doi.org/10.1080/17452759.2016.1139378
41. Getgood A M J, Kew S J, Brooks R, *et al*., 2012, Evaluation of early-stage osteochondral defect repair using a biphasic scaffold based on a collagen-glycosaminoglycan biopolymer in a caprine model. *The Knee*, vol.19(4): 422 430. https://doi.org/10.1016/j.knee.2011.03.011
42. Nemat-Nasser, S., Guo W G, and Cheng J Y, 1999, Mechanical properties and deformation mechanisms of a commercially pure titanium. *Acta Materialia*, vol.47(13): 3705 3720. https://doi.org/10.1016/S1359-6454(99)00203-7
43. Chichili D R, Ramesh K T, and Hemker K J, 1998, The high strain-rate response of alpha-titanium: experiments, deformation mechanisms and modeling. *Acta Materialia*, vol.46(3): 1025 1043. https://doi.org/10.1016/S1359-6454(97)00287-5
44. Gurao N P, Kapoor R, and Suwas S, 2011, Deformation behavior of commerically pure titanium at extreme strain rates. *Acta Materialia*, vol.59(9): 3431 3446. https://doi.org/10.1016/j.actamat.2011.02.018
45. Zysset P K Z, Guo X E, Hoffler C E, *et al*., 1999, Elastic modulus and hardness of cortical and trabecular bone lamellae measured by nanoindentation in the human femur. *Journal of Biomechanics*, vol.32(10): 1005 1012. https://doi.org/10.1016/S0021-9290(99)00111-6
46. Piotrowski B, Baptista A A, Patoor E, *et al*., 2014, Interaction of bone-dental implant with new ultra low modulus alloy using a numerical approach. *Material Science and Engineering: C*, vol.38: 151 160. https://doi.org/10.1016/j.msec.2014.01.048
47. Traini T, Mangano C, Sammons R L, *et al*., 2008, Direct laser metal sintering as a new approach to fabrication of an isoelastic functionally graded material for manufacture of porous titanium dental implants. *Dental Materials*, vol.24(11): 1525 1533. https://doi.org/10.1016/j.dental.2008.03.029

RESEARCH ARTICLE

Influence of electrohydrodynamic jetting parameters on the morphology of PCL scaffolds

Hang Liu[1], Sanjairaj Vijayavenkataraman[2], Dandan Wang[1], Linzhi Jing[1,3], Jie Sun[1,4*] and Kai He[4]

[1] National University of Singapore (Suzhou) Research Institute, Suzhou Industrial Park, Suzhou 215123, China
[2] Department of Mechanical Engineering, National University of Singapore, Singapore 117575, Singapore
[3] Department of Chemistry, National University of Singapore, Singapore 117543, Singapore
[4] Department of Industrial Design, Xi'an Jiaotong-Liverpool University, Suzhou 215123, China

Abstract: One of the important constituents in tissue engineering is scaffold, which provides structural support and suitable microenvironment for the cell attachment, growth and proliferation. To fabricate micro/nano structures for soft tissue repair and three-dimensional (3D) cell culture, the key is to improve fibre-based scaffold fabrication. Electrohydrodynamic (EHD) jetting is capable of producing and orientating submicron fibres for 3D scaffold fabrication. In this work, an EHD-jetting system was developed to explore the relationship between vital processing parameters and fibre characteristics. In this study, polycaprolactone (PCL) solution prepared by dissolving PCL pellets in acetic acid was used to fabricate the scaffolds. The influence of voltage, motorized stage speed, solution feed rate, and solution concentration on fibre characteristics and scaffold pattern were studied. Morphology of the EHD-jetted PCL fibres and scaffolds were analysed using optical microscope images and scanning electron microscope (SEM) images. Multi-layer scaffolds with the varied coiled pattern were fabricated and analysed. Cell attachment and proliferation have to be investigated in the future by further cell culture studies on these multi-layer coiled scaffolds.

Keywords: electrohydrodynamic jetting, 3D bioprinting, polycaprolactone scaffolds, soft-tissue, tissue engineering

*Correspondence to: Jie Sun, Department of Industrial Design, Xi'an Jiaotong-Liverpool University, Suzhou 215123, China; Email: jie.sun@xjtlu.edu.cn

Received: November 14, 2016; **Accepted:** December 14, 2016; **Published Online:** January 6, 2017

Citation: Liu H, Vijayavenkataraman S, Wang D, *et al*., 2017, Influence of electrohydrodynamic jetting parameters on the morpho logy of PCL scaffolds. *International Journal of Bioprinting*, vol.3(1): 72–82. http://dx.doi.org/10.18063/IJB.2017.01.009.

NOMENCLATURE

C	Concentration (wt%)
D	Nozzle to substrate distance (mm)
FR	Feed Rate (μL/min)
SS	Stage Speed (mm/s)
T	Temperature (°C)
V	Voltage (kV)

1. Introduction

To fabricate micro/nano structures for soft tissue repair and three-dimensional (3D) cell culture in regenerative medicine, tremendous efforts have been made to improve fibre based scaffold fabrication. Traditional scaffold fabrication methods, such as solvent casting and particulate leaching, gas foaming, phase separation, melt moulding, and freeze drying suffer from many inherent limitations, including the inability to precisely control pore size, pore geometry, pore interconnectivity, and spatial distribution of pores. Other relatively recent scaffold fabrication methods, such as fused deposition modelling (FDM) and extrusion method, suffer from the limitations of low resolution and

Influence of electrohydrodynamic jetting parameters on the morphology of PCL scaffolds. © 2017 Hang Liu, et al. This is an Open Access article distributed under the terms of the Creative Commons Attribution-NonCommercial 4.0 International License (http://creativecommons.org/licenses/by-nc/4.0/), permitting all non-commercial use, distribution, and reproduction in any medium, provided the original work is properly cited.

large diameter fibres ranging from 180–1000 μm[1]. Electrohydro-dynamic (EHD) spinning technology involves high speed non-linear electrohydrodynamics, complex rheology, and transport of charge, mass, and heat within the jet. The process consists of three stages: jet initiation, jet elongation with or without branching and/or splitting, followed by solidification of jet into nanofibers. High resolution fibres can be produced by this technique to mimic the nano-topographical elements in the extracellular matrix (ECM)[2-4]. The resultant micro-metre/nanometre fibres are usually disordered and pore size less than 20 μm[5]. The fabricated electrospun meshes are in a non-woven form, applied in wound dressing[6,7]. Continuous single fibre or uniaxial fibre bundles are required in tendon, muscle, cartilage, and meniscus replacement, in which the collagen fibres are organized either parallel or perpendicular to the surface of tissues[8]. Scaffolds with highly aligned fibres usually possess a greater level of mechanical anisotropy[3], which is preferred in soft tissue engineering. Having accurate fibre control on physical properties and patterns is critical for fabrication of biomimetic structures.

The traveling liquid jet stream is subjected to a variety of forces with opposing effects and as a result, various fluid instabilities also occur. The jet may undergo splitting into multiple sub-jets in a process known as splaying or branching[28]. This happens when changes occur in the shape and charge per unit area of the jet due to its elongation, and evaporation of the solvent. The splaying or branching process shifts the balance between the surface tension and the electrical forces, and the jet becomes unstable. In order to reduce its local charge per unit surface area, the unstable jet ejects a smaller jet from the surface of the primary jet. However, the key role in reducing the jet diameter from micrometre to nanometre is played by whipping instability, which causes bending or stretching of the jet. When the polymer jet becomes very long and thin, the time required for excess charge to redistribute itself along the full length of the jet becomes longer. The location of the excess charge then tends to change with the elongation. The repulsive coulombic forces between the charges carried with the jet elongate the jet in the direction of its axis until the jet solidifies. This leads to an incredibly high velocity at the thin leading end of the straight jet. As a result, the jet bends and develops a series of lateral excursions that grow into spiral loops with a thin fibre diameter.

To achieve aligned electrospun fibres, various types of electro-spinning setup with different dynamic collectors have been developed[9], such as disc collector[10], rotating drum with wire[11], and rotating tube with knife edge electrodes[12]. One of the first instances of aligned electro-spun fibres was demonstrated by Theron *et al*.; a thin rotating disc was used to collect the fibres[10]. Biodegradable nanofibrous scaffolds with aligned poly (l-lactic-co-e-caprolactone) [P(LLA-CL)] copoly-mer have been produced using this electrospinning setup for blood vessel engineering application. Baker *et al*. applied an electrospinning setup with a rotating drum/mandrel to collect aligned electrospun fibres for scaffold fabrication[13]. An electrospun mat, with the majority of fibres in one direction, was seeded with cells; the cells were observed to attach and grow along the prevailing fibre direction in the *in vitro* study.

Near-field electrospinning process (NFES)[14], is proposed to orientate micro and nano fibres via stage control where the electrode is positioned close to the substrate. Several studies have focused on NFES to evaluate substrate effects[15], patterns[16], and parameters optimization[17]. However, these achievements are only limited to 2D graphic and patterning applications. A quick solidification of fibres over very short distances between the nozzle and collector is normally required to build 3D structures. An EHD hot jet plotting technique has been applied to fabricate high resolution (i.e., a fibre diameter below 10 μm) 3D scaffolds[18]. This method is not applicable to temperature-sensitive materials, such as collagen and growth factors, or high melting point materials.

Park *et al*. introduced computer control into a self-developed EHD printing system to print complex patterns using various inks that are in industrial use, ranging from insulating and conducting polymers, to solution suspensions of silicon nanoparticles and rods, to single-walled carbon nanotubes[19]. Kim *et al*. experimented materials and operating conditions for high-resolution printing of layers of quantum dots with precise control[20]. Lee *et al*. investigated the generation of highly aligned and patterned silver nanowires (Ag NWs) using EHD-jetting[21].

In this work, an EHD-jetting system was developed to explore the relationship between processing parameters and fibre characteristics. High resolution scaf-

folds with controlled micron scale patterns were fabricated. PCL solution prepared by dissolving PCL pellets in acetic acid was used to fabricate 3D scaffolds. This study mainly investigated the influence of the stage speed on fibre characteristics and scaffold pattern. Morphology of the EHD-jetted PCL fibres and scaffolds were analysed using optical microscope images and scanning electron microscope (SEM) images. Multi-layer scaffolds with varied coiled pattern were fabricated and analysed. Cell attachment and proliferation have to be investigated in the future by further cell culture studies on these multi-layer coiled scaffolds.

2. Methodology

2.1 EHD-jetting System Design and Setup

As shown in **Figure 1**, the EHD-jetting system consists of a high precision motorized stage capable of XYZ motion, high voltage power supply (output DC voltage from 0 to 30 kV), and solution feeding system (syringe pump, syringe and nozzle). The solution feeding system consists of a syringe pump (NE-1000, New Era Pump System Inc., USA), syringe with internal diameter of 13 mm and volume of 5 ml, a flexible hose with internal diameter of 3 mm, and a stainless steel nozzle with internal diameter of 0.5 mm. The syringe is filled with sufficient PCL solution, which gives continuous solution supply during the EHD-jetting process.

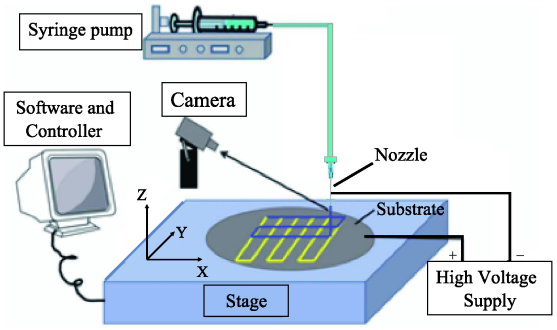

Figure 1. Sketch diagram of EHD-jetting system.

A three-axis precision stage (PRO165LM, Aerotech Company, USA) was used for scaffold fabrication of different geometries. The stage was driven by linear motors, with the X and Y axes having a travel distance of 150 mm with ±3 μm accuracy. The travel distance of Z axes was 50 mm with ±5 μm accuracy. Polished silicon wafers with diameter of 100 mm and thickness of 0.8 mm, were used as the substrate. The precision stage was controlled using Ensemble IDE software running on a desktop PC and connected through a serial USB port, gave the real-time position and velocity information for monitoring and compensation purposes.

2.2 Material Preparation

PCL is a type of biodegradable polyester normally used for fabrication of scaffolds. A solution of PCL is obtained by dissolving the PCL pellets in acetic acid. PCL pellets with an average molecular weight of 90 kDa, were purchased from Scientific Polymer Products Inc., USA. Acetic acid with 99.7% purity was purchased from Aladdin Industrial Corporation, USA. Material preparation involves dissolving the PCL pellets in acetic acid, and sonicating it in an ultrasonic bath at 60 °C until it turns into a colourless viscus liquid. Later on, the solution was degassed for few hours until there were no notable air bubbles.

2.3 Scaffold Characterization

Surface morphology of the PCL scaffold was observed using an optical microscope (BX51M, Olympus, Japan) at a magnification of ×50 and a scanning electron microscope (JSM-6510, JEOL, Japan) at an accelerating voltage of 15 kV. Fibre diameter was measured both using the optical microscopy images (using MShot Digital Imaging System software) and from the SEM. In this study, the fiber diameter was measured at 4 points on each fiber and an average value was taken.

2.4 Process Parameters

During the printing process, fibres were laid down on the substrate and a mesh was formed by the raster motion, shown as **Figure 2A**. Fibre characteristics such as fibre diameter and its uniformity, were adjusted by varying several controllable process parameters[22,23]. In this study, six parameters were considered to have major effects on fibre diameter as well as morphology, and they are discussed below:

(i) Solution Concentration (C): Weight volume ratio of PCL in acetic acid is considered as the solution concentration. During the solvent-based EHD-jetting process, one of the key requirement for fibre collection and 3D structure construction is whether the fibre would solidify over a short distance between the nozzle and the substrate. The concentration solution of 60% to 80% was used in this study.

(ii) Supply voltage (V): When a high voltage is ap-

plied between the nozzle and the substrate, charges will be induced within the solution. When a small volume of electrically conductive droplet is exposed to an electric field, the shape of the droplet starts to deform from the shape caused by surface tension alone. When a certain threshold voltage has been reached, the slightly rounded tip inverts and emits a jet of liquid.

(iii) Nozzle-to-substrate distance (D): In a conventional EHD-spinning process, the nozzle to substrate distance ranges from 10 mm to 30 mm[24], which leads to whipping. A smaller distance results in stronger electric field, which causes the solution to overcome the surface tension on the Taylor cone and initiate the EHD-jetting process.

(iv) Stage speed (SS): When the high voltage initiates the Taylor cone, it usually bursts out with an initial velocity of up to 5 m/s[25]. In order to avoid accumulation of solution at the nozzle tip, an appropriate stage speed should be chosen. In this study, the maximum stage speed for scaffold fabrication was set at 0.3 m/s.

(v) Solution feed rate (FR): The syringe pump supplies a constant solution flow, and the feed rate setting can directly affect the fibre formation. It is hard to form a Taylor cone when the feed rate is too low, for it cannot eject enough solution. However, the solution may accumulate at the nozzle tip under a higher feed rate and in turn produce thick fibres.

(vi) Temperature (T): PCL has a glass transition temperature about −60 °C and a low melting point of around 60 °C. Low melting point of the PCL makes it vulnerable during the EHD-jetting process. The temperature mainly influences the viscosity and conductivity of medium, thus changing the surface tension and electrostatic force under the applied electrical force.

2.5 Stage Motion Characterization

Effective fabrication area represents the part of the scaffold, which was fabricated when the actual robotic stage speed approximately equals to the preset stage speed. In this study, a rectilinear raster pattern was used as the standard print pattern as shown in **Figure 2A**.

Following this pattern, the stage first moves in horizontal zigzag directions. Next it moves in vertical zigzag directions to print a full single layer. Thus, a linear movement can be divided into 3 phases, the acceleration region, stable region, and the deceleration region. As shown in **Figure 2B**, position feedback displayed that the axis was moved from 0 mm to 40 mm, while the velocity feedback shows the 3-region variation. Then, each fiber began with an acceleration region, then reached the stable region, and finally ended at the deceleration region. Only the fiber fabricated under the stable region can be considered as the effective fabrication area. The stage was built on a servo loop controller, and can be auto-tuned, which involved driving the axis using a predefined input, measuring the resulting data, and calculating a set of servo gains that matched given criteria.

To define the stable region under a varied stage speed and acceleration, a stage tuning test was designed. In order to find the optimal stable region, stage speed was fixed and different stage performance under varied acceleration values and servo gains were

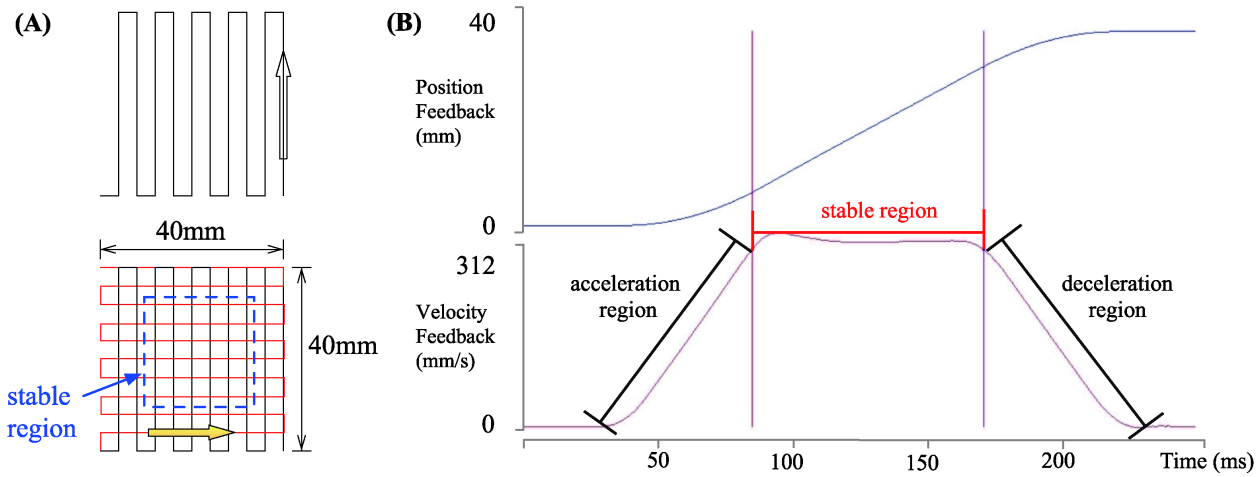

Figure 2. (A) Sketch of raster stage movement pattern; **(B)** Position feedback and velocity feedback of motorized stage axis (pre-set stage speed=300 mm/s).

compared. Stage performance was obtained from the feedback images. To select the best stage performance, the length of the stable region was compared, and the longest one was chosen as the best. When the stage reached a r elatively stable region, there still existed some fluctuation, and any error below ±5% was defined as sustainable error. Based on these criteria, a set of acceleration values with corresponding stable region length were found and listed in **Table 1**. In this study, all of the experimental results were based on the scaffold fabricated in the effective fabrication area.

Table 1. Stage motion characterization results

Stage speed (mm/s)	cceleration region (mm)	Stable region (mm)	Deceleration region (mm)
50	1.7	36.3	1.9
100	3.6	32.8	3.6
150	3.6	32.4	4.0
200	4.3	31.2	4.5
250	6.1	27.6	6.3
300	9.1	21.2	9.7

3. Results and Discussion

3.1 Grid Scaffold Structure and Process Parameters

Effects of two process parameters on fibre diameter were investigated: solution feed rate and motorized stage speed. In addition, the nozzle-to-substrate distance plays an important role in positioning and tuning the degree of solidification. If this distance was below 2.5 mm, the deposited fibres we always straight even at very slow stage speed values. If the nozzle-substrate distance was between 2 mm and 5 mm, straight fibres can only be obtained when the stage speed was larger than that of the jetting speed.

(1)Effects of Solution Feed Rate on Fibre Diameter

Relationship between solution feed rate and fibre diameter has been investigated. Solution feed rate was varied from 1.0 μL/min to 2.0 μL/min at increments of 0.5 μL/min. The other parameters were kept constant: voltage of 3.0 kV, nozzle-to-substrate distance of 3 mm, stage speed of 200 mm/s, and temperature of 20°C. Two concentrations of PCL solution were used: 60% and 70%. For 60% PCL, the measured fibre diameter varied from 18.9 μm to 36.0 μm. For the 70% PCL, the measured fibre diameter varied from 18.7 μm to 37.6 μm. In **Figure 3**, the variation of the solution feed rate vs the fiber diameter is shown. Solution feed rate at 2.0 μL/min always could generate thicker fibres, and the fibre diameter increases with the solution feed rate. Higher solution feed rate results in increased pressure from the pump acting on the Taylor cone, which leads to an increase in the volume of the solution that comes out of the nozzle. Therefore, higher solution feed rate always causes larger fibre diameter.

In this experiment, solution concentration did not have significant influence on the fibre diameter. Both 60% PCL and 70% PCL exhibited similar trends. However, there are other factors that were influenced by varying solution concentration, such as electrical conductivity, surface tension, viscosity, and solvent evaporation rate. All of these factors determine the amount of solution being stretched out from the nozzle tip under high voltage, thus affecting fibre formation. During the process initiation, the surface tension of the solution should be overcome, and then the EHD jets will be stretched. Less acetic acid means fewer frees ions, and a decrease in electrical conductivity. Thus, less solution volume was pulled out of the nozzle under higher concentration. These multiple factors work together to determine the fibre diameter, and some of them are significantly affected by solution concentration and feed rate.

(2) Effects of Stage Speed on Fibre Diameter

Stage speed has significant influence on the positioning of EHD jetted fibres. When this speed is much lower than the speed of jetting, linear, aligned microstructures were achieved even when the motion stage movement was linear. Air turbulence or buckling of solid fibres disturbs the linear deposition of fibres. When the two speeds are closer, the deposited fibres were linear and aligned straight due to the mechanical drawing force. When the stage speed exceeds the jetting speed, fibre diameter can be tuned by varying the stage speed.

Table 2 shows the relationship between stage speed and fibre diameter. The range of the stage speed used were 100 mm/s to 300 mm/s at increments of 50 mm/s; the supply voltage was 3.0 kV, nozzle-substrate distance was 3.0 mm, and the solution feed rate was 1.5 μL/min. Two different PCL concentrations, 60% and 70%, were used for this experiment.

As shown in **Figure 4**, fibre diameter decreases with increased stage speed. Faster stage speed can effectively reduce the volume of dispensed solution on the substrate, and hence, by increasing the stage speed, thinner fibres can be fabricated. For 70% PCL solution, when the stage speed was 100 mm/s, the average fibre diameter was around 32.8 μm, and when the stage

Table 2. Optical microscope images of scaffold pattern under varied stage speed (FR=1.5 μL/min, D=3 mm, V=3 kV, and T=20 °C). Scale bar 400 μm

		Stage speed (mm/s)				
		100	150	200	250	300
60% PCL	Scaffold pattern	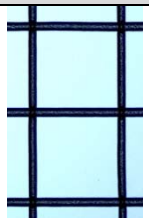		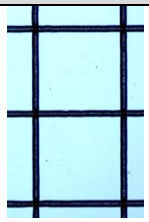	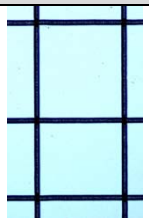	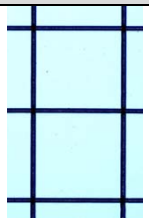
	Fiber diameter (μm)	37.8	30.7	29.5	25.0	23.2
70% PCL	Scaffold pattern	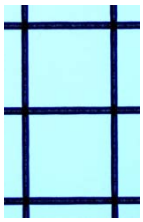	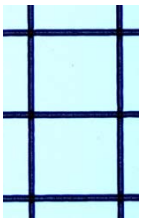	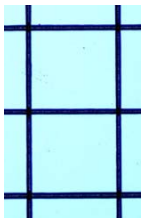	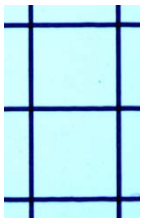	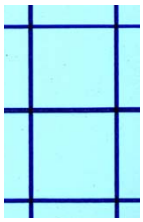
	Fiber diameter (μm)	32.8	30.0	23.7	20.7	19.3

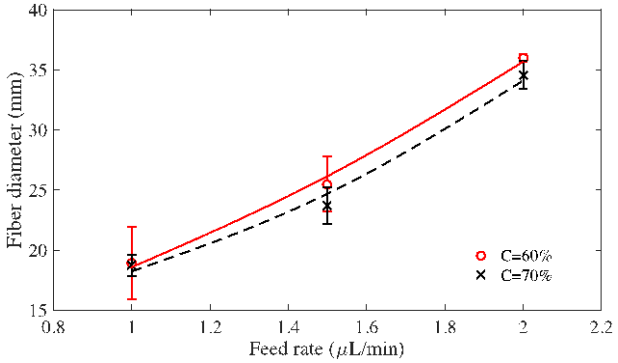

Figure 3. Relationship between feed rate and fibre diameter (V=3 kV, D=3 mm, SS=200 mm/s, and T=20°C).

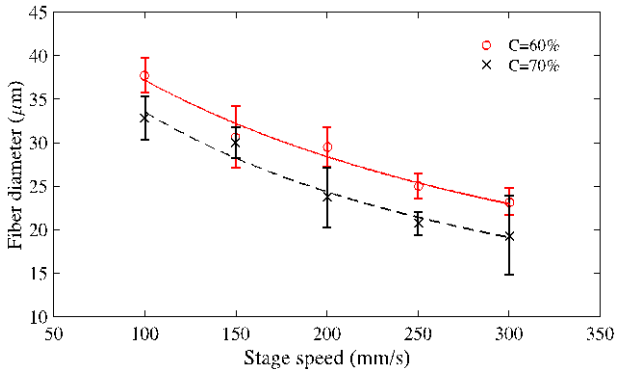

Figure 4. Relationship between feed rate and fibre diameter (FR=1.5 μL/min, D=3 mm, V=3 kV and T=20°C).

speed was increased to 300 mm/s, the average fibre diameter decreased to 19.3 μm.

3.2 Coiled Structure and Influencing Factors

Coiled structure has more surface area than the normal mesh structure and hence provides more area for the cells to attach and grow. It is also expected to provide better pore interconnectivity and hence increased cell-cell interaction. Coiled structure scaffold is based on the control of the unstable bulking/whipping behaviour observed during EHD-jetting process, in which the unstable jet fiber can be positioned on the substrate by the combined control of process parameters. This section discusses the effects of PCL properties, stage speed, solution feed rate, and solution concentration on the formation of a coiled structure.

(1) Effects of PCL chemical property on EHD-jetting Process

In EHD-jetting process, the pendent drop of polymer solution under electric field is influenced by many forces: columbic, electric, viscoelastic, surface tension, air drag and gravitational force. Among them, electric, viscoelastic and surface tension are the three main forces working on the EHD jetting process, and the last two forces are closely relevant to the viscosity of solution.

PCL shows high solubility in many polar solvents, such as tetrahydrofuran and acetic acid[26]. As a hydrophobic, semi-crystalline polymer, the crystallinity of PCL tends to decrease with increasing molecular weight (MW). The good solubility of PCL, its low melting point (59–64 °C) and exceptional blend-com-

patibility has stimulated extensive research into its potential application in the biomedical field. The solubility of PCL is strongly dependent on the MW of polymer. Hence, the viscosity of the polymer solution is proportional to the MW of PCL, for the same concentration of solution. As the PCL has a low melting point, the viscosity of the polymer solution decreases rapidly with the increase of temperature, thus lowering the viscoelastic force acting on the Taylor cone during EHD-jetting. Moreover, during the printing process, the polymer chain tends to orient along forced direction and solidifies on substrate upon evaporation of the solvent in which the temperature and humidity show significant influence on the solvent evaporation rate[29–30]. Therefore, the temperature variation directly affects the EHD jetting process and the morphology of the scaffold.

(2) Effects of Process Parameters on the Layout of Scaffold

In this experiment, process parameters were C=60% and 70%, FR=1 μL/min, D=3 mm, V=3 kV, and T=25°C. A transition from coils to waves and finally to straight fibres was observed, with the variation of the stage speed, as shown in **Table 3**. Two critical speeds were observed to aid in this transition between two shapes: straight, and coiled/waved structures, namely 100 mm/s and 250 mm/s, when C=60%.

When the stage speed was relatively slow, the electrical force, pressure from the pump, and the other forces take charge of the formation of the fibres. Since the stage moves very slowly, there is enough time for the fibres to fold and form coiled/wave structures. However, when the speed increases, the mechanical drawing force of the stage play a main role, and the fibres align in a straight line. With the increase of the stage speed, the fibre diameter becomes thinner and thinner. At a certain point, when the fibre diameter is too thin, the mechanical drawing force generated by the robotic stage will lose control due to the small fibre diameter and the fibres become coiled or wave-shaped again. Splaying might also play a role in the formation of coiled / wave structure but further research is required to study how significant the effect is. This explains the two critical transition speeds of 100 mm/s and 250 mm/s. At C=70%, the lower bound of the transition speed holds good at 100 mm/s while straight to coiled/wave structure transition is not seen at 250 mm/s. As mentioned above in the case for C=60%, at lower stage speed, there is enough time for the fibres to fold and form coiled/wave structures. But at higher speeds (>250 mm/s), while C=60% is easy to trigger the coiled/wave structure, C=70% yields fibres that are not thinner enough to form the coiled/wave structure due to the higher solution concentration. Hence, there is no transition from straight to coiled/wave structure is seen.

(3) Effects of Stage Speed on the Coiled Scaffold

To investigate the influence of stage speed on the coiled scaffold pattern, the process parameters were set as following: nozzle-to-substrate distance of 3 mm, solution concentration of 60%, solution feed rate of 1.5 μL/min, ambient temperature of 25#C, and the stage speed was varied from 100 mm/s to 250 mm/s at increments of 50 mm/s. **Table 4** shows the optical microscope images of fabricated single layer scaffolds.

In this experiment, the temperature was 25#C, which is 5#C higher than the previous single layer grid structure fabrication (**Table 2**). With the increase of temperature, the solution viscosity decreased, aiding the traveling liquid jet stream to flow easily, being subject to a variety of forces. And then, the EHD jetting process undergoes an instable phase, which directly results in the formation of the coiled structure scaffold. The stage speed plays a s econdary role in this experiment by just guiding the scaffold pattern. Therefore, all the scaffold patterns are coiled and the stage speed variation resulted in slight differences in the coiled structure morphology. During the EHD-jetting process, the liquid jet stream exiting from the nozzle is subjected to a variety of forces with different effects. If the forces are unbalanced, instability of the jet occurs. The increased surface tension at the Taylor cone and the electrical force causes the whole EHD-jetting process to be unstable during this period and forms coiled structures. However, by tuning the parameters, consistent coiled patterns were obtained. For instance, at a s tage speed of 100 mm/s, the coiled structure was more uniform when the feed rate was increased from 1.5 to 2 μL/min.

From **Table 4**, when the stage speed is low, there were more coiled loops in a single fibre. Apart from this, the low stage also resulted in thicker fibre diameter. Comparing the fibres printed at a stage speed of 100 mm/s with that of 150 mm/s, the fibre diameter is smaller and the loop diameter is larger. Both the low stage speed and high stage speed have less likelihood to fabricate a uniform coiled pattern. For both the concentration values of 60% and 70%, the coils were unstable and non-uniform at the extreme ends of stage

speed, namely at 100 mm/s and 250 mm/s.

As shown in **Table 4**, an increasing stage speed from 100 mm/s to 250 mm/s results in stretching of the EHD-jetted fibres to form loose spiral structure scaffold. The structural uniformity linearly decreases with stage speed. Under a smaller stage speed, the fibre was mainly stretched by electrical field, and the mechanical drawing force only plays a guiding role in positioning the fibres along the motion direction. The shape of deposited structure is determined by the relative velocity and the instability of jetting, while the other processing parameters are kept constant. As the stage speed was increased to 250 mm/s, the mechanical drawing force becomes an important influencer in drawing the fibres, thus resulting in loose spiral structures rather than the uniform coiled structure.

3.3 Multilayer Scaffold Fabrication

From the insights gained by the experiments done in the previous sections on single layer scaffolds of grid and coiled structure, multi-layer scaffolds were fabricated using PCL material. SEM images show the surface topography, morphology features of the multi-layer scaffolds (**Figure 5**). The process parameters of this grid structure scaffold were C=60%, V=3 kV, D=3 mm, FR=2 µL/min, SS=250 mm/s, and T=25#C, as shown in **Figure 5A**. In this structure, the average fibre diameter and pore size were 15 µm and 400 µm respectively. The fibers are precisely oriented. **Figure 5B** and **5C** shows the front and rear view of the multi-layer coiled structure scaffold. The process parameters used in fabricating the multi-layer structure were

Table 3. Optical microscope images of single layer scaffold under varied stage speed (FR=1 µL/min, D=3 mm, V=3 kV, T=25 ºC). Scale bar 400 µm

	Stage speed (mm/s)					
	50	100	150	200	250	300
60%PCL	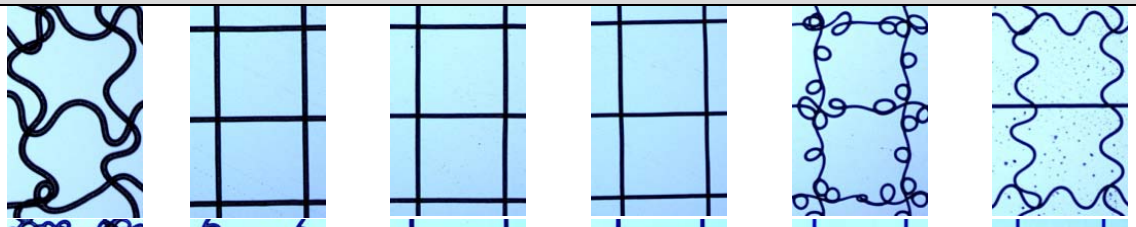					
70%PCL	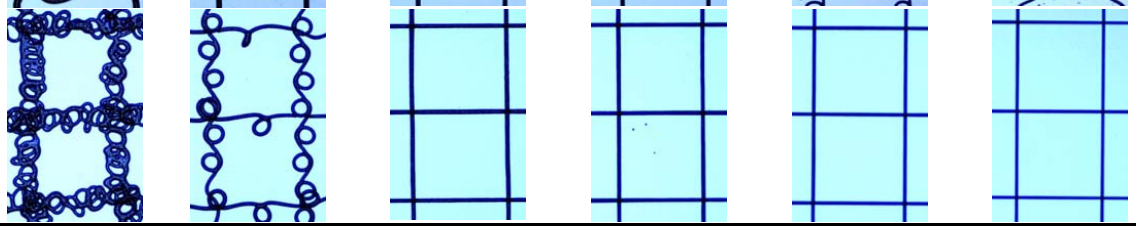					

Table 4. Optical microscope images of single layer scaffold under varied stage speed and solution feed rate (C=60%, D=3 mm, V=3 kV, T=25#C). Scale bar 400 µm

Feed rate	Stage speed (mm/s)			
	100	150	200	250
1.5µL/min	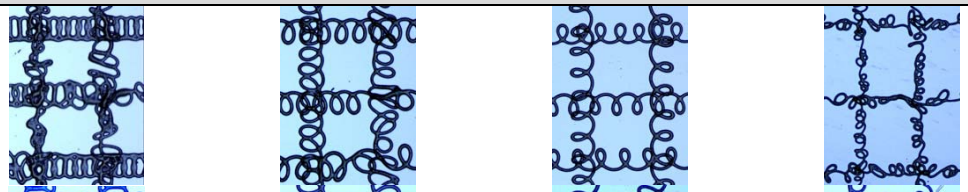			
2.0µL/min	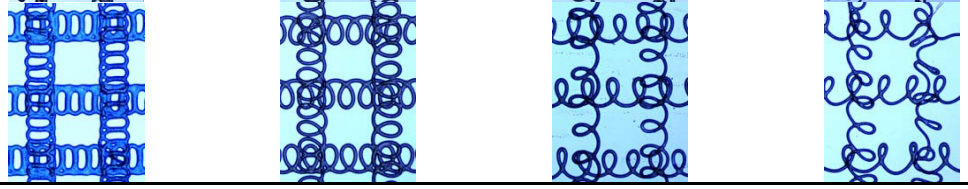			

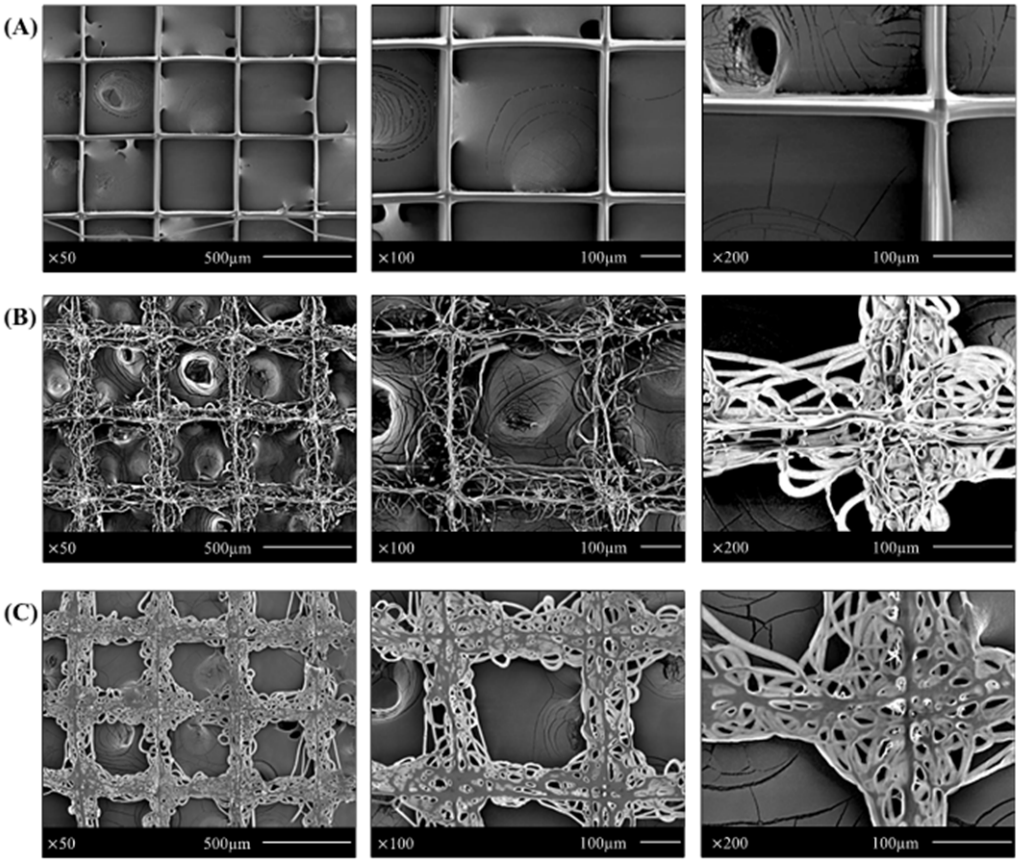

Figure 5. SEM images for fabricated multi-layer scaffolds: **(A)** gird structure scaffold; process parameters are C=70%, V=3 kV, D=3 mm, FR=2 μL/min, SS=250 mm/s, T=25 ^{o}C; **(B)** front view of coiled structure scaffold; process parameters are C=60%, V=3 kV, D=3 mm, FR=2 μL/min, SS=250 mm/s, T=25 ^{o}C; **(C)** rear view of the coiled structure scaffold.

C= 60%, V=3 kV, D=3 mm, FR=2 μL/min, SS= 250 mm/s, and T=25 °C.

A proper scaffolds' physical property is one of the most important prerequisites for tissue engineering applications, which include thickness, porosity, strength, and the ability for the cells to attach and grow. Porosity(Π) is defined as the percentage of void space in a solid, and it is a morphological property independent of the material[27]. It is calculated by using Equation (1)

$$\Pi = 1 - \rho_{scaffold} / \rho_0 \quad (1)$$

where $\rho_{scaffold}$ is the density of the EHD-jetting fabricated scaffold and ρ_0 is the bulk density of the PCL. Porosity of biomimetic scaffolds plays a critical role in tissue formation both *in vitro* and *in vivo*. Comparing **Figure 5A** and **5B**, it is easy to conclude that void space of coiled structure scaffold is much smaller than the grid structure scaffold, which means the porosity of coiled structure is smaller than the gird structure. However, the surface area of coiled structure is higher than the grid structure, thus increasing the cell attachment area, which might benefit the cellular growth. In the coiled structure scaffolds, the small holes with different sizes might afford the diversity of cell attachment.

While the grid structure was obtained at a concentration of 70%, coiled structure was obtained at a concentration of 60%, keeping all the other parameters the same. In this experiment, the stability of the jet decreased with the solution concentration, which directly results in the formation of coiled structure. Besides, the printing temperature may also trigger the formation of coiled structure. Moreover, comparing the front view and the rear view of the coiled scaffolds, the first layer was flattened, and the reasons might be insufficient time for solidification due to the low concentration (60%), and thinner fibre diameter.

It is worth mentioning that the fabrication of coiled and wave structure scaffolds, both single layer and multi-layer, using the process parameters given, possessed both repeatability and reproducibility. At least

15 scaffolds were fabricated for each combination of process parameters and used for SEM measurement and cell culture study. The SEM results show that around 80% of the samples show very similar microstructure patterns under the same fabrication condition combination.

4. Conclusion

EHD-jetting technique can be used to direct-write high-viscosity solution into continuous high-resolution fibres. Thus, EHD-jetting could be used for fabrication of multi-layer scaffolds with various morphology and resolution that could be achieved by tuning key process parameters: the stage speed, the solution concentration, the nozzle-to-substrate distance, the temperature, and the applied voltage. The mechanical drawing force controlled by the stage speed plays a critical role in the determination of resolution, positioning, and alignment of the fibres. Arrayed diverse structures like the coiled scaffolds can potentially be applied in soft tissue repair and 3D cell culture in regenerative medicine. Cell attachment and proliferation has to be investigated in the future by further cell culture studies on these multi-layer coiled scaffolds.

Conflict of Interest and Funding

No conflict of interest was reported by the authors. This research is supported by the Jiangsu Province Science and Technology Support Programme, China under Grant No BE2013057 and Suzhou Science and Technology Program under Grant No. SYG201418.

References

1. Yeong W Y, Chua C K, Leong K F, *et al.* 2004, Rapid prototyping in tissue engineering: challenges and potential. *Trends in Biotechnology*, vol.22(12): 643–652. http://dx.doi.org/10.1016/j.tibtech.2004.10.004
2. Wang X, Drew C, Lee S H, *et al.* 2002, Electrospun nanofibrous membranes for highly sensitive optical sensors. *Nano Letters*, vol.2(11): 1273–1275. http://dx.doi.org/10.1021/nl020216u
3. Li W J, Laurencin C T, Caterson E J, *et al*. 2002, Electrospun nanofibrous structure: a novel scaffold for tissue engineering. *Journal of Biomedical Materials Research*, vol.60(4): 613–621. http://dx.doi.org/10.1002/jbm.10167
4. Min B M, Lee G, Kim S H, *et al.* 2004, Electrospinning of silk fibroin nanofibers and its effect on the adhesion and spreading of normal human keratinocytes and fibroblasts *in vitro*. *Biomaterials*, vol.25(7): 1289–1297. http://dx.doi.org/10.1016/j.biomaterials.2003.08.045
5. Megelski S, Stephens J S, Chase D B, *et al*. 2002, Micro and nanostructured surface morphology on electrospun polymer fibers. *Macromolecules*, vol.35(22): 8456–8466. http://dx.doi.org/10.1021/ma02044a
6. Jin H J, Fridrikh S V, Rutledge G C, *et al.* 2002, Electrospinning bombyx mori silk with poly (ethylene oxide). *Biomacromolecules*, vol.3(6): 1233–1239. http://dx.doi.org/10.1021/bm025581u
7. Vijayavenkataraman S, Lu W F, and Fuh J Y H, 2016, 3D bioprinting of skin: A state-of-the-art review on modelling, materials, and processes. *Biofabrication*, vol.8(3): p032001. http://dx.doi.org/10.1088/1758-5090/8/3/032001
8. Chizhik S A, Wierzcholski K, Trushko A V, *et al.* 2011, Properties of cartilage on micro- and nanolevel. *Advances in Tribology*, vol.2010. http://dx.doi.org/10.1155/2010/243150
9. Teo W E, and Ramakrishna S, 2006, A review on electro-spinning design and nanofibre assemblies. *Nanotechnology*, vol.17(14): R89. http://dx.doi.org/10.1088/0957-4484/17/14/R01
10. Theron A, Zussman E, and Yarin A, 2001, Electro-static field-assisted alignment of electrospun nanofibers. *Nanotechnology*, vol.12(3): 384. http://dx.doi.org/10.1088/0957-4484/12/3/329
11. Bhattarai N, Edmondson D, Veiseh O, *et al.* 2005, Electrospun chitosan-based nanofibers and their cellular compatibility. *Biomaterials*, vol.26(31): 6176–6184. http://dx.doi.org/10.1016/j.biomaterials.2005.03.027
12. Teo W E, Kotaki M, Mo X, *et al.* 2005, Porous tubular structures with controlled fibre orientation using a modified electrospinning method. *Nanotechnology*, vol.16 (6): 918. http://dx.doi.org/10.1088/0957-4484/16/6/049
13. Baker B M, and Mauck R L, 2007, The effect of nanofiber alignment on the maturation of engineered meniscus constructs. *Biomaterials*, vol.28(11): 1967–1977. http://dx.doi.org/10.1016/j.biomaterials, 2007.01.004
14. Sun D, Chang C, Li S, *et al.* 2006, Near-field electrospinning. *Nano Letters*, vol.6(4): 839–842. http://dx.doi.org/10.1021/nl0602701
15. Sun D, Lin L, Wu D, *et al.* 2007, Electrospun ordered nanofibers on Si and SiO_2 substrate. In *2nd IEEE International Conference on Nano/Micro Engineered and Molecular Systems, NEMS'07*, IEEE, pp.72–76.
16. Chang C, Limkrailassiri K, and Lin L, 2008, Continuous near-field electrospinning for large area deposition of orderly nanofiber patterns. *Applied Physics Letters*, vol.93 (12): 123111.

http://dx.doi.org/10.1063/1.2975834

17. Padmanabhan T, Kamaraj V, Magwood L, *et al.* 2011, Experimental investigation on the operating variables of a near-field electrospinning process via response surface methodology. *Journal of Manufacturing Processes*, vol.13(2): 104–112. http://dx.doi.org/10.1016/j.jmapro.2011.01.003
18. Wei C, and Dong J, 2013, Direct fabrication of high-resolution three-dimensional polymeric scaffolds using electrohydrodynamic hot jet plotting. *Journal of Micromechanics and Microengineering*, vol.23(2): 025017. http://dx.doi.org/10.1088/0960-1317/23/2/025017
19. Park J U, Hardy M, Kang S J, *et al.* 2007, High-resolution electrohydrodynamic jet printing. *Nature Materials*, vol.6(10): 782–789. http://dx.doi.org/10.1038/nmat1974
20. Kim B H, Onses M S, Lim J B, *et al.* 2015, High-resolution patterns of quantum dots formed by electrohydrodynamic jet printing for light-emitting diodes. *Nano Letters*, vol.15(2): 969–973. http://dx.doi.org/10.1021/nl503779e
21. Lee H, Seong B, Kim J, Jang Y, *et al.* 2014, Direct alignment and patterning of silver nanowires by electrohydrodynamic jet printing. *Small*, vol.10(19): 3918–3922. http://dx.doi.org/10.1002/smll.201400936
22. Croisier F, Duwez A S, Jérôme C, *et al.* 2012, Mechanical testing of electrospun PCL fibers. *Acta Biomaterialia*, vol.8(1): 218–224. http://dx.doi.org/10.1016/j.actbio.2011.08.015
23. Wang H, Vijayavenkataraman S, Wu Y, *et al.* 2016, Investigation of process parameters of electrohydro-dynamic jetting for 3D printed PCL fibrous scaffolds with complex geometries. *International Journal of Bioprinting*, vol.2(1): 63–71. http://dx.doi.org/10.18063/IJB.2016.01.005
24. Kowalewski T, Błoński S, and Barral S, 2005, Experiments and modelling of electrospinning process. *Technical Sciences*, vol.53(4).
25. Koombhongse S, Liu W, and Reneker D H, 2001, Flat polymer ribbons and other shapes by electrospinning. *Journal of Polymer Science Part B: Polymer Physics*, vol.39(21): 2598–2606. http://dx.doi.org/10.1002/polb.10015
26. Woodruff M A and Hutmacher D W, 2010, The return of a forgotten polymer — polycaprolactone in the 21st century. *Progress in Polymer Science*, vol.35(10): 1217–1256. http://dx.doi.org/10.1016/j.progpolymsci.2010.04.002
27. Karageorgiou V and Kaplan D, 2005, Porosity of 3D biomaterial scaffolds and osteogenesis. *Biomaterials*, vol.26(27): 5474–5491. http://dx.doi.org/10.1016/j.biomaterials.2005.02.002
28. Garg K. and Bowlin G L, 2011, Electrospinning jets and nanofibrous structures. *Biomicrofluidics*, vol.5(1): 013403. http://dx.doi.org/10.1063/1.3567097
29. Lee A, Jin H, Dang H W, *et al.*, 2013, Optimization of experimental parameters to determine the jetting regimes in electrohydrodynamic printing. *Langmuir*, vol.29(44): 13630–13639. http://dx.doi.org/10.1021/la403111m
30. Pillay V, Dott C, Choonara Y E, *et al.*, 2013, A review of the effect of processing variables on the fabrication of electrospun nanofibers for drug delivery applications. *Journal of Nanomaterials*, vol.13(1): 789289. http://dx.doi.org/10.1155/2013/789289

PERSPECTIVE

Roles of support materials in 3D bioprinting – Present and future

Ratima Suntornnond*, Jia An and Chee Kai Chua

Singapore Centre for 3D Printing, School of Mechanical and Aerospace Engineering, Nanyang Technological University, Singapore 639798, Singapore

Abstract: Bioprinting has been introduced as a new technique in tissue engineering for more than a decade. However, characteristics of bioprinted part are still distinct from native human tissue and organ in terms of both shape fidelity and functionality. Recently, the combination of at least two hydrogels or "multi-materials/multi-nozzles" bioprinting enables simultaneous deposition of both model and support materials, thus advancing the complexity of bioprinted shapes from 2.5D lattice into micro-channeled 3D structure. In this article, a perspective on the roles of second bioinks or support materials is presented and future outlook of sacrificial materials is discussed.

Keywords: hydrogel, support materials, bioprinting, additive manufacturing, tissue engineering

*Correspondence to: Ratima Suntornnond, Singapore Centre for 3D Printing, School of Mechanical and Aerospace Engineering, Nanyang Technological University, Singapore; Email: ratima001@e.ntu.edu.sg

Received: November 4, 2016; **Accepted:** December 7, 2016; **Published Online:** January 4, 2017

Citation: Suntornnond R, An J and Chua C K, 2017, Roles of support materials in 3D bioprinting – Present and future. *International Journal of Bioprinting*, vol.3(1): 83–86. http://dx.doi.org/10.18063/IJB.2017.01.006.

1. Introduction

Bioprinting is an emerging technology that shows potential for regenerative medicine and other biomedical applications[1–3]. Unlike other 3D printing techniques which print non-living materials, bioprinting incorporates living materials during the printing process. However, the bioprinted structures are still different from complex native human tissue or organ. One reason is that "Bioink" which mostly refers to hydrogels has a relatively low mechanical integrity compared to other 3D printing materials such as metals, ceramics and polymers[4–7]. Some of the hydrogels are highly biocompatible and even able to promote tissue growth and tissue formation, but hydrogels that have good biocompatibility usually have low printability and low mechanical strength before and during printing. For example, collagen and gelatin-methacrylate (GelMA) has good biocompatibility, but their printability is poor and the mechanical strength is low. The viscosities of both hydrogels are low at the human body temperature (or before crosslinking stage). This may favor direct printing of cell-hydrogel suspensions without any change in environment or equipment such as temperature control unit[2,8], but it is difficult to print them into 3D shapes without using strength enhancement strategy (e.g. chemical crosslinking or adding thickener). A second reason is that there is a lack of sufficient support materials suitable for bioink. Support, also known as sacrificial material or structure, is a basic but important concept in 3D printing. It allows the fabrication of overhang features and complex internal structures. Similarly, in 3D bioprinting, it is difficult to print 3D complex shapes and geometries without using support. Therefore, at the current stage, bioprinting of complex hollow structures that can completely mimic human's vascular systems or hollow organs such as heart or kidney is very challenging. Single material printing will not be sufficient to provide all the required properties (including biocompatibility, mechanical integrity and printability)[1–9]

Roles of support materials in 3D bioprinting — Present and future. © 2017 Ratima Suntornnond, et al. This is an Open Access article distributed under the terms of the Creative Commons Attribution-NonCommercial 4.0 International License (http://creativecommons.org/licenses/by-nc/4.0/), permitting all non-commercial use, distribution, and reproduction in any medium, provided the original work is properly cited.

for bioprinted 3D complex hollow structures.

2. Roles of Support Materials in Bioprinting

Recently, printing beyond 2.5D (2.5D shape is the shape that comes from repeatedly printing a 2D pattern in Z direction without changing the pattern in any layer) grid structure and simple tubes into the micro-channeled and hollow structures represent a great advancement in bioprinting[10,11]. It is no l onger stacking layer by layer in the same pattern. To form small channels or hollow tubes, a second "bioink" is used. The second bioink acts as support material or sacrificial material. As shown in **Figure 1**, the second ink acts as mold or sacrificial materials to create a hollow structure or track for perfusion purpose. This technique normally composes of chemically crosslinked hydrogel especially UV crosslinked hydrogel such as GelMA[11] or polyethylene glycol diacrylate (PEGDA)[12] as model materials and usually thermo-responsive hydrogels such as pluronic F127 or agarose as support materials[2]. By incorporating both types of hydrogels, the complex hollow or complex track pattern in 2.5D level or microfluidic level is possible to be fabricated.

Even though the complex track has more advancement compared to just 2.5D lattice structure, in the reality, the real human organ is never in 2.5D plane. Rather, human organ is an intricate 3D structure which has a very complex shape, fine details and topography. Therefore, the technique in **Figure 1** is not sufficiently adequate to bring 3D bioprinting to the level of printing a human organ. This is due to the fact that only one of the materials, either model or support materials (mostly support material), has the good mechanical strength which is responsible for the shape stability and shape integrity.

Another recent advancement is the development of freeform reversible embedding of suspended hydrogels or "FRESH" technique, which allows 3D structure to be fabricated by using gelatin bath as the support material with many types of other hydrogels as model materials such as alginate with calcium chloride ($CaCl_2$) or fibrinogen and thrombin[13]. However, this technique needs precision control in temperature in addition to positional control. Gelatin is thermo-responsive which will start to melt when the temperature is above 30#C[2]. Therefore, temperature control is critical for "FRESH". Moreover, the "FRESH" technique is batch by batch specific so the crosslinked agent must be pre-mixed with gelatin bath first. Lastly, because of gelatin bath, the printing temperature needs to be lower than 30#C (around 22–25 °C) which is not ideal for printing cells over a prolonged period. To date, "FRESH" is considered one of the most advanced techniques. To sum up, a list of support materials for bioprinting is shown in **Table 1**.

Here comes the question, what is the next advancement for support material in bioprinting? In 3D printing, support materials always play an important role to create overhanging and hollow structures. As shown in **Figure 2** which is an anatomical heart model, the overhanging part (**Figure 2A**) needs a support to

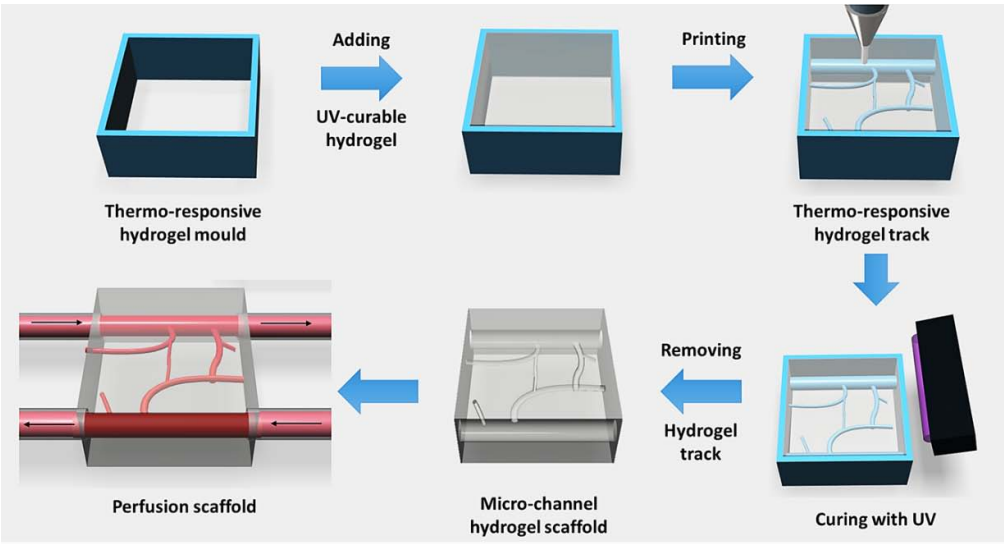

Figure 1. Schematic of hollow structure or track fabrication using two different types of hydrogels. UV curable hydrogel is model material whereas thermo-responsive hydrogel is sacrificial materials.

Table 1. Common support hydrogels in bioprinting

Support hydrogel	Model hydrogel	Bioprinted form	References
Gelatin and derivatives	Alginate, Fibrin and collagen	3D hollow structure	[13]
Agarose	GelMA, SPELA*, PEGDMA** and PEGDA	2.5D complex track	[14]
Pluronic and derivatives	GelMA and Agarose	2.5D complex track and micro-pattern	[11,15]

*Star poly(ethylene glycol-co-lactide) acrylate
**Poly(ethylene glycol) dimethacrylate

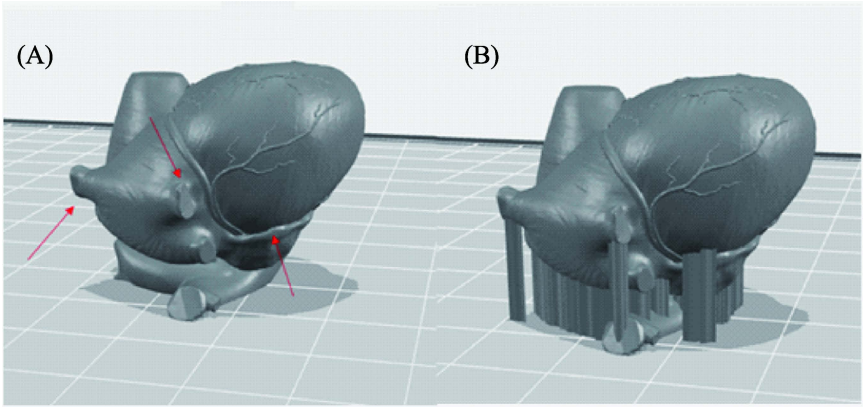

Figure 2. **(A)** Computer model of anatomical heart (red arrows pointed the overhanging parts) and **(B)** Computer model of anatomical heart with support structure.

hold even in other 3D printing techniques (Figure 2B). It is almost impossible for bioprinting to fabricate this structure without using support. However, comparing the materials that have been used in fused deposition modelling (FDM) with hydrogels or bioinks for bioprinter, the mechanical strength of the FDM materials is typically stronger[4–16]. The current hydrogels that have been used with bioprinter are too soft to hold the shape. Moreover, with the high water content, osmosis pressure will affect the interaction between model and support materials (e.g. water travels by osmosis pressure to another hydrogel which will lead to change in concentration, viscosity and mechanical properties). Thus, the requirements needed in bioprinting for fabricating 3D complex hollow structures are: (i) the material (including both model and support) must have sufficient shape integrity and can be printed in a cell friendly environment. To ensure biocompatibility properties, the bio-derived materials or even extracellular matrix (ECM) derived materials are preferred. Furthermore, to enhance mechanical properties, strong bio-derived materials such as silk or hydroxyapatite can be integrated with the model hydrogel as the composite natural materials; (ii) there is no or minimal reaction between model and support materials; and (iii) support materials must be easily removable without sacrificing cell viability. In order to achieve this property, either the concentration of model and support materials need to be similar or there is an interaction to create wall between model and support materials. For example, if model material contains Ca^{2+} and support contains alginate, the wall can be created by semi physical crosslinked reaction of alginate and calcium ion. All the mentioned techniques need to involve with the advancement of materials science and chemistry to understand the nature of materials and reaction mechanism.

3. Conclusion

It is evident that support materials are essential for both 3D printing and bioprinting. In 3D printing, the support materials have been used to fabricate complex structures with high resolution, which should be applicable to bioprinitng as well. The support materials may also be applied for upscale printing, organ printing and the advancement in tissue model for drug delivery and other related biomedical applications. In terms of achieving 3D complex hollow structures, it is challenging to rely on single material to accomplish it. The 2.5D complex track by using sacrificial materials has proved its application for lab-on-a chip and organ-on-a chip level. Nevertheless,

in order to scale up beyond micro-level, further improvements in materials research such as new biocomposite material or novel derived natural materials for both model and support materials for bioprinters are needed.

Conflict of Interest and Funding

No conflict of interest was reported by the authors.

Acknowledgements

Singapore Centre for 3D Printing (SC3DP) is supported by the Singapore National Research Foundation (NRF).

References

1. Murphy S V, Atala A, 2014, 3D bioprinting of tissues and organs. *Nature Biotechnology*, vol.32: 779–785. https://dx.doi.org/10.1038/nbt.2958
2. Suntornnond R, An J, Chua C K, 2016, Bioprinting of thermoresponsive hydrogels for next generation tissue engineering: A review. *Macromolecular Materials and Engineering*. https://doi.org/10.1002/mame.201600266
3. Lee J M and Yeong W Y, 2016, Design and printing strategies in 3D bioprinting of cell-hydrogels: A review. *Advanced Healthcare Material*. https://doi.org/10.1002/adhm.201600435
4. Schuurman W, Khristov V, Pot M W, *et al*., 2011, Bioprinting of hybrid tissue constructs with tailorable mechanical properties. *Biofabrication*, vol.3: 021001. https://doi.org/10.1088/1758-5082/3/2/021001
5. Cheah C M, Leong K F, Chua C K, *et al.*, 2002, Characterization of microfeatures in selective laser sintered drug delivery devices. *Proceedings of the Institution of Mechanical Engineers, Part H: Journal of Engineering in Medicine*, vol.216: 369 –383. https://doi.org/10.1243/095441102321032166
6. Yeong W Y, Chua C K, Leong K F, *et al.*, 2007, Comparison of drying methods in the fabrication of collagen scaffold via indirect rapid prototyping. *Journal of Biomedical Materials Research — Part B Applied Biomaterials*, vol.82: 260–266. https://doi.org/10.1002/jbm.b.30729
7. Kok Y H, Tan X P, Loh N H, *et al.*, 2016, Geometry dependence of microstructure and microhardness for selective electron beam-melted Ti–6Al–4V parts. *Virtual and Physical Prototyping*, vol.11: 183–191. https://doi.org/10.1080/17452759.2016.1210483
8. Ozbolat I T and Hospodiuk M, 2016, Current advances and future perspectives in extrusion-based bioprinting. *Biomaterials*, vol.76: 321–343. https://dx.doi.org/10.1016/j.biomaterials.2015.10.076
9. Murphy S V, Skardal A and Atala A, 2013, Evaluation of hydrogels for bio-printing applications. *Journal of Biomedical Materials Research Part A*, vol.101A: 272–284. https://doi.org/10.1002/jbm.a.34326
10. Kucukgul C, Ozler S B, Inci I, *et al*., 2015, 3D bioprinting of biomimetic aortic vascular constructs with self-supporting cells. *Biotechnology and Bioengineering*, vol.112: 811–821. https://doi.org/10.1002/bit.25493
11. Kolesky D B, Truby R L, Gladman A S, *et al.*, 2014, 3D bioprinting of vascularized, heterogeneous cell-laden tissue constructs. *Advanced Materials*, vol.26: 3124–3130. https://doi.org/10.1002/adma.201305506
12. Hoch E, Tovar G E M and Borchers K, 2014, Bioprinting of artificial blood vessels: Current approaches towards a demanding goal. *European Journal of Cardio-Thoracic Surgery*, vol.46: 767–778. https://doi.org/10.1093/ejcts/ezu242
13. Hinton T J, Jallerat Q, Palchesko R N, *et al.*, 2015, Three-dimensional printing of complex biological structures by freeform reversible embedding of suspended hydrogels. *Science Advances*, vol.1. https://doi.org/10.1126/sciadv.1500758
14. Bertassoni L E, Cecconi M, Manoharan V, *et al.*, 2014, Hydrogel bioprinted microchannel networks for vascularization of tissue engineering constructs. *Lab on a Chip*, vol.14: 2202–2211. https://doi.org/10.1039/C4LC00030G
15. Müller M, Becher J, Schnabelrauch M, *et al*., 2013, Printing thermoresponsive reverse molds for the creation of patterned two-component hydrogels for 3D cell culture. *Journal of Visualized Experiments*: e50632 e50632.
16. Boparai K, Singh R, Singh H, 2015, Comparison of tribological behaviour for Nylon6-Al-Al_2O_3 and ABS parts fabricated by fused deposition modelling. *Virtual and Physical Prototyping*, vol.10: 59–66. https://doi.org/10.1080/17452759.2015.1037402

INTERNATIONAL JOURNAL OF BIOPRINTING

ISSN (print): 2424-7723

ABOUT THE JOURNAL

International Journal of Bioprinting is a biannual, double-blind peer-reviewed, open access journal. This journal focuses on the use of 3D printing technology with materials that incorporate viable living cells or biological elements to produce tissue or biotechnological products. Further discourses and technological advancements in bioprinting are the goals behind acceptance of high-quality basic and applied research: from concept creation to fabrication of the bioprinting process, associated clinical applications as well as social implications.

Whioce Publishing, official publisher for the journal welcomes researchers to submit their papers relevant to bioprinting for consideration via **http://ijb.whioce.com/** For general enquiries and order for prints and reprints, please write in to **IJB@whioce.com** for a fast response.

SUBMIT YOUR PAPERS HERE

WHIOCE
PUBLISHING PTE. LTD.

ABOUT THE PUBLISHER

Whioce Publishing in Singapore is a registered publisher of excellent quality academic journals for an international readership. We deliver exceptional editorial support for the advancement and dissemination of scientific research by linking readers and researchers with networks and industries. We have ambitions to get our journals indexed in prominent databases such as EI, SCI, SSCI and AHCI, thereby aiming to be a first-class knowledge platform for researchers worldwide.

Whioce Publishing also engages in publishing e-books, organizing academic conferences and educational trainings, and providing translational services.

International Journal of Bioprinting is an
independent open access journal published
by Whioce Publishing Pte.Ltd.

WHIOCE PUBLISHING PTE. LTD.
PROVIDING
FIRST-CLASS SCIENTIFIC INFORMATION
FOR TOP SCHOLARS

Whioce Publishing Pte.Ltd.
7030 Ang Mo Kio Avenue 5
#04-15 Northstar@AMK
Singapore 569880
Tel: +65 65702707/65702718
Fax: +65 65702803

See www.whioce.com/contact for a full list of offices and contact information.

Whioce Publishing Pte.Ltd. is a company registered in Singapore (No. 201427293E), whose registered office is at 7030 Ang Mo Kio Avenue 5 #04-15 Northstar@AMK Singapore 569880